2022

NUMERICAL AND SCALING STUDY ON APPLICATION OF INKJET TECHNOLOGY TO AUTOMOTIVE COATING

Masoud Arabghahestani Dr.
University of Kentucky, mar243@uky.edu
Author ORCID Identifier:
https://orcid.org/0000-0001-7349-2331
Digital Object Identifier: https://doi.org/10.13023/etd.2022.376

Right click to open a feedback form in a new tab to let us know how this document benefits you.

NUMERICAL AND SCALING STUDY
ON APPLICATION OF INKJET TECHNOLOGY
TO AUTOMOTIVE COATING

DISSERTATION
_____

A dissertation submitted in partial fulfillment of the
requirements for the degree of Doctor of Philosophy in the
College of Engineering at the University of Kentucky

By

Masoud Arabghahestani

Lexington, Kentucky

Co- Directors: Dr. Kozo Saito, Professor of Mechanical Engineering

and Dr. Nelson Akafuah, Associate Professor of Engineering Technology

Lexington, Kentucky

2022

ABSTRACT OF DISSERTATION

NUMERICAL AND SCALING STUDY
ON APPLICATION OF INKJET TECHNOLOGY
TO AUTOMOTIVE COATING

A thorough literature review identified lack of precision control over quality of droplets generated by the currently available industrial sprayers and a growing need for higher quality droplets in the coating industry. Particularly, lack of knowledge and understanding in continuous inkjets (CIJ) and drop-on-demand (DOD) technologies is identified as significant. Motivated by these needs, this dissertation is dedicated to computational fluid dynamics (CFD) and scaling studies to improve existing inkjet technologies and develop new designs of efficient coating with single and/or multiple piezoelectric sensors to produce on-demand droplets. This dissertation study aims at developing a new DOD type coating technology, but it required understanding the effects of paint viscosity on droplet generation mechanism, an effective droplet delivery method to the coating surface, painted surface quality and control system of the DOD among others. Waterborne (WB) paints are chosen as the working liquid to identify three different DOD designs capable of creating a stream of mono-dispersed droplets. Volume-of-fluids (VOF) multiphase model explored the droplet creation process and effects of various parameters on the droplets' quality. The law approach scaling analysis identified scaling laws to scale up these numerical results conduced for the laboratory-scale DOD to the large industrial scale inkjet nozzles.

KEYWORDS: Inkjet Printing, Numerical Simulation, Scaling Analysis, Droplet Generation, DOD Inkjet Nozzles.

Masoud Arabghahestani

(Name of Student)

08/29/2022

Date

NUMERICAL AND SCALING STUDY
ON APPLICATION OF INKJET TECHNOLOGY
TO AUTOMOTIVE COATING

By
Masoud Arabghahestani

Prof. Kozo Saito
Co-Director of Dissertation

Dr. Nelson Akafuah
Co-Director of Dissertation

Prof. Jesse Hoagg
Director of Graduate Studies

08/29/2022
Date

ACKNOWLEDGMENTS

I wish to express my sincere gratitude to all people who provided guidance and support during the course of this long journey to complete this dissertation. I have greatly benefited from their kind help and support, and they have made my graduate study experience, the best I could ever hope for.

First and for most, I would like to thank my main advisor Dr. Kozo Saito for enabling me to study and perform my PhD dissertation at the University of Kentucky and take advantage of his great knowledge. His continued supports and insights into various subjects helped me to find ways to overcome all the difficulties on the way and enabled me to study the problem deeply and thoroughly.

Second, I am greatly thankful and appreciative of Dr. Nelson K. Akafuah and Dr. Mark Doerre, who never hesitated to spare time to provide technical supports along the way.

Third, I would like to thank my committee members, Dr. Dušan P. Sekulić and Dr. Yang-Tse Cheng for reviewing my dissertation and providing guidance for me to improve the quality of this dissertation.

Forth, I would like to acknowledge Dr. John Stencel, Dr. Tianxiang Li, Dr. Adnan Ahmad Darwish, Dr. Ahmad Abubaker and Essa Salem for their in-valuable comments and helpful discussions and supports along the way.

And finally, I would like to thank my family for their encouragements and moral supports that made the entire process a lot easier.

TABLE OF CONTENTS

LIST OF TABLES

LIST OF FIGURES

CHAPTER 1. INTRODUCTION

1.1 Current Technologies Used in Automotive Spray Coating

Different layers of coat and paint are generally applied to the surface of the cars using a selected type of sprayer. There have been many different types of atomizers proposed to generate droplets and they each have their advantageous and disadvantageous. A spray is defined as the disintegration of liquid ligaments into smaller size droplets. Spray atomizers can be driven by various mechanisms. Aerodynamic, mechanical, ultrasonic, and electrostatic forces are only few of the processes that can be used. The characteristics of the droplets depend on the quality of the atomization process which depends on the type of the atomizer, liquid properties, environmental effects and the geometrical properties of the atomizer itself. Thus, different types of atomizers are suitable for different applications.

In automotive coating sector, spray coating is mainly done with either conventional air spray devices/guns or high-speed rotary bell atomizers, with the latter being the major technology used for these applications in the recent years. Spray booths are required for spray coatings. These are enormous, climate-controlled enclosures that aid in increasing the paint's transfer efficiency (TE) onto a target while also directing overspray (paint particles that do not coat the automobile and float in the air) and solvents into an emission abatement area of the booths. The main sprayer technologies used in automotive industries will be explained in detail in the following section and some of the general issues related to their application will be discussed.

Air sprays, airless sprays, air-assisted airless sprays, HVLP sprays, and rotary sprayers are all examples of conventional atomizers. In the following, some of these atomizers that are more common for coating purposes will be explained further.

1

1.1.1 Conventional Air Spray Devices and Equipment

The earliest technology is traditional air spray (siphon/gravity/pressure feed), which rose to popularity in the 1920s with the rise of the automobile and furniture industries. These spray guns were used for over 100 years to apply the paint on the car bodies for many years, mainly in smaller scales, due to two main advantages that they laid claim to; control and versatility. In terms of control, this is the procedure that can be controlled the greatest. When properly trained, the spray operator can adjust the spray pattern from a small dot to a big production-style pattern. This allows them to spray little or large areas without having to change guns or nozzles. And in terms of versatility, these devices offer the capability to be used with the widest range of working liquids.

This method is still used by some of the smaller paint shops all around the world, however, there is a major setback which limits the application of these device with the lower transfer efficiency. The lower transfer efficiency may cause negative effects on both the worker's health and the environment with the wasted paint/coat which is higher than that of the deposited paint/coat. The following section summarizes studies on the performance and applications of these inkjets. It should be mentioned the pioneer experimental study by Nukiyama and Tanasawa (Nukiyama & Tanasawa, 1938) on their first significant contributions to the study of the conventional sprayer devices was one of the first studies that shed more light on this technology. They successfully provided an empirical formula to associate the droplet sizes to gas and liquid speeds as well as liquid characteristics. They found that liquid and gas viscosities, densities, liquid surface tension, and the liquid and gas velocity and flow rates were the most influential parameters impacting droplet sizes. Even though the performance of the nozzle and how each of the

2

factors affects the droplet characteristics change based on the properties of the design, droplet sizes normally increase as the flow rate increases, and they decrease as the flow rate decreases (Masters, 1979; Schick, 2006). The gas pressure (shaping air pressure), however, has a reverse relationship with the size of the droplets as increasing the air pressure can significantly decrease the size of the droplets in most conventional sprayers (Lefebvre, 1989).

The interactive nature of these elements may generate discrepancies in the results when analyzing specific spray parameters that affect droplet size distribution. Each of the characteristics listed above, such as liquid density, can have an impact on liquid viscosity and even surface tension (Schonhorn, 1967). As a result, interactions among influential parameters should be carefully investigated to obtain reliable conclusions from research on traditional air spray systems. This brings up another point: droplet size distributions are heavily impacted by interactions between spray device design and ambient conditions such as temperature and humidity. The effective spray device's design not only requires operational parameters such as inherent liquid, operational velocities, and pressures, but also external parameters such as ambient temperature and humidity.

1.1.2 High Volume Low Pressure (HVLP) Devices

The high-volume low-pressure (HVLP) sprayers are designed based on the idea to reduce over spray paint. HVLP sprayers use the high volume of air rather than the high pressure of air which the conventional spray atomizers use. HVLP guns were first developed in response to environmental regulations enacted in some areas of California (Fettis, 2008). (Heitbrink, Verb, Fischbach, & Wallace, 1996) compared the TE and the

effects of HVLP and conventional atomization sprayers on the spray concentrations, by conducting experiments in a downdraft spray painting booth. They concluded that the HVLP can provide significantly higher transfer efficiency than the conventional spray-painting gun. (Tan & Flynn, 2000) presented an experimental evaluation of mathematical model for estimating the transfer efficiency of HVLP sprays. They also investigated the effects of gun-to-surface distance and nozzle pressure on the agreement between measurement and prediction of transfer efficiency. (Darroch, 1997) presented two different type of HVLP guns, an air conversation sprayer gun and a turbine-driven system HVLP gun.

The HVLP guns have advantages and dis advantages over the conventional spray guns. The main benefit of the HVLP guns is that they typically provide much higher transfer efficiencies (over 50%, which is generally much higher than that of the conventional spray guns). Consequently, they reduce the material cost, waste treatment cost and the cost of spray booth maintenance. Compared to the conventional spray guns, however, they suffer from a poor finish quality and expensive cost and operation.

1.1.3   Rotary Bell Atomizers

Electrostatic rotary bell sprayers (ERBS) are one of the most widely used applicators in the coating industries, particularly in the industries with higher rates of production (Toda, Salazar, & Saito, 2012). Rotary bell atomizers showed promising results due to a consistency in their spray pattern and their high atomization rates. With the growing need for higher quality of droplets in various industries, the earlier electrostatic

rotary bell sprayers which are inherent in poor quality of atomization are no longer valid for top coating but only for the primer coating which requires less surface finish quality.

The recent advancements in the electrostatic rotary bell sprayers helped to apply these electrostatic rotary bell sprayers to top coating and even metallic paint applicators in some industries. Electrostatic rotary bell sprayers consist of four major components: (1) valves to provide pathways for paint, solvents, and shaping air, (2) a rotating disk to provide the essential centrifugal forces, (3) a turbine to rotate the bell and (4) the shaping air ring. Figure 1.1 shows a schematic of a typical simple rotary bell sprayer.
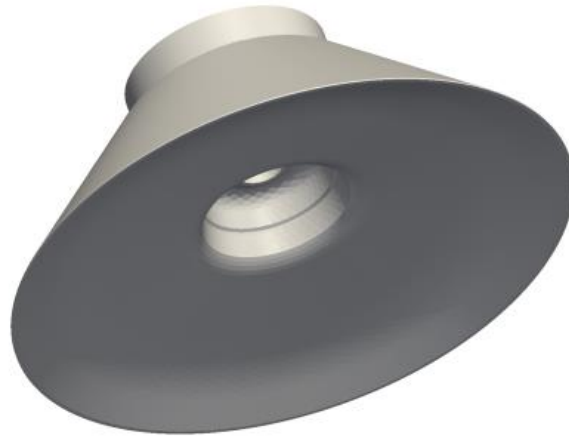
Figure 1.1 A typical schematic of simple rotary bell sprayers, adopted from (Andersson, 2013), reproduced with the permission of Dr. Björn Andersson.

Many researchers have studied the effects of various operating parameters on the performance of electrostatic rotary bell sprayers (Darwish Ahmad, Abubaker, Salaimeh, & Akafuah, 2018; Darwish Ahmad et al., 2019; Domnick, Scheibe, & Ye, 2005, 2006; Guettler, Knee, Ye, & Tiedje, 2020; Im, Lai, Yu, & Matheson Jr, 2004; J. Liu, Yu, & Guo, 2012; Mark et al., 2013). (Marshall, 1954) and (Dombrowski & Lloyd, 1972) made some of the early contributions towards understanding the physics behind the atomization

process from rotary bell atomizers. They suggested three possible different modes of droplet formation. These three different modes are schematically shown in Figure 1.2, on the rotary bell atomizers. It intends to show three different mechanisms identified as (a), (b) and (c) in the figure to produce droplets. The first mechanism (a) is to directly produce droplets from the bell which produces the torus with the most uniform sizing. The second mechanism (b) is to use the ligament breakup to form the liquid ligaments from the liquid flow where the torus around the bell periphery disintegrates into droplets and detaching from the bell itself. The second mechanism produces less uniformly distributed droplet sizing than the first mechanism. The third mechanism (c) is the film breakup mechanism where the liquid is detached from the bell in terms of films and sheets of liquid. They experience multiple disintegrations over time by imposition of aerodynamic waves which grow in amplitude until fragments of sheets are detached, producing droplets as the result of these multiple disintegration processes. The third mechanism produces the least uniform distribution of the droplets sizing among all three mechanisms. (Frost, 1981) proposed a criterion to predict the outcome atomization mechanism from a rotary bell atomizer, given the operation conditions introduced to it.

(a) (b) (c)
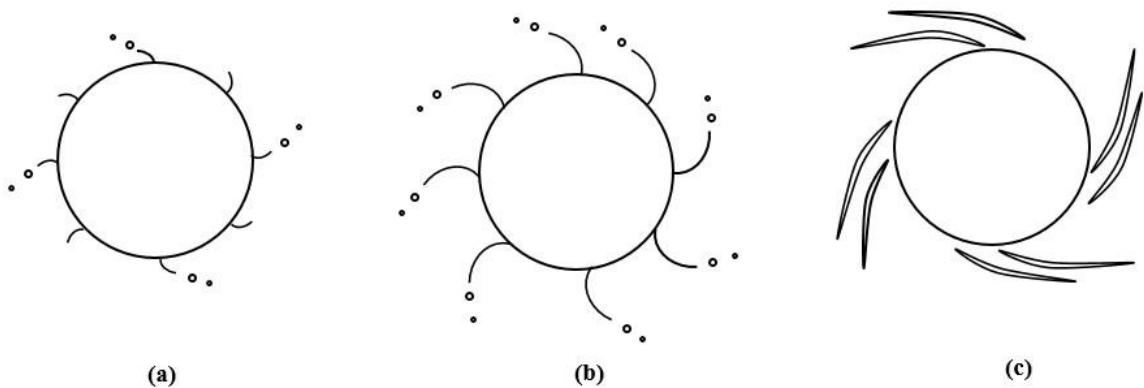
Figure 1.2 Different modes of liquid breakup from rotary bell atomizers; (a) direct drop formation, (b) ligament breakup and (c) film breakup (sheet formation),

6

adopted from (Poozesh, 2015), reproduced with the permission of Dr. Sadegh Poozesh.

Experimental methods in comparison to theory and numerical computation dominated the study of the electrostatic rotary bell sprayers for a long time, mainly because the control mechanism involves in multi parameters and an accurate description on how each of these multi parameters behaves requires complex physical equations, and some of them are often unknown.

Due to the recent progress in high speed computation, the computational methods became an approximate and inexpensive way to conduct parts of these studies in the more recent years (Osman, Adamiak, Castle, Fan, & Simmer, 2015; Pendar & Páscoa, 2019). Because computation capabilities are limited in completely understanding the spray process, however, a combination of experimental and computation methods is received the practically most attractive way to study and comprehend the complex nature of the spray process (J. Liu et al., 2012; Peng, Wang, Wang, & Ling, 2016).

(Hines, 1966) studied the effects of various parameters on the atomization process from electrostatic rotary bell sprayers and provided some formulations to predict the droplet size generated from the rotary bell sprayers, depending on the liquid properties introduced to it. (Huang, Lai, & Meredith, 2000) developed a numerical simulation model to fully estimate the airflow and droplets transport map and showed a higher transfer efficiency and droplet speed by increasing the electrostatic field for electrostatic rotary bell sprayers. (Ye & Domnick, 2017) investigated the atomization process from multiple atomization devices and obtained the linear relationship between Sauter Mean Diameter (SMD) and the rotary bell cup's radius.

7

The following summarizes factors that influence droplet size distributions from rotary bell atomizers.

(1) Three major inlet liquid properties including viscosities, surface tensions, and rheology being the most influential in determining the distributions of droplet size;

(2) The inlet flow rates of liquid and air into the atomizer;

(3) Geometrical configurations of the cup and disc; and

(4) The rotational speed of the bell. Because of their relevance during droplet formation, the bell's rotational speeds and inlet liquid flow rates, according to published data, are found to be most influential in determining droplet size distributions.

Table 1.1 presents a summary of typical and conventional atomizers, their droplets' size range and related advantages against other similar types.

Table 1.1. A summary of some of the conventional atomizers, (Srinivasan, 2006), reproduced with the permission of Dr. Vedanth Srinivasan.

Atomization Type		Droplet Size Range (µm)	Advantages	Disadvantages
Pressure Atomization	Plain Orifice	20-250	Simple, rugged, cheap	Narrow spray angle, solid spray cone

				Increased pressure
	Simplex	25-200	Simple, cheap, Wide spray angles	supply, very sensitive to applied pressure
	Duplex	20-200	Simple, cheap, Wide spray angle, Good atomization over a wide range of liquid flow rates	Increased liquid flow rate leads to narrow spray angle
	Dual-orifice	20-250	Good atomization, Constant spray angle	Poor atomization in transient stage, design complexity, Passage blockage
	Spill return	25-200	Simple, good atomization over a range of flow rates	Flow rate dependent spray angle, higher power consumption
	Fan spray	100-1000	Good atomization, elliptical spray pattern	High supply pressure
Rotary Atomization	Spinning disk	10-250	Good monodispersity	Satellite droplets, 360° spray pattern

			of droplets, independent control of atomization and flow rate	
	Rotary Cup	10-300	Capable of handling slurries, high viscosity materials	Requirement for air blast and high-power requirement
Two-fluid atomization (air assisted)	Internal mixing	50-400	Good atomization, low clogging, handle high viscosity liquids	High air power, other Auxiliary device
	External mixing	20-140	Good atomization, no risk of liquid backup into air line	Requirement for external source of high pressure air, limited air/liquid ratios
Two-fluid atomization (air blast)	Plain-Jet	15-150	Simple, cheap, good atomization	Narrow spray angle

	Prefilming	25-150	Good atomization at high ambient pressures, wide spray angles	Poor atomization at low air velocities
Effervescent atomization		25-350	Simple, good atomization, low risk of plugging, soot reduction	Requirement for separate air supply
Electrostatic atomization		0.1-1000 300-600 100-250	Fine and uniform droplets	Very low flow rates, Sensitive dependence on liquid electrical properties
Ultrasonic atomization	Nebulizers	1-5 (55 KHz) 30-60 (50 KHz)	Very fine uniform droplets, low spray rates	Incapable of handling high flow rates

1.2 Background of Inkjet Technology

The process of liquid jets disintegration has been a subject of study for a long time in the literature due to its significant impacts on variety of applications in different industries such as healthcare, automotive, coating, painting, food, combustion,

microfluidic devices and pharmaceutical industries (Masoud Arabghahestani, Akafuah, Li, & Saito, 2022; Masoud Arabghahestani, Akafuah, & Saito, 2021; M Arabghahestani & Karimian, 2017; Masoud Arabghahestani, Poozesh, & Akafuah, 2019; Basaran, 2002; Darwish Ahmad et al., 2019; Gao, Hossain, Matsuoka, & Nakamura, 2017; Lefebvre, 1989; Li et al., 2020; H. Liu, 2002; Poozesh, 2015; Poozesh, Akafuah, & Saito, 2015; Poozesh, Akafuah, Campbell, Bashiri, & Saito, 2020; Poozesh, Saito, Akafuah, & Graña-Otero, 2016; A. J. S. Salazar, K. , 2008).

Liquid jets disintegration process is the basis for investigation of droplet formation, which is the result of liquid ligament breakup. This phenomenon is highly complex and physical characteristics of it are yet to be fully discovered. These complexities regarding the atomization process, result in undesirable or random spray or droplet characteristics such as wide ranges of droplet sizes, irregular spatial distributions, satellite or bouncing droplets, longer ligament breakup lengths, spray jets and many others.

The nature of the liquid jet breakup phenomenon and the possible characteristics of the generated droplets are highly influenced by different parameters and phenomena such as turbulence, cavitation, particle interactions, fluid properties, and the geometrical properties of the sprayer itself (Masoud Arabghahestani et al., 2021; Bang, Kim, & Kim, 2003; Brown & McDonell, 2006; Lefebvre, 1989; Nasr, Yule, & Bendig, 2013; Rayleigh, 1892; R. D. Reitz, 1978). To explain the various regimes encountered as a function of operation parameters, it is necessary to understand the forces influencing the liquid jet and affecting its breakup process. There are four basic breakup regimes that correspond to various combinations of liquid inertia, surface tension, and aerodynamic forces acting on the jet (Lefebvre, 1989; Lin & Reitz, 1998; R. Reitz & Bracco, 1982; R. D. Reitz, 1978).

For the generation of desirable size droplets, a thorough understanding of the mechanism which controls the generation process is crucial. For this purpose, researchers have introduced various creative design concepts including different types of small to large-scale atomizers. Disintegration of liquid filaments emanating from a nozzle into droplets have been widely investigated recently (Akafuah, Salazar, Saito, & Srinivasan, 2009; Antonopoulou, Harlen, Rump, Segers, & Walkley, 2021; Avvaru, Patil, Gogate, & Pandit, 2006; Conto, 2019; Janna, 1976; Lefebvre, 1989; H. Liu, 2002; Lohse, 2022; Herman Wijshoff, 2018; W. Zhang, Liu, Liu, Jia, & Xi, 2019). Various mechanisms such as nozzle cavitation (Bergwerk, 1959) and liquid turbulence (Grant & Middleman, 1966; R. Reitz & Bracco, 1982; R. D. Reitz, 1978) have been recognized as the most significant factors to influence the breakup phenomenon. Other researchers have studied the governing forces with the most significant influence on the liquid breakup process from the nozzles (Masoud Arabghahestani et al., 2021; Swerin, 2018).

The mechanism of liquid breakup inside a nozzle holds stochastic nature which makes the traditional experimental and theoretical investigations difficult. The concept of inkjet printing was first introduced in the early 1950s, when the technology was only used to recreate digital images and documents by producing and transferring ink droplets to a paper substrate. A rapid progress in the inkjet technology has brought broader applications of the inkjet technology to industries such as Micro-Electro-Mechanical systems (MEMS) (Fakhfouri et al., 2008; Fischer, Mäntysalo, & Niklaus, 2020; Lessing et al., 2014), spraying processes (Akafuah et al., 2009; Z. Wang & Nagao, 2014), electronic industries (Caglar, 2010; Eshkalak et al., 2017; H.-H. Lee, Chou, & Huang, 2005; Mei, Lovell, & Mickle, 2005), drug delivery (Kolakovic et al., 2013), DNA arranging (Liou & Wu, 2017)

13

and finally, coating and painting industries (Masoud Arabghahestani et al., 2021; López, Diez, & Odriozola, 2007; Maisch et al., 2016). Efforts have been devoted to improve the quality and performance of the inkjets in printing technology, but the progress in coating and painting lags behind in related applications (Akafuah et al., 2009; Basaran, 2002; Burr, Tence, Le, Adams, & Mutton, 1996; Poozesh, 2015; Poozesh et al., 2015; Herman Wijshoff, 2010). Researchers at the University of Kentucky's IR4TD have proposed two new types of atomizers: ultrasonically-driven cavitating atomizers (UCA) (Akafuah et al., 2009) and ultrasonic ligament atomizer (ULA) (Avvaru et al., 2006). They numerically and experimentally investigated their performance and identified one of challenges to be solved before prototyping tests is to deal with high viscosity fluids, including the paint widely used in automotive industries to coat automobile body and parts.

Inkjets nozzles can mainly be categorized in two types: continuous inkjet (CIJ) and drop-on-demand (DOD) (S. D. Hoath, 2016; Y. Wang, Bokor, & Lee, 2004). CIJ, one of the oldest inkjet technologies, can create continuous breakups of liquids to produce a continuous stream of droplets by a regular pressure modulation unit. This technology creates high-pressure continuous stream of droplets by using Plateau-Rayleigh instability (Chuang, 2011) and is capable of generating up to 165,000 droplets per second. Droplets are charged with variable positive and negative charges, separated by some neutral droplets called guard droplets to avoid undesirable repulsion, as they form and pass through an electrostatic field (typically, a variable electrostatic field). CIJ inkjet nozzles are capable of producing droplets with higher kinetic energies which help the droplets to travel a long distance relative to the substrate and gain higher frequency compared to the similar models. In addition, the CIJ's continuous stream of inks can reduce the frequency of clogging and

cleaning. CIJ technology, however, has its limitations: its applications such as high-speed droplets splash, more satellite droplets, limits in controlling the droplet sizes and harder due to implementation of electrostatic fields for the inkjet, and a relatively low transfer efficiency. Figure 1.3 shows a simple illustration of the CIJ droplet generation process, where droplets are generated at the left-hand side nozzle and moving to the right, creating a continuous stream of droplet.

Figure 1.3 Schematic of CIJ technology droplet generation.

DOD inkjets, driven by pressure or heat gradients generated by piezoelectric sensors or spot heaters, can generate an intermittent stream of droplets with lower kinetic energy, at the time the droplets are needed. In addition, using these inkjet nozzles can eliminate the need for electrostatic fields as the undesired droplets are not generated, thus, increase the transfer efficiency of the process. Figure 1.4, a sample numerical simulation result for DOD inkjet, shows how the droplets are generated by the left-hand side nozzle and moving to the right.

Figure 1.4 Schematic of DOD technology droplet generation.

These inkjet nozzles, however, have the relatively lower droplets' generation rate and lower kinetic energies compared to CIJ. Therefore, for commercial applications, multiple nozzles are required to be placed closed to each other and depending on the applications, some of these nozzles would stay idle for longer periods of time. This can

increase the probability of nozzle clogging that can interrupt the droplet formation or decrease the quality of the printing or painting.

Figure 1.5 illustrates the mechanism of generating droplets from CIJ and DOD inkjet nozzles. As it can be seen from part (a), the CIJ nozzles require a more sophisticated procedure to direct the favorable drops towards the substrate and attempt to recycle the undesired droplets.
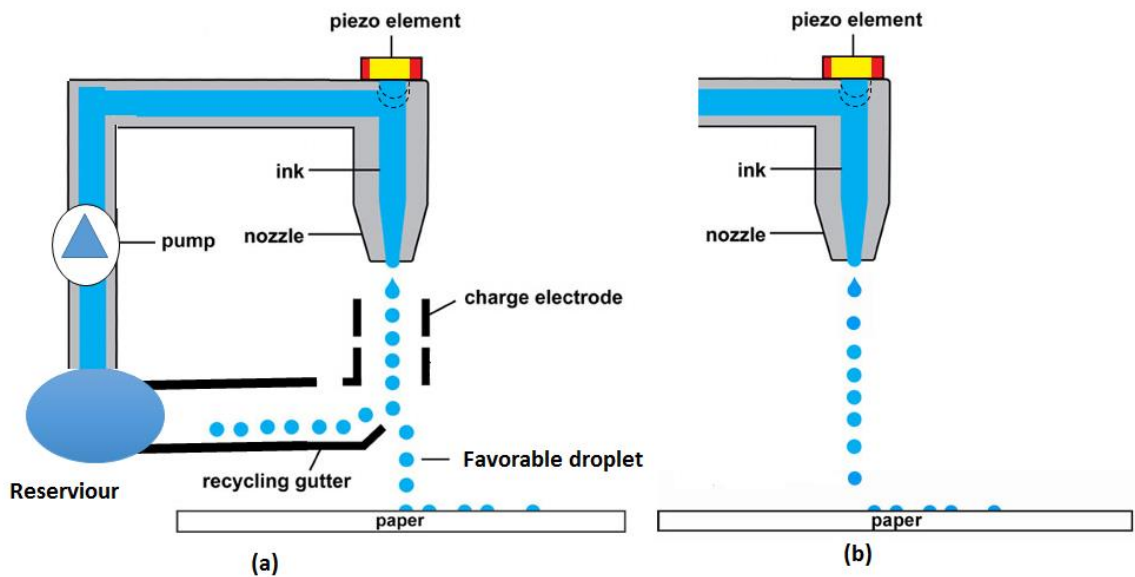
Figure 1.5 (a) CIJ inkjet working mechanism and (b) DOD inkjet working mechanism (Poozesh, 2015), reproduced with the permission of Dr. Sadegh Poozesh.

DOD inkjets can also better control the characteristics of the droplets compared to CIJ. There are two major types of DOD inkjets: piezoelectric driven and thermal driven inkjets. Even though the mechanism triggering these two types of DOD inkjets have major similarities, there are some differences that can change the applications of these two inkjet types. In thermal-driven inkjets, an electric current pulse generates heat inside the nozzle using a heated plate that causes small bubbles to form in the regions closer to the heated

plate. This can slowly increase the pressure and thus mobilize a small volume of liquid to form the droplets at the nozzle. Thermal inkjets usually require volatile components to promote the vapor bubble formation and involve high vapor pressure solvents and lead to increased temperatures that can limit the application of these inkjets.

Figure 1.6 shows a schematic of the DOD droplet generation process. The piezoelectric inkjets consist of a piezo sensor, a durable container for the inks, a mechanism of refilling the ink container, air entrances, a durable stand to fix the gap between the head and the targeted substrate, and a piezo controller including a software to control the movements of the piezo material. The piezo sensor changes shape by applying the electric current to it and creates a pressure pulse, forcing the working liquid to move towards the nozzle's orifice. These inkjets have a wider range of application compared to the thermal inkjets as there are fewer limitations for the working liquid that can be input to the nozzle head. The piezoelectric driven inkjet nozzles, however, are generally more expensive since the piezoelectric material comes at higher prices. Figure 1.6 (a) illustrates a simple presentation of DOD inkjet using piezoelectric sensor and its droplet generation mechanism.
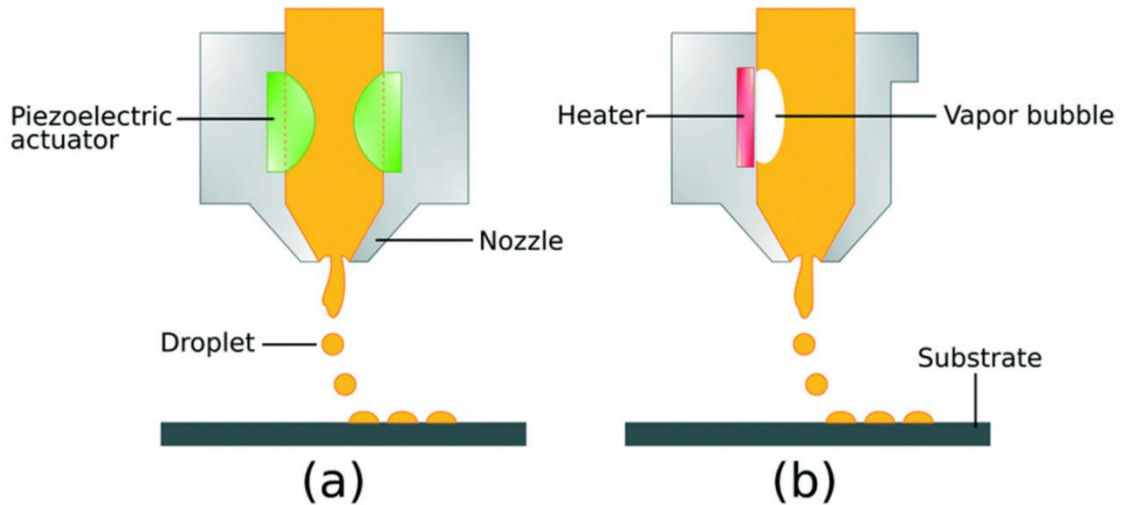
Figure 1.6 DOD Inkjets operated based on two different mechanisms: (a) piezoelectric actuators and (b) heated plates, adopted from (Mahmood, 2021).

As an alternative to these two types of inkjet nozzle, actuators can be used to create the positive and negative gradients inside the nozzle head. Such systems work very similar to that of piezoelectric-driven nozzles, but there are some differences in the geometry of the nozzle and how the actuators are placed. One main difference is that, unless specific methodology is used, actuator-driven nozzles produce continuous stream of droplets.

The whole process of DOD inkjet droplet generation can occur in a timespan of less than 50 µs, meaning that even a high-speed camera image of 10,000 frame per second only can capture one or two frames before the droplets hit the target. In addition, the very small droplet sizes generated from the inkjet nozzles require high precision accuracy tools, which are often expensive and even not available in the market, to capture the details of the process. Because of the difficulty in experimental methods, numerical methods may become an attractive alternative tool. Note, in a scientific research, there are three methods known to exist, experiment, theory and computation. Each offers unique strengths but also

weaknesses. For interested readers, the following references are available (Emori, Saito, & Sekimoto, 2000; K Saito & Williams, 2015; Wilson, 1990)

Numerical simulations can be conducted using a numerical model, which is constructed based on assumptions and hypotheses. If they are adequate in correctly describing the current inkjet problem, the numerical modeling or numerical simulations are expected to provide results which are relevant to understand the mechanisms that control the process. Numerical methods, however, require validation by experiments, therefore, the combination of experiments and numerical simulations become a widely recommended tool in scientific research. This combination is chosen for this dissertation to study the liquid breakup phenomenon from the inkjet nozzles. In the following, objectives and overview of this dissertation are provided, and the next chapter provides a detailed literature review to justify the objectives of this dissertation.

1.3   Objectives of this Dissertation

The main objectives of this research are summarized as follows:

1. To tackle two major issues, the low transfer efficiency and chemical waste problems, which are currently faced by the automotive coating and painting industry. This research proposes three novel droplet-on-demand inkjet nozzles that can work with higher viscosity fluids such as those of industrial grade paints. These three new designs use one or a combination of multiple piezoelectric sensors to generate the pressure gradients required for disintegration of liquid jets, with a precision control over the characteristics of the liquid droplets generated from the nozzle.

2. To provide physical insights on the liquid filament breakup process from inkjet nozzles and the effective parameters and forces on the characteristics of the droplets generated from the nozzle under specific operating conditions.

3. To precisely control the properties of the droplets: the velocity, frequency, size and impingement location.

4. To find operation conditions for the proposed inkjet nozzles to produce monodispersed droplet streams which are desired by the coating and painting industry.

The achievement of the above-mentioned research objectives can help automotive coating and painting industry in the following five aspects:

1. Developing an on-demand droplet generation sprayer using the inkjet technology.

2. Developing a simulation model to study the liquid breakup process from a modulated DOD inkjet nozzle and study the effects of the modulation parameters such as amplitude and frequency of the formation and characteristics of the droplets.

3. Providing precision control over the droplets size and frequency that are crucial droplet properties in this industry.

4. Reducing the satellite droplets and over sprayed paint.

5. Increasing the transfer efficiency and precisely controlling the droplet hitting locations to achieve two-tone painting without masking and reduce the pollution and operation cost.

1.4   Overview of this Dissertation

Chapter 1 provides basic information regarding the inkjet printing technology and introduces the main technologies that are currently being used in automotive coating and painting industries and states their weak areas and strong suits. In addition, this chapter provides a detailed background on inkjet printing technologies; such as how it started, what applications it encompassed over time, improvements made to its concept over the course of history and potential applications suggested for it by researchers in the field. Lastly, this chapter summarizes the objectives and the flow of information in this dissertation.

Chapter 2 provides an extensive literature review on the inkjet printing technology, strengths, weaknesses, potentials for improvement, and the problems that this technology has been facing over the course of history. These problems were grouped in three main categories including problems related to meniscus generation and backpressure in the nozzle, droplet size related issues, and issues regarding generation of unfavorable satellite droplets. This chapter ends by introducing scaling analysis as a viable tool to study problems related to this technology.

Chapter 3 provides the details of three inkjet designs that showed potentials towards being used in the automotive coating and painting industries and replace the conventional sprayers in this industry. These designs include a simplistic UPA model that uses basic procedures to provide acceptable droplets, SPD printhead that uses one piezo sensor in the form of an actuator to provide the essential energy required for breaking up the liquid ligaments, and a final DPD that uses two piezo electric sensors to provide a higher degree of control over the droplets' characteristics. This chapter presents the working concept, the isometric view, and the CAD designs with dimensions to replicate the studies conducted in this work.

21

Chapter 4 summarizes the concept of multiphase flow system and different models available to numerically study the multiphase flow problems. This chapter also details the numerical methodology adopted for this study, including the governing equations, and suggests alternative models for similar future studies. This chapter ends with the validation of the proposed numerical model with literature values to ensure that the model is capable of accurately capturing the physics that governs the inkjet problem.

Chapter 5 explains scaling analysis, the concept of scaling, and applications to small-scale industrial models. The chapter is divided into three main sections: the first section introduces the scaling analysis and benefits from scaling studies, the second section explains similar scaling studies with major governing forces from the literature, and the final section explains the unique role of the scaling analysis study to achieve the goals of this work.

Chapter 6 presents the results from this study and provides interpretations and discussion on them. This chapter consists of three sections: section 1 provides the UPA nozzle results and explains how this nozzle can better control the droplet characteristics with a simple pulse wave to the nozzle. Sections 2 and 3 summarize the numerical calculation results on the two new piezo-assisted-atomizer designs proposed in this study and list the advantages of using these designs over the current sprayers for such applications.

Chapter 7 concludes this study by presenting its contributions to our current knowledge and to the targeted industries. It also provides a list of potential study items for future studies.

CHAPTER 2. LITERATURE REVIEW

2.1   Overview of Inkjet Printing Technology

As mentioned in the previous chapter, inkjet technology has been considered for many different applications as the result of more recent developments related to this technology. Spray combustion, spray drying, spray cooling, spray deposition, aerosol generation, automotive coating and painting are among these potential applications. Each of these applications requires a very distinct set of droplet characteristics such as droplet size, generation frequency and spatial distribution to obtain the optimum outcome. Inkjet printing technology provides a number of options for achieving this ideal condition, including the ability to create controllable droplets with predetermined sizes, speeds, and orientations. However, there are many issues to be tackled along the way of using this technology in the related industries. Limiting satellite droplet occurrence and reducing the droplet sizes (A. Castrejón-Pita, Castrejón-Pita, & Martin, 2012) are two of the main issues to address. The following summarizes the current status of inkjet technology development.

2.2   Meniscus Generation and Backpressure in The Nozzle

The first problem is related to generation of backpressure in the orifice of the inkjet nozzle. Generation of a meniscus is the first step in forming and emanating the droplets and it is inevitable. However, for piezoelectric sensors driven DOD inkjet technology and depending on the working conditions of the sensors and ink refilling pressure, a negative pressure gradient can happen at the orifice of the nozzle and the meniscus would then be vacuumed inside the nozzle instead of being emanated from it.

This issue can be addressed by comparing the volume flow rate emanating from the nozzle and the ink flow rate into the chamber and was identified as the first step for an inkjet nozzle to work. To address this issue, the emanating volume rate of the nozzle is first determined and then this volume rate is implemented as the ink refilling volume rate. This can assure the inkjet nozzle to be close to the working condition range. The chamber refilling volume rate can be slightly different from the emanating volume rate of the nozzle; however, a significant difference can interrupt the performance of the nozzle.

Having a significantly lower refilling rate would cause a backpressure at the orifice of the nozzle as it causes the meniscus to transfer inside the nozzle. Unlike the first case, having a higher refilling volume rate would generate a spray instead of droplets from the nozzle and it is desirable, as the best performance would be a chain of the same size droplet without any interruption. There will be more explanations on the meniscus generation process in the following sections as it can be the cause for more issues in the droplet generation as well.

2.3   Droplet Size

The inkjet technology is growing rapidly by finding a wide range of applications as explained earlier. Targeting variety of applications requires capability of generating quality droplets with various unique properties including desired size, speed, generation frequency and mass flow rate. Some industries are experiencing extreme needs for an improved high-quality inkjet system, which necessitate a thorough understanding of the effects of all the various characters on the quality and properties of the generated droplets.

Due to a wide range of applications and with reviewing recent publications, there are two current main issues related to industrial applications of this technology. One of the most important challenges is about the desired range of size of the droplets, whose diameter can be as small as 2 µm or even below that for specific applications, for instance, in coating applications on arrays of gene chips and some microfluidic devices. A careful review of the recent literature found that the typical size of the generated droplets were nearly the size of the inkjet nozzle (Chen & Basaran, 2002), even though there have been some innovative methods proposed more recently to reduce the droplet size relative to the nozzle size. In the following, some of these studies will be explained further.

(J. Kimura, Y. Kawana, & T. Kuriyama, 1989) presented a novel enzyme immobilization method, in which an inkjet nozzle, originally designed for a printing equipment, was utilized to deposit precise enzymes into a silicon on sapphire (SOS) device. They used a nozzle with a 50 µm orifice that used a pressure pulse (wave) to increase the pressure to push the enzymes outside the nozzle and pull to help them detach it from them nozzle. They reported enzyme droplets as small as 48 µm, which is about the same size as the diameter of the nozzle orifice. (Bernardini, Rampy, Howell, Hayes, & Frederickson, 1991) investigated the potential application of inkjet technology in neurobiological research. They performed various types of experiments using the 52 µm diameter nozzle on different tissues and reported 50 µm diameter drops in their experiments. (Sakai, 2000) proposed the use of electric pulses to modulate an actuator to decrease the droplet diameter from a given inkjet nozzle. He used a nozzle with the orifice size of 32 µm in diameter and reduced the droplet diameter to 23 µm, about 70% of the orifice diameter.

Another study implementing the waveform inputs to the piezoelectric sensors was presented by (Chen & Basaran, 2002). They conducted experiments testing various voltage forms induced to the piezoelectric sensors in the inkjet nozzle to investigate their effects on the droplet size emanated from the nozzle. They used a nozzle with the orifice size of 70 µm in diameter and recorded droplets as small as 32 µm in size, which is about 45% of the nozzle diameter, the highest reductions of droplet size shown for similar cases to our study. Figure 2.1 shows the time evolution of droplet generation for their work.
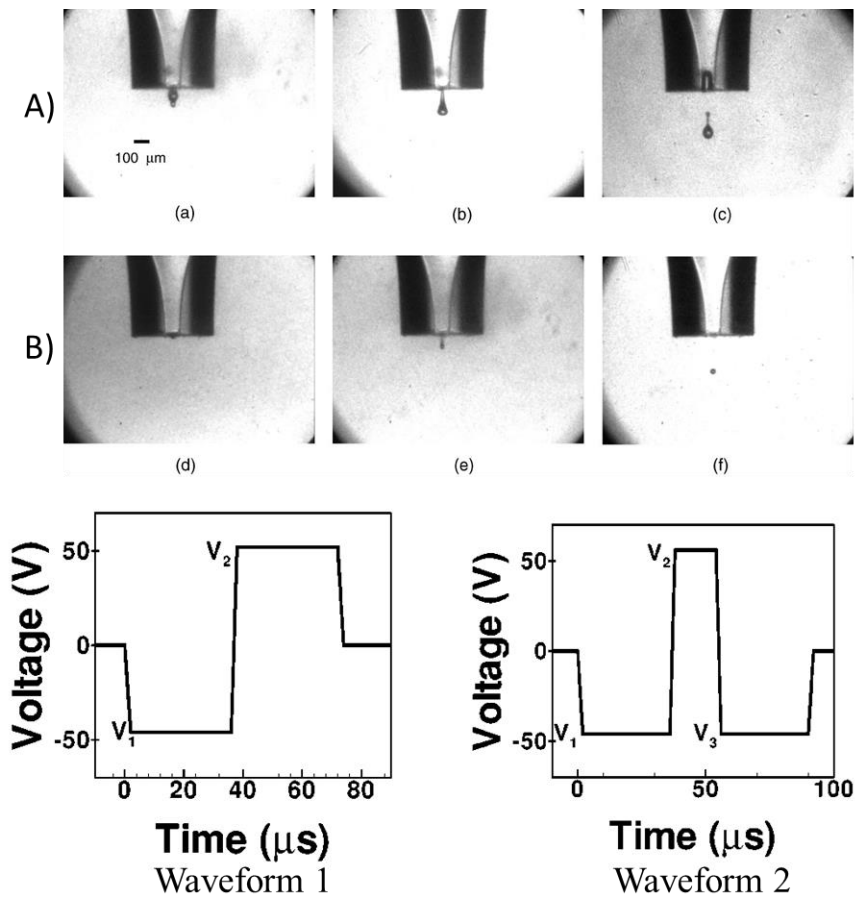
Figure 2.1 Time evolution of filament separation and droplet generation with two waveforms implemented at 84, 104, 144 ms for A) Waveform 1, B) Waveform 2, reproduced from (Chen & Basaran, 2002), with the permission of AIP Publishing.

Recently, (Poozesh, 2015) conducted CFD simulations to investigate the effects of the push-pull waveform mechanism on the characteristics of the droplets such as the droplet size and to identify the optimum waveform to produce the smallest size droplets, given a specific size inkjet nozzle. Table 2.1 summarizes all the above mentions results.

Table 2.1. Inkjet nozzle and generated droplet sizes in the recent literature

Reference	Industrial Application	Nozzle Diameter (μm)	Droplet Diameter (μm)
(J. Kimura, Y. Kawana, & T. J. B. Kuriyama, 1989)	Enzyme deposition and immobilization	50	48
(Bernardini et al., 1991)	Dispensing liquids in neurobiological research	50	52
(Brennan, 1999)	Arraying of biologically active materials	40	50
(Sziele, Brüggemann, Döring, Freitag, & Schügerl, 1994)	Injection of sample drops in capillary electrophoresis	60	60
(Perçin, Atalar, Levent Degertekin,	Dispensing (a) water (b) photoresist	(a) 60 (b) 110	(a) 50 (b) 94

& Khuri-Yakub, 1998)			
(Laurell, Wallman, Nilsson, & Microengineering, 1999)	Chromatography	60	50
(Sakai, 2000)	DOD inkjet printing	32	23
(Chen & Basaran, 2002)	DOD inkjet printing	70	32
(Gan, Shan, Eriksson, Lok, & Lam, 2009)	Polymeric inkjet printing (a) DI water (b) PEDOT	50	(a) 28 (b) 62
(A. Castrejón-Pita et al., 2012)	DOD inkjet printing	100	38

High accuracy fabrication applications such as gene cells coating require a small and high precision diameter nozzle, which requires a special equipment and facility for fabrication. In addition, the quality of the droplets generated by a small micro-scale size nozzle has exhibited slightly different behaviors with more complexity from larger diameter droplets. Many studies have attempted to generate smaller droplets without reducing the nozzle size, e.g., (A. Castrejón-Pita et al., 2012; Chen & Basaran, 2002). An innovative use of a waveform movement was suggested to produce smaller droplet sizes without reducing the nozzle diameter below a critical size. This approach can help produce

smaller size droplets by manipulating governing forces such as capillary, inertial and viscous forces and adding an instantaneous external force to the flow inside the nozzle. Implementing the waveform causes the liquid ligaments to reach the breakup diameter before reaching the nozzle orifice. The simplest force of these waveforms proposed in the literature is a combination of push-pull waveform. The potential effects of changing the waveforms have been evaluated in the more recent years in the literature. Although, the proposed designs have critical differences, they all use the same concept of making the protruded meniscus to break up before its diameter reaches the nozzle diameter.

There have been several new designs of inkjet nozzles employing amplifier and input signals using controllers (Gan et al., 2009). As it has been observed in theirs experiments, generating smaller droplets using such techniques usually accompanies with generation of satellite droplets in the process and the characteristics of the generated droplets depend only on the properties of the printhead design. An example of applying the push and pull to reduce the droplet size is using acoustic focusing method used by (Hon, Kwok, Li, & Ng, 2010). Figure 2.2 presents a schematic of filaments generated from by printheads applying these push-and-pull forms. This schematic presents a push-pull voltage applied to the nozzle head. During the push phase, a large size meniscus is formed and pushed out of the nozzle orifice. This meniscus is then separated from the orifice walls and ejected from the nozzle head during the following pull phase. Using such waveforms typically produces droplets of at least the size of the nozzle and the reason for that is that the formed meniscus develops over the push phase until it reaches the same size (sometimes even larger) as the nozzle orifice itself.
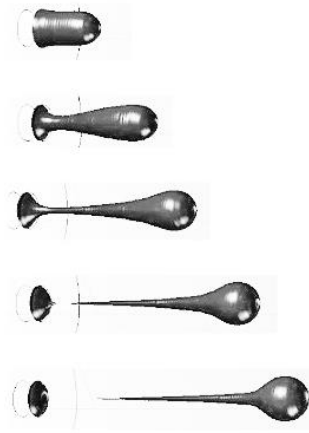
Figure 2.2 Time evolution of filament separation with a sample imposed push and pull waveform (Poozesh, 2015), reproduced with the permission of Dr. Sadegh Poozesh.

There are other methods proposed to reduce the size of droplets from a print head, e.g., a nozzle-less design. These methods are, however, highly complex and have not yet been applied in industry due to the difficulty in precision control and restriction in types of liquids to be used. Given the importance of these designs, however, many researchers have kept looking for efficient printhead designs. Castrejón-Pita et al. (A. Castrejón-Pita et al., 2012) achieved a push-and-pull-based method, capable of generating up to 40% smaller than the nozzle size, using an external jaw to transfer energy to the cavity to generate fine droplets. Figure 2.3 shows the concept of their creative design which consists of six different steps. Step (a) is steady state which is followed by steps (b) and (c) where meniscus moves into the cavity behind the nozzle. In step (d), the meniscus collapses and extends, generating a high-speed jet (step e), and finally at step (f) this jet breaks up forming a single small droplet.
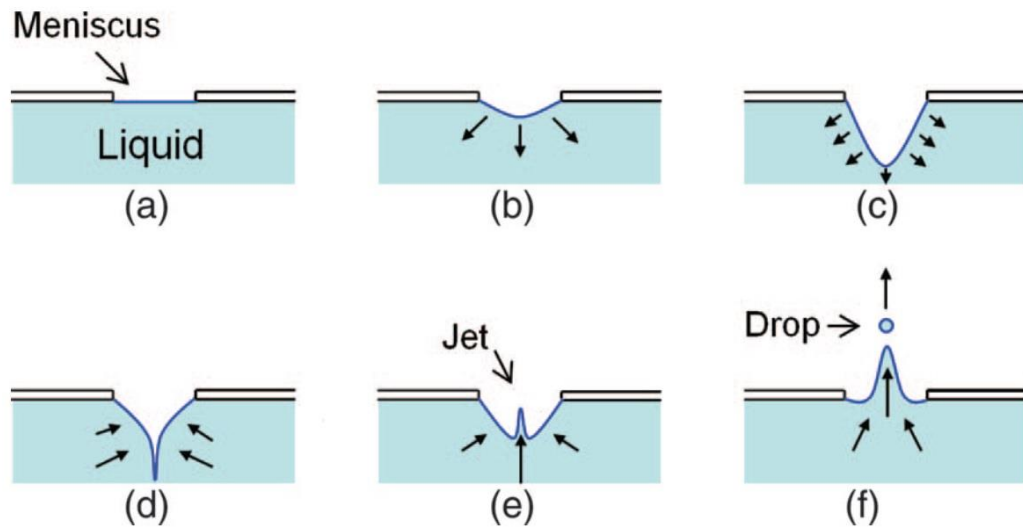
Figure 2.3. Principle for jetting: (a) steady state, (b) and (c) meniscus moves into the cavity behind the nozzle, (d) fast collapse of the extended meniscus, (e) a high speed jet is formed, and (f) under the proper conditions, this jet breaks up and a single small droplet is formed, reproduced from (A. Castrejón-Pita et al., 2012), with the permission of AIP Publishing.

Although progress has been made mostly based on the above-mentioned experimental studies, there are only a few numerical studies to fully target the issues brought up before.

Numerical models, when they are validated by proper experiments (Hollister et al., 2005), become a unique, effective and efficient tool to design a new droplet generator, test its performance, and optimize the design. Numerical modeling is an effective way to obtain detailed data on new designs and their performance. Here, the numerical model developed by (Poozesh, 2015) is applied to examine the effects of various factors on lowering the

droplet sizes to obtain the optimized working conditions. Figure 2.4 shows a schematic of the mechanism proposed here, adopted from (Poozesh, 2015).
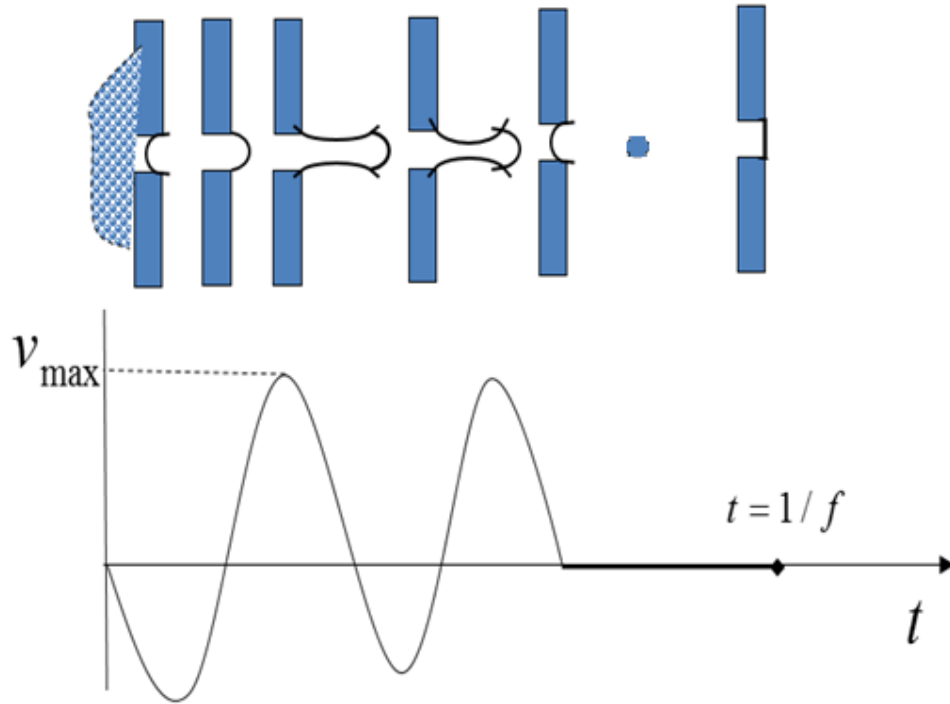
Figure 2.4 A sinusoid function mechanism proposed by (Poozesh, 2015) which provided the baseline mechanism for the current study, reproduced with the permission of Dr. Sadegh Poozesh.

2.4   Satellite Droplet Generation

Satellite droplets are smaller size auxiliary drops following the main drops generated from the nozzle of the inkjets. Satellite drops are undesirable as their characteristics are not controllable. They can move in undesired or random directions, drastically reducing the quality of printing. These drops are an undesired by-product generated during the process of the ligament formation and its break-up phase. Some studies suggest the process of ligament formation and its breakup from the nozzle as the

reason for the formation of satellite droplets, which can be further clarified by comparing

the kinetic energy of the filament formed outside the orifice with the energy that is needed

to overcome the surface tension energy. It is important to reduce the possibility of

generation of these satellite droplets, but it is also difficult to do so because the physical

characteristics of the nozzle, its input conditions, and the liquid properties all influence the

formation of these drops. As of today, although a lot of effort was made to reveal the root

cause mechanism on the formation of satellite droplets, it still remains unknown.

Figure 2.5 presents four photographs of an evolution of a typical liquid filament

formed outside a DOD inkjet nozzle orifice. It shows the characteristic elongated tail and

the satellite droplet formation.
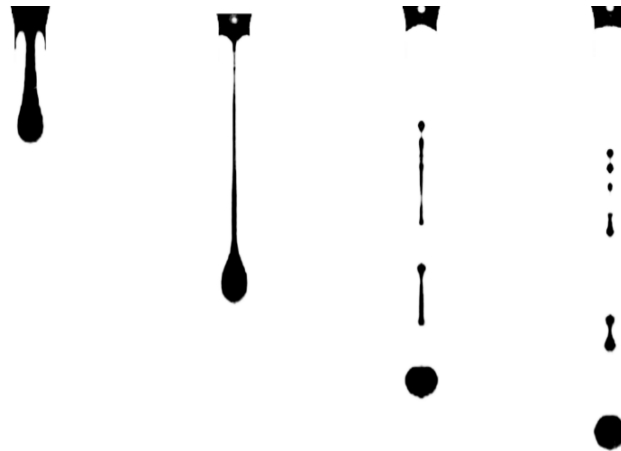
Figure 2.5 Evolution of a typical liquid filament formed outside a DOD inkjet nozzle
orifice, showing the characteristic elongated tail and the satellite droplet
formation, adopted from (Poozesh, 2015), reproduced with the permission of Dr.
Sadegh Poozesh.

Figure 2.6 schematically compares an ideal single droplet formation process with

an undesired satellite droplet formation. Figure 2.6 (a) shows single droplet formation

where the liquid thread forms an almost spherical droplet without breakup, and Figure 2.6

(b) shows a primary droplet accompanied by a satellite droplet. Figure 2.6 presents two modes of generating satellite droplets that are more commonly observed from similar systems. The satellite droplets formed in the process (a) will usually be absorbed back to the primary droplets very quickly, while satellite droplets formed in the form of (b) are, however, undesired droplets with random speed and trajectory and stay unmerged.
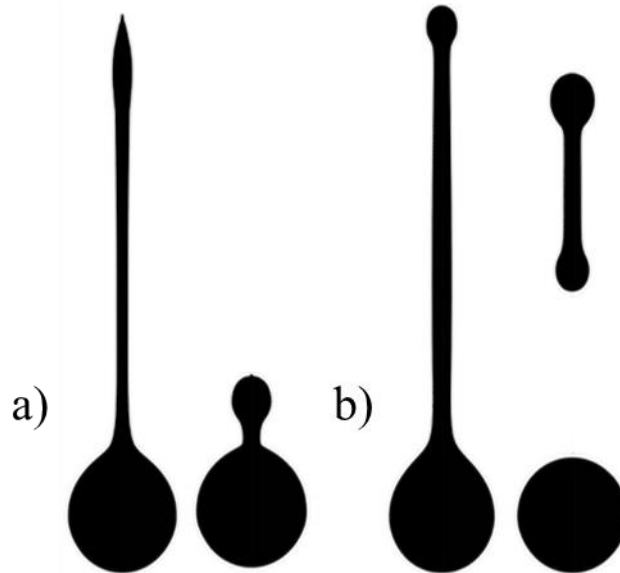
Figure 2.6 (a) Single droplet formation where the liquid thread form an almost spherical droplet without breakup, and (b) A primary droplet accompanying with a satellite droplet (Poozesh, 2015), reproduced with the permission of Dr. Sadegh Poozesh.

There is rich literature devoted to better understanding of the ligament breakup procedure and formation of undesired satellite droplets. Some divided the entire satellite formation process into several different regimes and studied mechanisms specific to each of these different regimes. Key studies on the formation of satellite droplets and liquid ligament breakup are summarized in the following.

(Fromm, 1982) studied filament breakup mechanisms and explained the dynamics of droplet formation process from a droplet-on-demand nozzle using a marker-and-cell

method. (Eggers & Dupont, 1994) solved a one-dimensional slender-jet equation system to theoretically investigate the liquid breakup process. (Shi, Brenner, & Nagel, 1994) solved, with a primary focus on the liquid breakup exactly at the time of filament pinch-off, a system of one-dimensional equations to theoretically investigate the generation and pinch-off of low viscosity drops. (D. Zhang & Stone, 1997) investigated, with the boundary element method (BEM), the droplet formation process in Stokes flow into a viscous ambient fluid and found that the length of droplets at the breakup stage increased significantly with an increase in the ratio of droplets' viscosity to the external fluid's viscosity.

Hauser and Edgerton (Edgerton, Hauser, & Tucker, 1937; Hauser, Edgerton, Holt, & Cox Jr, 2002) were among the first few to find the governing physical laws that control the formation of satellite droplets. They conducted a series of various experiments to study the formation of the primary and satellite droplets using high-speed photography and reported the exact shape of the satellite droplets which were formed during the entire process. (X. Zhang & Basaran, 1995) investigated, with high-speed photography, the formation and behavior of primary and satellite droplets of a solution of glycerol and water to find the effect of the liquid flow rate and tube radius on the capillary tube. (Henderson, Pritchard, & Smolka, 1997) observed the detailed process of droplets' pinch-off in a high viscous fluid placed in a capillary tube, for both the primary and satellite droplets. (Dong, Carr, & Morris, 2006) studied the dynamics of droplet generation from a DOD inkjet nozzle using piezoelectric sensors. They investigated the effects of various factors such as viscosity of the working liquid and surface tension on the quality of the drops and performance of the nozzle head. They observed two separate modes of liquid breakup from

the process; When the liquid thread formed a nearly spherical droplet without breaking apart, single droplet was produced, and multiple breakups occurred when the primary droplet was followed by one or more satellite droplets. Further study is, however, required to clarify the role of viscosity and surface tension on the formation of satellite droplets.

The computational methods have also been extensively applied to study the formation mechanism of satellite droplets. (Gueyffier, Li, Nadim, Scardovelli, & Zaleski, 1999) developed a three-dimensional simulation based on volume-of-fluids method (VOF) to predict the dynamics of satellite droplets formation from similar nozzle. (X. Zhang, 1999) employed volume-of-fluids model to study the growth and breakup dynamics of pendant droplets into air ambient. He reported a critical liquid flow rate after which droplets did not form. (J. Castrejón-Pita, Morrison, Harlen, Martin, & Hutchings, 2011) conducted a small-scale experiment to produce on-demand droplets from an inkjet-nozzle-based system and simulated the performance of a large-scale DOD inkjet printing system using a shadowgraph technique. They further developed an in-house numerical model based on the Lagrangian finite-element method to study the same system. Their numerical model was validated against experiments and became a benchmark model for studying similar systems. Their results did not match with the full-scale experimental results, however, possibly because they disregarded the effects of gravity which might influence on the full-scale droplets. (Kim & Baek, 2012) studied the same system numerically and presented a jetting behavior diagram identifying different liquid breakup regimes to predict the performance of the nozzle based on dimensionless groups, the Oh, We and Ca numbers. (A. Castrejón-Pita et al., 2012; Castrejon-Pita, Castrejon-Pita, & Hutchings, 2012) provided the necessary conditions for the liquid ligament to breakup into droplets based on

their experimental data and in terms of two dimensionless π numbers of aspect ratio and Ohnesorge number. (Poozesh et al., 2015; Poozesh et al., 2016) developed numerical models based on volume-of-fluids method to predict the performance of droplet-on-demand nozzles based on non-dimensional numbers, We, Oh, Re, Ca and Ω (a non-dimensional number developed based on pulsation frequency). They provided extensive regime maps identifying the droplet formation mechanism from the nozzle based on these non-dimensional numbers and presented a novel mechanism to better control the breakup mechanism and the size of generated droplets.

2.5 Role of Scaling Analysis Study in This Field

Before proceeding to explain about the mathematical formulations and numerical methodologies, it is noteworthy to provide some information about one of the most significant tools at hand for investigating effective factors on liquid ligament disintegration process. Scaling analysis helps us to identify the major governing forces which control liquid jet disintegration and droplet formation. The traditional experimental approach in scale modeling is to design scale model experiments to validate assumptions based on which scaling laws were developed (Emori et al., 2000; Kozo Saito, 2008; K Saito & Williams, 2015). Due to the difficulty associated with precision-controlled physical experiments of inkjet droplet flow dynamics, it would be of a great help if numerical experiments can substitute or supplement the physical experiment in the production of fine liquid droplets.

(Antonopoulou, Harlen, Walkley, & Kapur, 2020; Masoud Arabghahestani et al., 2021; Kim & Baek, 2012; Poozesh et al., 2015; Poozesh et al., 2016) conducted numerical modeling with dimensional analysis to understand and predict the performance of nozzles.

(K Kuwana, Hassan, Singh, Saito, & Nakagawa, 2008) applied a combined approach of scale and numerical modeling to solve problems associated with the steel teeming process, (Ghosh, Rezaee, Honaker, & Saito, 2015) took the combined approach in solving coal mining safety problems, and (Kumar et al., 2020) on developing a new device to capture fine coal particles. (Nakamura, Yamashita, & Saito, 2006) also conducted numerical scale modeling over micro-diffusion flames.

Employing scaling analysis techniques combined with numerical experiments has merits over scale model experiments alone regarding time and consistency. Numerical modeling itself also has limitations associated with assumptions employed for governing equations that the numerical model uses, whether they can correctly represent physical process of the phenomena of concern or not. Physical experiments, however, no matter how simple they are, are irreplaceable by numerical models (Kazunori Kuwana, Sekimoto, Saito, & Williams, 2008). A direct presentation of nature is only possible by physical experiments, through which observers may access the secret mystery of nature by their direct observations. As to the role of experiments, it is noteworthy to mention that Poozesh (Poozesh, 2021) recently addressed the emergence and surge of data-driven modeling as a new opportunity to leverage experimental data in model development, in comparison to the traditional first-principle-based scale modeling, which attempts to find pi-numbers made up of physical forces and energies that govern the phenomenon of concern and proper correlations among pi-numbers. The law approach (Emori et al., 2000) is available to accomplish the first aim, while scale model experiments achieve the second aim. His mention of data-driven modeling, such as artificial intelligence, can be added as a new tool to scale modeling.

There are four main dimensionless numbers known to contribute to the performance of the nozzle using Newtonian working fluids. They are the Re, We, Ca, and Oh, each defined as follows.

$$Re = \frac{Inertial\ forces}{Viscous\ forces} = \frac{\rho U R}{\mu}$$

$$We = \frac{Inertial\ forces}{Surface\ Tension\ forces} = \frac{\rho U^2 R}{\sigma}$$

$$Ca = \frac{Viscous\ drag\ forces}{Surface\ Tension\ forces} = \frac{\mu U}{\sigma}$$

$$Oh = \frac{Viscos\ forces}{\sqrt{(Inertial\ \times\ Surface\ Tension)forces}} = \frac{\mu}{\sqrt{\rho R \sigma}}$$

(2-1)

Where, ρ is the density of the liquid flow (kg/m3), U is the inlet velocity of the liquid flow (m/s) (characteristic velocity chosen in this work), R is the nozzle radius (m) (characteristic length chosen in this work) and σ is the surface tension of the liquid flow (N/m). Note that the shaping air velocity is also important to determine the performance of the nozzle. However, since the inkjet designs proposed in this work operates using more complicated designs, there will be a need for more dimensionless numbers to account for extra forces affecting the performance of the nozzle design. There will be a more detailed scaling analysis presented in the next chapters of this dissertation to explain more about the scaling analysis conducted in this work. This dissertation uses a detailed and modified scaling analysis to study the effects of the influential factors on the characteristics of the droplets generated from the inkjet nozzle and to provide general jetting behavior diagrams to predict the performance of the nozzle based on the operating conditions, geometrical properties and the liquid properties.

2.6   Closure

Chapter 2 conducted a thorough literature review on the inkjet technology, the fundamental mechanisms affecting the liquid jet disintegration process, and the most critical issues associated with the liquid jet breakup and droplet formation process. This literature review revealed no single general mechanism which is solely responsible for the droplet formation process including both the main and satellite droplets. There are multiple forces which are simultaneously affecting the process of producing the quality droplets, complicating the process of droplet formation. Typical forces identified include: the inertial force of fluids (both the working liquid and air), the viscous forces of air and liquids, the surface tension forces of liquids, and the static and dynamic pressure forces (Masoud Arabghahestani et al., 2021). The current study also offers detailed jetting behavior diagrams to predict the performance of the nozzle more accurately based on the governing forces in this mechanism.

CHAPTER 3. DESIGNING VARIOUS NOZZLES

3.1   Introduction

The paint spray cycle process of an automobile can be complicated depending on the final design of the painting, while relatively simple visualizations available in literature can assist our understanding, e.g., Figure 3.1, a schematic of cross section of a typical automobile spray booth and painting process (A. J. Salazar, 2013). The cross-section dimension of automobile paint booth varies depending on the type of vehicles, large and small and automobile manufacturers' preference, but a typical dimension for painting midsize passenger vehicles is: 10 m height x 6.5 m width. The typical paint booth consists of air supply plenum which provides a downward flow of well-regulated temperature and humidity-controlled air. This air will be first filtered to remove all types of contaminants before it enters to the upper paint booth section through an air inlet section which provides uniform two-dimensional downward flow with the average approximate velocity of 1 m/s. Supply of a well-aligned downward airflow to the upper section affects the trajectory of sprayed paint particles and paint transfer efficiency; if the downward airflow is not well-regulated, the trajectory of paint particles toward the target will fluctuate causing an unfavored painted surface quality. At the paint booth upper section, the following process will take place.
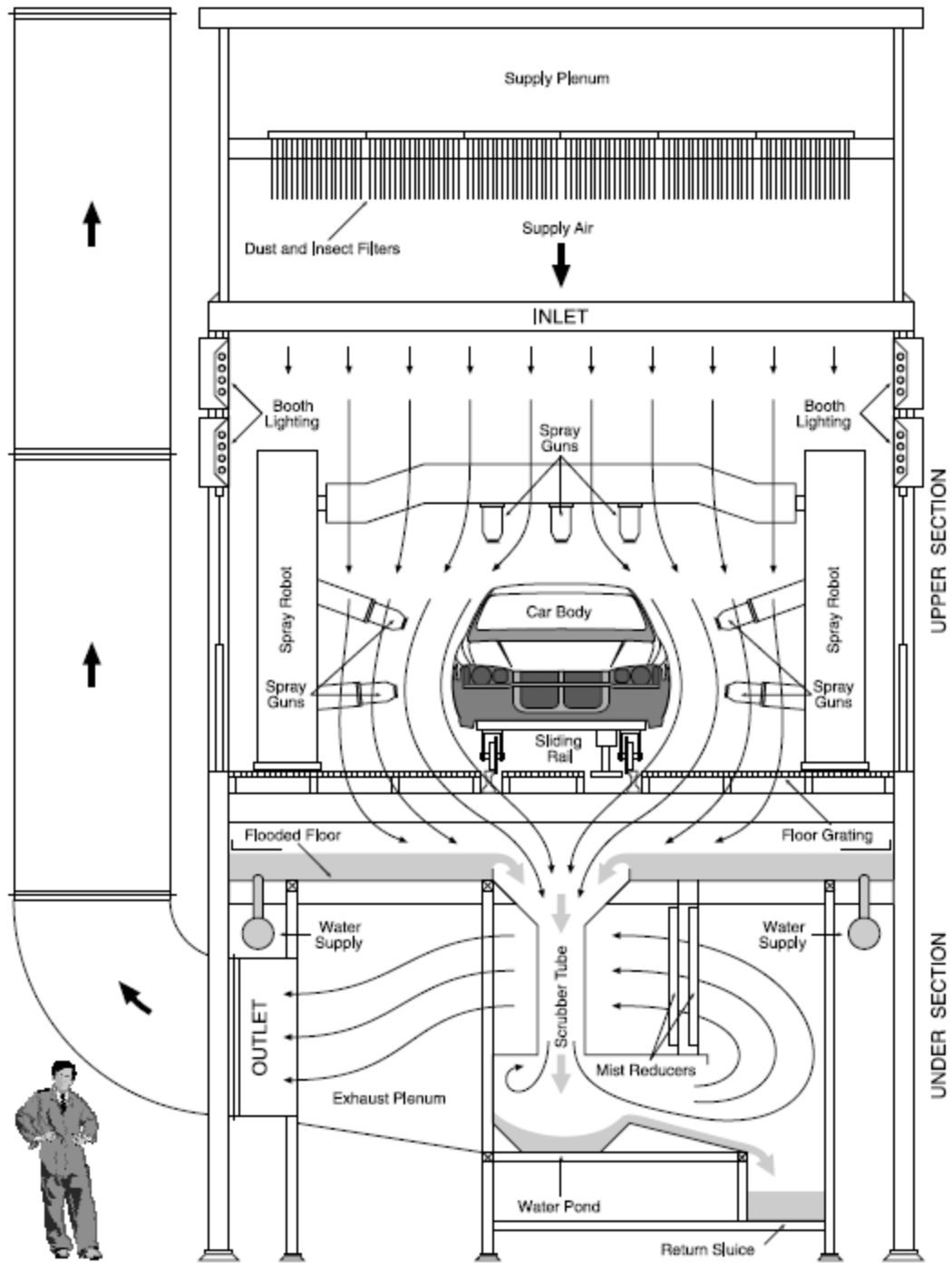
Figure 3.1 Schematic of a typical automobile spray booth and painting process, reprinted/adapted by permission from Springer Nature: (A. J. Salazar, 2013).

After atomizing the liquid (paint) by the chosen atomizer, the droplets are transferred towards the targeted part of the vehicle, however, only a portion of the droplets can reach the target successfully and coat that. This portion can be quantified with the so-called variable Transfer Efficiency (TE), which is defined as the ratio of the amount paint droplets that coats the targeted vehicle (after decomposing on the vehicle) over the total amount of paint that needs to be supplied to the chosen atomizer in order to achieve the complete process.

There have been many efforts devoted to improving this number to optimize the process and reduce the cost and chemical pollutions from the process, however the typical percentage for transfer efficiency is reported to be only 50 to 60 percent (Fettis, 2008), which is relatively a low number. Having this relatively low number for TE has been a significant issue in automobile industries since it makes the coating process more expensive and time consuming. In addition, low transfer efficiency is a health and environmental concern since it has detrimental effects over time on both workers' health and environment. Surveys show that improving the TE can save millions of dollars in cost for the coating industries in the cost of paint, utilities, equipment, and material usage. To have a better perspective about this, for example, the United States had close to two million vehicles exported in 2018. Knowing the percentage of the chemical waste and the cost, such low numbers for the TE can add a significant and unnecessary expense to this industry in some of the most developed countries. A simple conservative estimate on the waste of paint material only is roughly $100 for each vehicle production, where TE = 60 % for all three different (primer, top and clear) coating is assumed. It suggests a total of $200M paint material waste for the year 2018 only. Interestingly, this estimate does not include other

expenses which are necessary to capture and treat the waste paint and contaminated air, and the initial capital investment for facility and equipment (Toda et al., 2012). If the above additional waste is included in the calculation, the coast associated with the total waste will be much higher.

In addition, it can also reduce the organic compounds emission as the result of long coating processes. There have been efforts to alleviate this problem and some of them from the literature have been included in the following. One of the methods to improve the transfer efficiency is by implementing the surface modification techniques. (Carrino, Moroni, & Polini, 2002) studied the possible effects of cold plasma parameters and electrical discharge on the polymeric surface's adhesion and wettability. By implementing this technique, they achieved an optimized polymeric surface adhesion with changing the characteristics of discharge treatment process. (Conner, Atkar, Rizzi, & Choset, 2002; Conner et al., 2005; Shirinzadeh et al., 2007) investigated the painting and droplets trajectories emanating from gun sprays and the effects of various parameters on deposition of painting with uniform thickness all over the targeted substrate.

There are various factors identified affecting the transfer efficiency of the coating process depending on the type of atomizer being used in the process and some of them are mentioned in the following (I. Lee, Kim, Koo, & Sprays, 2012). Liquid coating characteristics, spray booth conditions such as temperature and humidity, the type of atomizer being used and the target surface characteristics such as the geometry, surface roughness and its distance to the atomizer. Overall, when the transfer efficiency is not close to 100 percent, there will be a substantial amount of chemical compounds left each time at the end of the coating process and that needs to be treated to avoid pollution and

contamination in the environment. The process of using extra paint in the system is called overspray and the amount of extra paint that can be successfully captured at the end of process is called overspray capturing efficiency. Capturing as much overspray paint as possible is fundamentally necessary for the environment, however the energy required to do that is substantial and is another possible issue in the coating process to tackle in the future. To summarize this, capturing as much overspray paint as possible with the least amount of energy usage is preferred in the coating procedure.

This chapter presents the main three inkjet designs as a precision painting and coating technology for the future with nearly 100% TE. The ideas and concepts for these inkjet designs are generated to overcome the current most urgent challenges and needs, the low TE, non-uniform droplet generation and not providing an on-demand setup for generating the droplets at-will.

3.2   Ultrasonic Pulsation Atomizer (UPA)

The first model that was used in this study is an Ultrasonic Pulsation Atomizer (UPA) that uses sinusoidal waveforms in its working liquid inlet. Figure 3.2 presents an isometric view of the conceptual UPA inkjet model employed in this work and Figure 3.3 details how this model operates. In short, the working liquid (e.g. waterborne paint) is introduced to the nozzle using a constant pressure paint chamber and is pushed towards the nozzle orifice using an external force that could be introduced from an actuator or a membrane. The paint will then be under the influence of the shear force due to presence of the shaping air stream and the shear duct helps to keep this shear force for longer periods of time so that the liquid breakup process is completed. Different parts of this atomizer are named in these figures as well for having a better understanding of different components and the

procedure of generating droplets. UPA atomizer consists of a liquid injection nozzle, liquid

flow inlet and a co-flow air inlet and a shear duct to direct the flow towards the target.

Sinusoidal wavelength inputs are employed as the pulsation form to the liquid flow at the

inlet. Droplets are carried by the air to the targeted substrate.
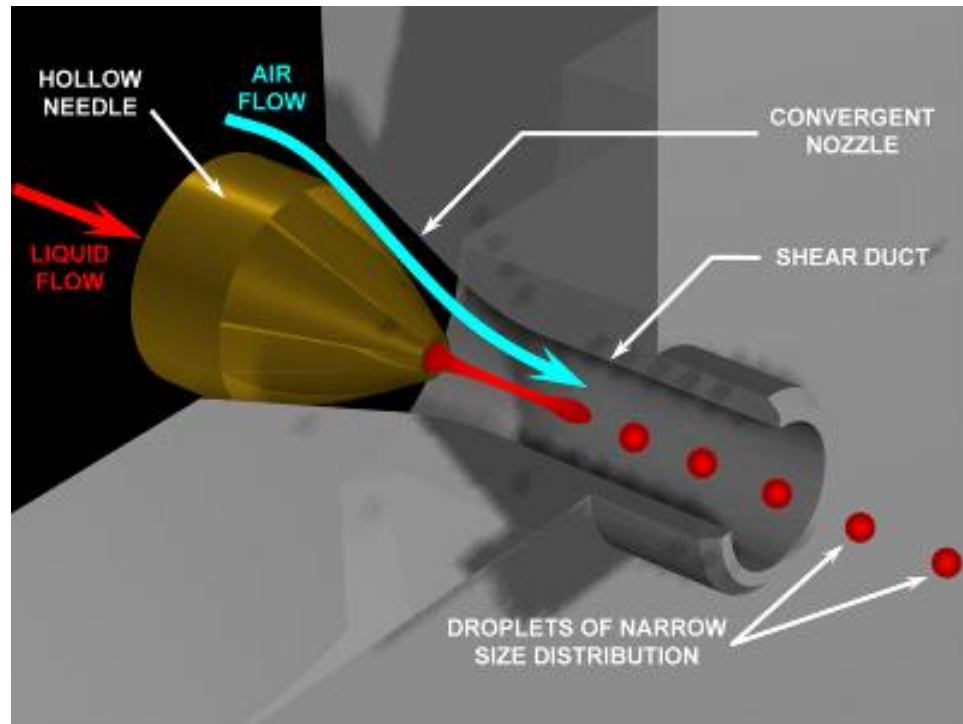
Figure 3.2 Isometric view of the UPA working concept. A continuous liquid flow was
provided at the liquid inlet shown on the left-hand side with solid red arrow and
air was provided through an annular area surrounding the circular nozzle to
stabilize the production process of well-regulated droplets coming out from the
outlet of the nozzle on the right-hand side of UPA. The diameter and length of
shear duct attached to the hollow needle can be determined based on the type of
liquid, velocity of the droplet and the airflow rate to optimize the steady flow of
quality droplet generation at the end. For more details, see (Salazar, A. J. Saito,
K., 2008; Arabghahestani, M., Akafuah, N. K., & Saito, K., 2021), reproduced
with the permission of Dr. Kozo Saito.
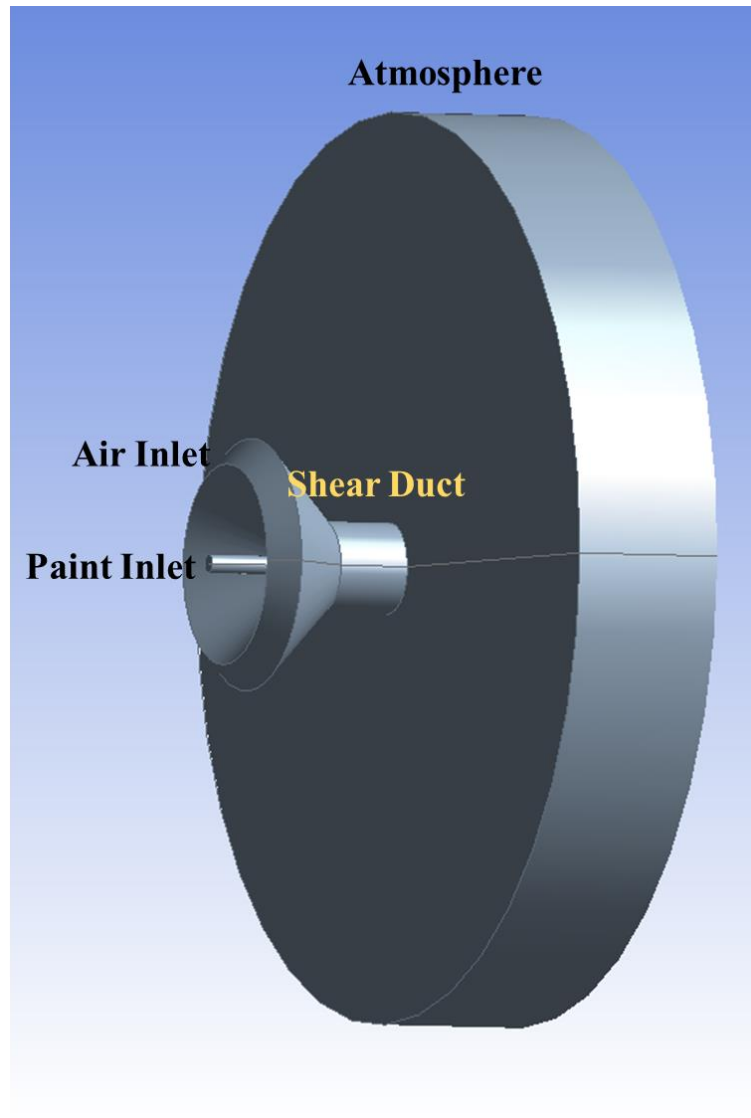
Figure 3.3 Isometric 3-dimentional view of the ultrasonic pulsation atomizer domain employed in the present study.

Figure 3.4 presents the detailed dimensions of the UPA printhead domain that is used in this study. Note that this figure presents the domain around the printhead as well and not only the printhead.
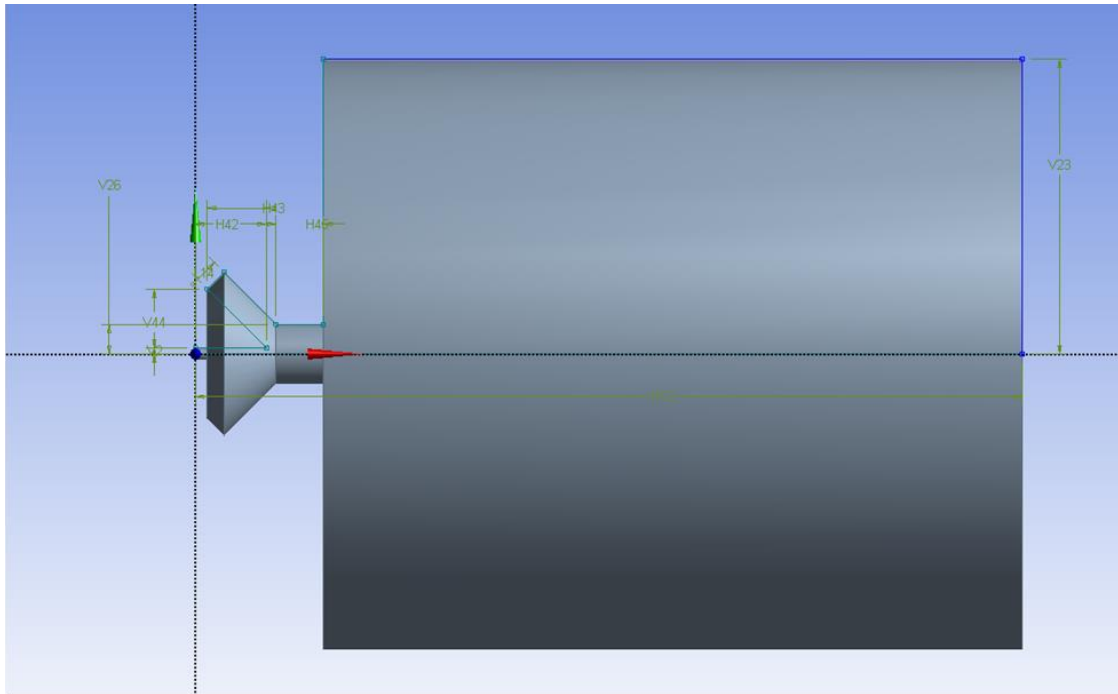
H12 = 3.5mm	H42= 0.3mm	H43 = 0.25mm	H45 = 0.2mm
L14 = 0.1mm	V2 = 0.025mm	V44 = 0.25mm	V26 = 0.125mm
V23=1.25mm			

Figure 3.4 Design dimensions of the UPA Printhead domain.

This simple design can provide precision control over the characteristics of the droplets, given the right inlet conditions. It provides a benchmark for the future printheads using the scaling analysis tools to scale the results. Figure 3.5 shows the working concept of the new UPA printhead which is expected to satisfy the following characteristics: droplets whose diameter is precisely controlled, e.g. 50 - 100 μm, can travel in a straight line for a minimum of 2.5 mm to a target surface and are able to hit the same target with high precision (any variation should not exceed half a diameter of the droplet). It is expected to precisely control the droplet frequency, number, and spacing as well.
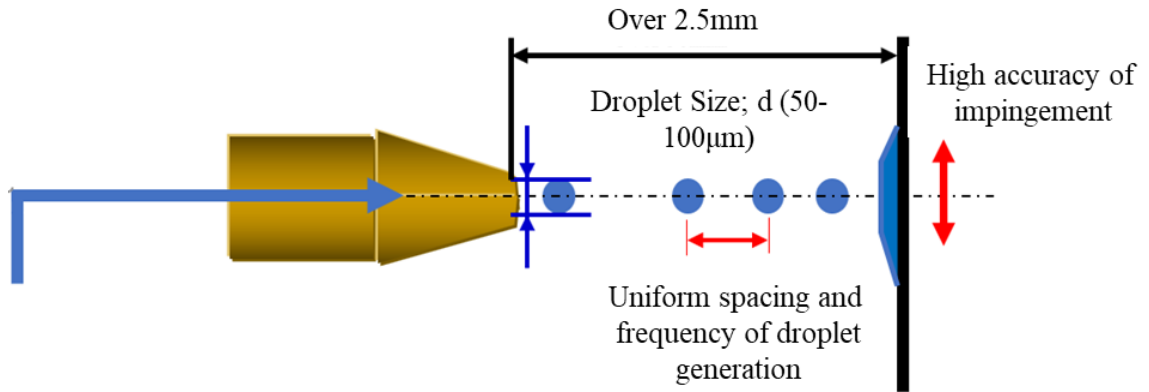
Figure 3.5 The working concept of the new UPA printhead.

3.3 Single-Piezo-Driven (SPD-DOD) Inkjet Printhead

The second model shares some similarity with that of (Poozesh, 2015) which worked well with low viscosity fluids but not for high viscosity working fluids. Therefore, this study focused on the improvement of single-piezo-driven DOD inkjet printhead for high viscosity fluids. Figure 3.6 (a) shows isometric 3-dimentional view of the single-piezo-driven inkjet printhead and Figure 3.6 (b) the XY planar view of the single-piezo-driven inkjet printhead, which is adopted from (Poozesh, 2015). Figure 3.7 presents an isometric exploded view of the single-piezo-driven DOD Inkjet printhead, also adopted from (Poozesh, 2015). There is a total of seven different key parts shown there; each of them plays a different role to properly operate this atomizer. They are: (1) an air chamber, (2) a liquid chamber, (3) a spray base that acts as a connector of the two chambers and provides the mount for other components, (4) a liquid nozzle to supply the liquid, (5) an air nozzle to supply the air, (6) a piezoelectric transducer and (7) a small shear duct to direct the flow towards the target.

49

To move the liquid towards the liquid nozzle, sinusoidal wavelength inputs are employed as pulsation to the liquid flow using the piezoelectric transducer. The droplets are then carried by the air to the targeted substrate. Note that each design carries unique name to distinguish it from other designs employed in this study.
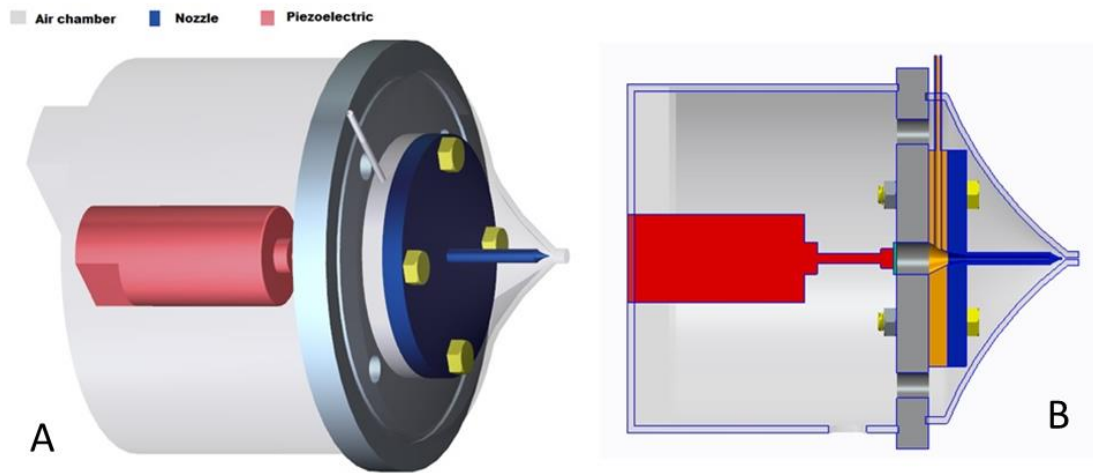
Figure 3.6 (a) Isometric 3-dimentional view of the Single-Piezo-Driven inkjet printhead and (b) the XY planar view of the Single-Piezo-Driven inkjet printhead, adopted from (Poozesh, 2015), reproduced with the permission of Dr. Sadegh Poozesh.
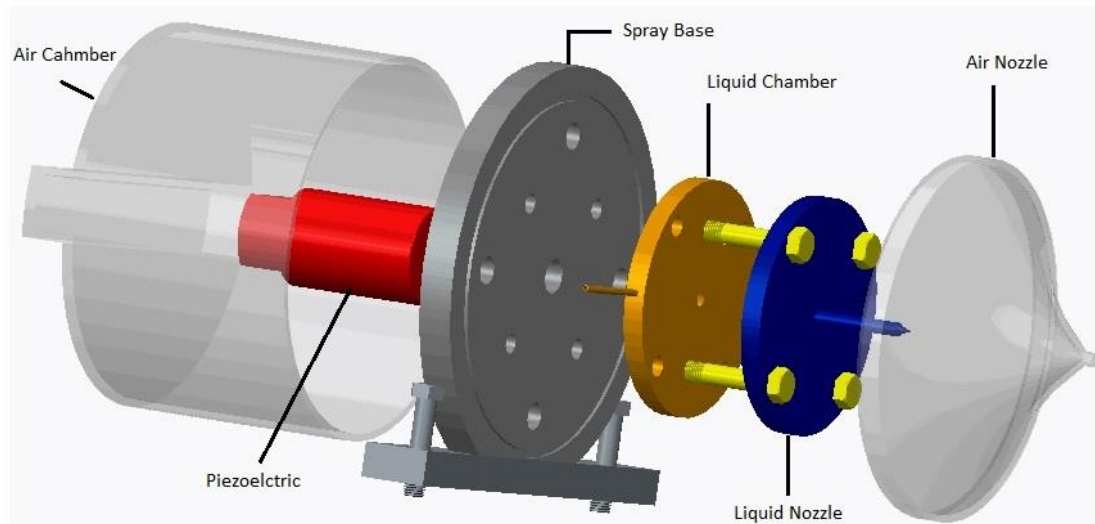
Figure 3.7 Isometric exploded view of the Single-Piezo-Driven DOD inkjet printhead, adopted from (Poozesh, 2015), reproduced with the permission of Dr. Sadegh Poozesh.

Figure 3.8 presents detail dimensions of the main components of single-piezo-driven (SPD-DOD) inkjet printhead. Detail dimensions are provided there to help production of this inkjet printhead. Good design that helps effective and precision manufacturing, known as design for manufacturability, may be of interest to researchers and engineers. The top and front view of the nozzle and air nozzle shown below can assist in the production of this type of nozzle, however, no details on manufacturing methods, e.g., precision laser-cutting, mechanical drilling, chemical edging, etc. were provided, since the issue goes beyond the scope of this dissertation.

Air Chamber

1.1 O_THICK

8

42.7

6.5

SECTION A-A

22.3

Ø 55

A   A

Ø 6

Piezoelctric

5.1

2

6.5

28

2

R0.3

10

2

SECTION A-A

Ø 14

Ø 5

Ø 1.5

A   A

Ø 3

Spray Base

0.5

5

SECTION A-A

Ø 5

(4x) Ø 3

20

10

A   A

(4x) Ø 4

Ø 50

20   10

Ø 60

Liquid Chamber

3

2.5   SECTION A-A

Ø 1

15

0.1 THICK

(4X) Ø 3

A   A

10

1

10

Dimensions in mm

52
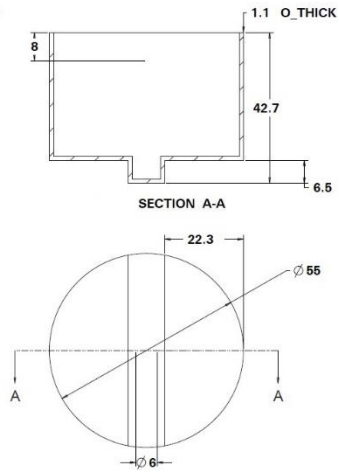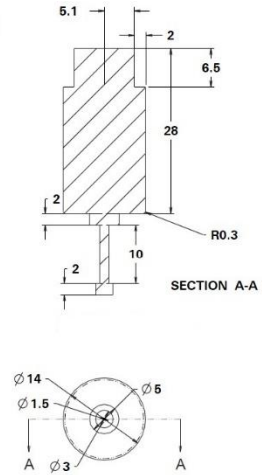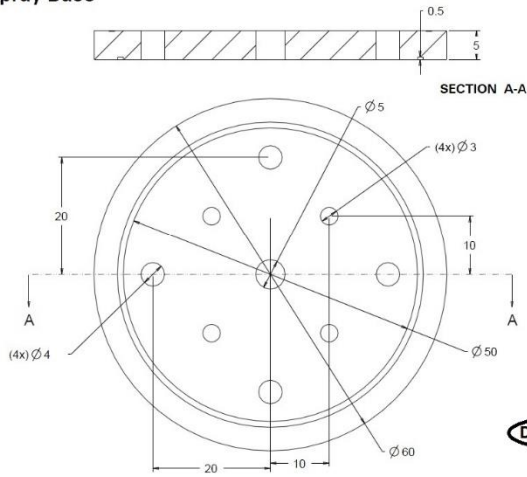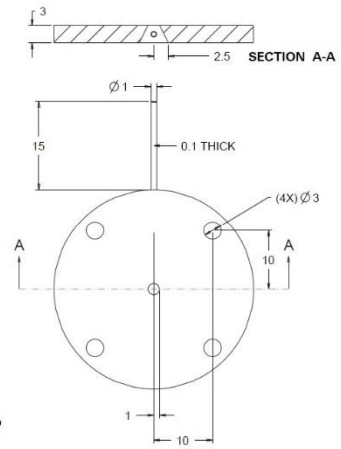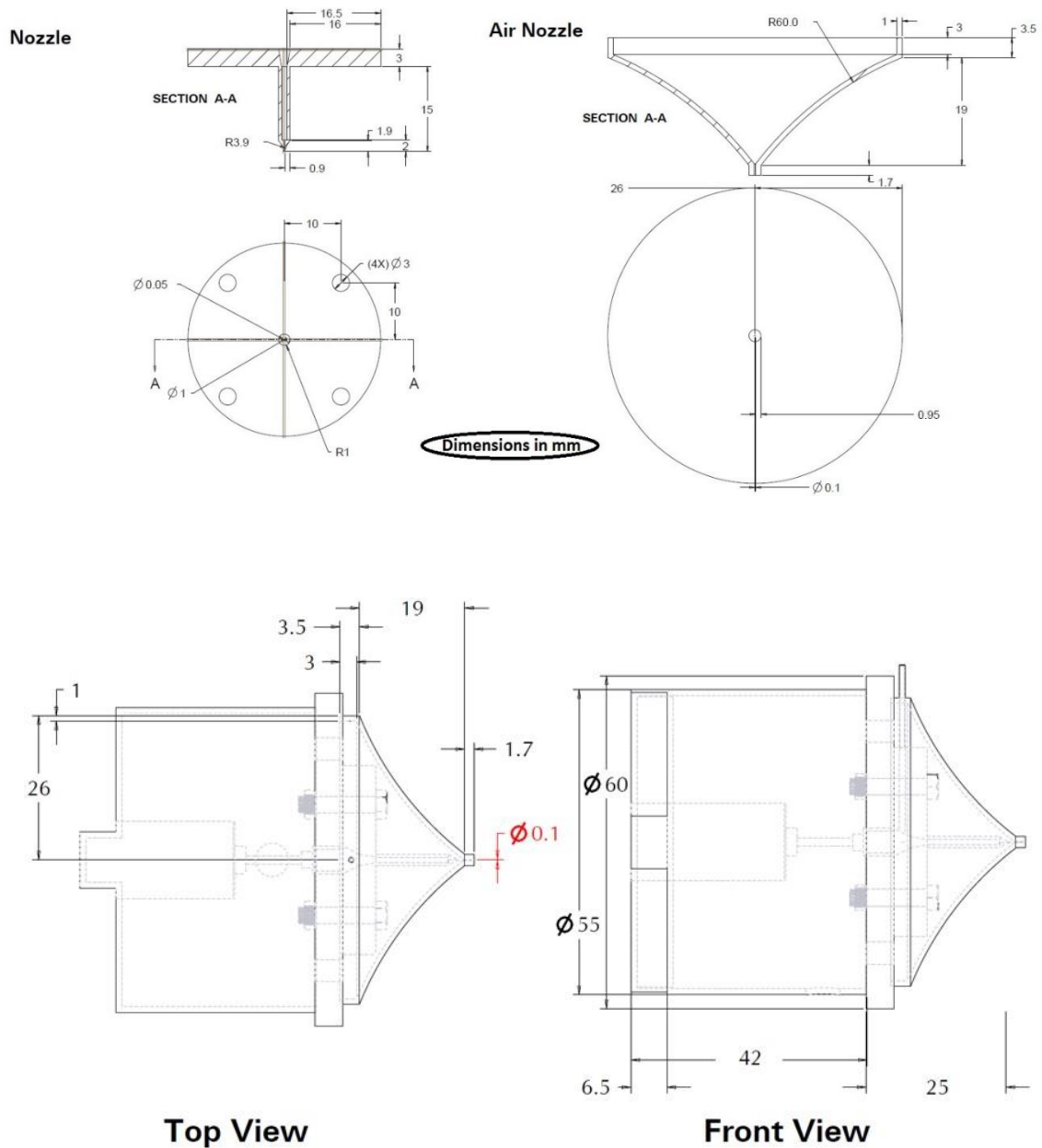
Figure 3.8 Components and their dimensions of the Single-Piezo-Driven (SPD-DOD) Inkjet Printhead, adopted from (Poozesh, 2015), reproduced with the permission of Dr. Sadegh Poozesh.

Figure 3.9 shows the working concept of the new SPD-DOD inkjet printhead. This new (SPD-DOD) inkjet printhead prototype is expected to satisfy the following specific characteristics: (1) droplets travel in a straight line for a minimum of 50 mm to a target

surface, (2) precisely control the droplet size, e.g. 25 - 100 μm, (3) a precision hitting of the target with high accuracy of half a diameter of the droplet, and finally (4) a precision control of the droplet frequency, number, and spacing.
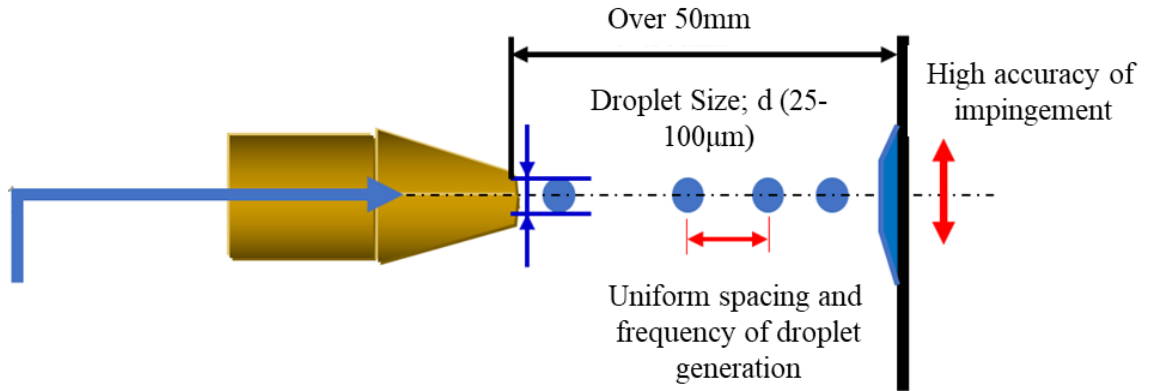
Figure 3.9 The working concept of the new SPD inkjet printhead.

3.4   Double-Piezo-Driven (DPD-DOD) Inkjet Printhead

The SPD-DOD has unique painting capability as explained in the above, but it may not work well for higher viscosity working liquids (closer to those of industrial paints) due to the limited piezo-driven force. To improve this limitation, double-piezo-driven inkjet printhead is proposed.   Attempts have been made to design and fabricate a new digital paint atomizer prototype for single and multiple nozzles. The DPD-DOD atomizer is designed for non-metallic water-borne paint. The working concept of this atomizer is similar to that of the SPD inkjet shown in Figure 3.9. The new prototype should be able to achieve the following: droplets travel in a straight line for a minimum of 25 mm to a target surface, be able to precisely control the droplet size, e.g. 25 - 100 μm, should have high accuracy and precision of hitting the same position on a target surface, any variation should

not exceed half a diameter of the droplet and finally, be able to precisely control the droplet frequency, number, and spacing.

The proposed DPD-DOD digital atomizer offers color mixing capability on the surface, 2-tone painting without masking, wider custom design colors and finishes, higher controllability with higher transfer efficiency of nearly 100%, and comparable spray gun flow rate (i.e. 250-500 cc/min) by adopting 20*20 array of nozzles/orifices.

Figure 3.10 shows a partial cross-sectional schematic of the proposed sprayer, which is a modified version of a commercially available single nozzle printhead (Microfab). This system comprises of a cylindrical chamber with a dynamic outlet nozzle cap on its lower side. A nozzle plate that can be perforated to accommodate multiple orifices is mounted on the cap. The closed end of the cylinder chamber is connected to a flexible rubber membrane, which is mechanically coupled to an electromagnetic actuator. The actuator is driven by electrical pulses from a waveform generator under precise computer controls. The movable nozzle cap is also driven by a piezoelectric ceramic transducer to aggravate naturally occurring perturbation within the nozzle to promote and facilitate the breakup process. Contrary to creating unordered hydrodynamic instabilities with conventional instabilities, this DPD-DOD can produce desired droplets on demand with two major effects: the actuator pushes the liquid and simultaneously the movable cap draws liquid filament outside. This unique feature of the system results in not only producing under-controlled droplets with desired size, but also ejecting high-velocity droplets suitable for adequate penetration during coating. Worthy to note that the movable nozzle plate is changeable with other nozzle plates with more orifices.
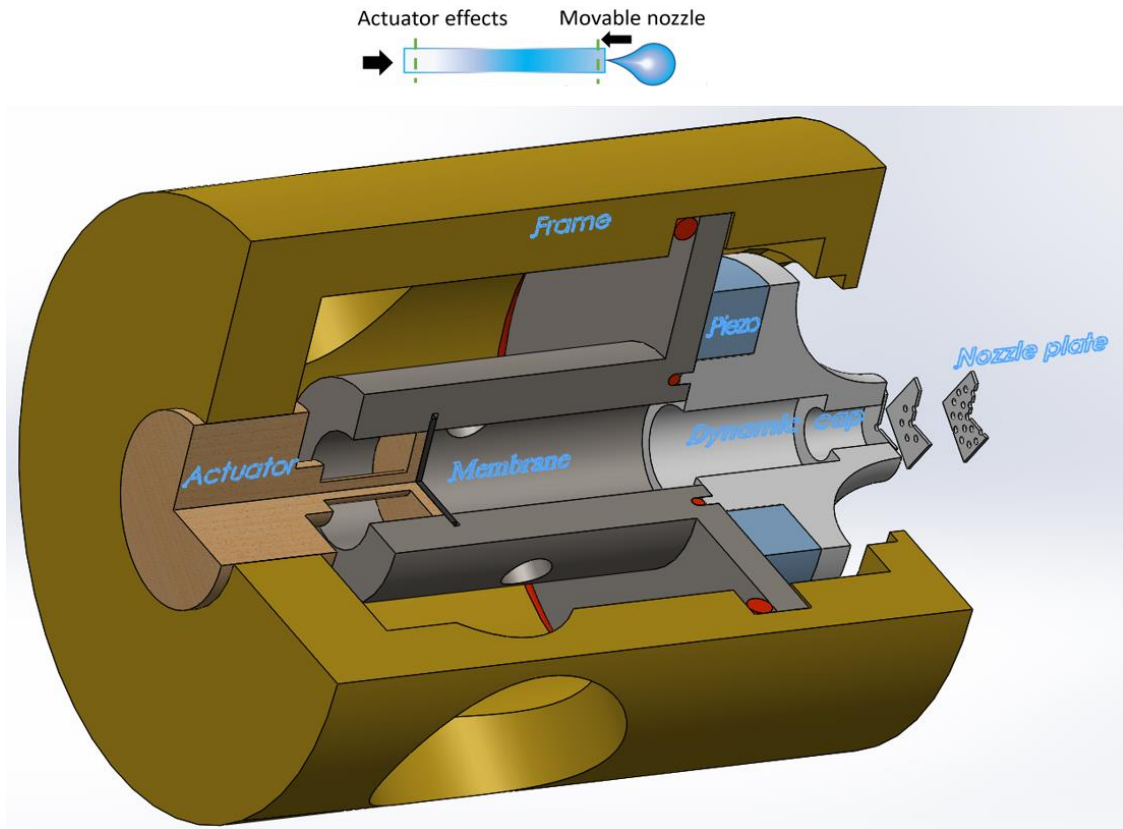
Figure 3.10 The initial CAD model of the new atomizer print head to be tested with using CFD simulations.

3.5   Closure

This chapter summarized three different inkjet printheads employed in this study. For each model, the CAD design, a list of their components and some of their main dimensions are provided for any researchers who are interested in reproducing numerical calculation results which will be presented in the later chapters. The Figure 3.10 design is expected to produce a stream of uniform quality droplets from higher viscosity working liquids (closer to those of industrial paints). This design uses two piezo electric sensors to provide the necessary instabilities and waves required to generate the droplets. The computational domains generated for each of these designs will be presented in the next chapter, where the details about the computational grid will also be presented.

CHAPTER 4. NUMERICAL METHODOLOGY

4.1   Introduction

Numerical simulations for scale modeling are designed based on scale modelling concepts introduced in the literature (Kozo Saito, 2008; K Saito & Williams, 2015; Toda et al., 2012). This combined use of numerical simulations and scale modeling was used to investigate details in the droplet atomization process. It will also help studies on the performance of the new designs and improve the atomization efficiency for its application in automotive industry. The following multiphase flow section offers basics of the multiphase flow and the numerical methods available to study the related problems.

4.2   Multiphase Flow

The multiphase flow in fluid mechanics is the simultaneous flow of materials with two or more thermodynamic phases. These phases can be made up of only one chemical component (e.g., liquid water and water vapor), or numerous separate chemical components (e.g. flow of oil and water). Multiphase flow phenomena are common in nature, e.g., falling rain drops to the surface of the earth, spreading forest fires through the mixture of air, combustible fuel gas and solid particles, hurricane moving on the surface of the ocean, just to name a few. Many industries also use the technology consisting of multiphase flow system, e.g., fluidized bed, breaking up liquids, transporting small particles by airflow, drilling fluids, etc.

The two general numerical simulation methods for multiphase flows are: Euler-Euler and Euler-Lagrange. A multiphase flow model can be written with each phase's local instant variables to match boundary conditions at all phase interfaces. Numerical equations

can be derived to replace each phase's local instant description with a collective description of the phases. Specific equations for (volume of fluid) VOF model will be discussed later in this chapter. Figure 4.1 presents a typical representation of multiphase flow containing two phases in a commercial code, ANSYS FLUENT, which uses mathematically formulated averaging methods. Note that graphs like Figure 4.1 can be plotted based on different variables, but volume fraction is the mostly commonly used factor for such analysis.
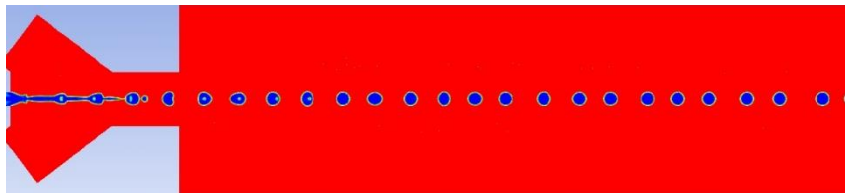
Figure 4.1 A typical representation of multiphase flow containing two phases in ANSYS FLUENT.

There is a larger selection of commercial or open-source codes available for multiphase flow simulations. This study, however, selected to use ANSYS FLUENT, because there are three main methods available under the category of Euler-Euler approach in the last versions of ANSYS FLUENT commercial software package as explained below:

4.2.1 Mixture Model

The mixture model is a simplified model to simulate the multiphase flows and can be used in different ways. Some of these ways are listed in the following (ANSYS FLUENT documentation):

1- It can be used for modeling multiphase flow with different phases moving at different velocities, assuming local over small spatial length scales.

2- It can be used to calculate the non-Newtonian viscosity.

3- Last but not the least, it can be used to model homogeneous multiphase flows with very strong coupling and phases moving at the same velocity.

By solving the momentum, continuity, and energy equations for the mixture, the volume fraction equations for the secondary phases, and algebraic formulas for the relative velocities, the mixture model could model N phases (fluid or particulate). Sedimentation, cyclone separators, particle-laden flows with low loading, and bubbly flows with a low gas volume fraction are examples of typical applications.

It is important to mention the limitations associated with numerical models. Physical limitations that need to be considered for the mixture model available in ANSYS FLUENT (ANSYS FLUENT documentation) are as follows:

1- Mixture model is not available for the density-based solvers.

2- Mixture model can only work with cases with no more than one compressible ideal gas. However, compressible liquids can be defined with no limits using user-defined functions.

3- Potential limitations with streamwise periodic flow boundary conditions with specific mass flow rate.

4- Some cavitation models in the mixture model cannot be used with LES turbulence model.

5- Mixture model cannot be used in conjunction with solidification and melting modeling.

6- The mixture model cannot be used for inviscid flows.

7- The shell conduction model for the walls cannot be used with the mixture model.

4.2.2   Eulerian Model

The Eulerian model in ANSYS FLUENT can be used to model separate phases in the domain that are interacting with each other. There is no limitation in the types, number or the combination of phases present in the domain for the software, however, depending on the number of phases and the complexity, there may be some limits for the memory requirements and convergence behavior. This model in ANSYS FLUENT does not have discrete difference between fluid-fluid and fluid-solid multiphase flows. This model is a complex and yet capable model available in ANSYS FLUENT. It is more suitable for complex problems where higher accuracy or more details are required and is compatible with a large number of turbulence models with no phase or mixture limits. It requires a large computation load to solve both the continuity and momentum equations for each phase in the entire domain unlike the VOF model that will be explained later.

The Eulerian model available in ANSYS FLUENT (ANSYS FLUENT documentation) has the following major limitations:

1- Inviscid flows cannot be modeled using this method.

2- Cannot be used in conjunction with solidification and melting modeling.

3- Potential limitations with streamwise periodic flow boundary conditions with specific mass flow rate.

4- This model is not compatible with Reynolds Stress turbulence model.

4.2.3   Volume of Fluids Model (VOF)

The volume of fluid (VOF) model is another model available in ANSYS FLUENT to study multiphase flow problems. VOF can model any number of immiscible fluids by solving a single set of momentum equation in the entire domain and tracking the volume

fractions of each phase in the whole domain. The steady or transient monitoring of any liquid-gas interface, the prediction of jet or liquid breakups, the motion and physics of bubbly fluids, the movement of liquid after a dam break, and the steady or transient tracking of any liquid-gas interface are all examples of typical applications. This model generally requires lower computation load than the Eulerian model since the momentum equation is only solved once for the entire domain unlike in the Eulerian model. It is suitable to study the less complicated multiphase-based problems.

The VOF model available in ANSYS FLUENT (ANSYS FLUENT documentation) has the following major limitations:

1- VOF model is not available for the density-based solvers.

2- A single fluid phase or a combination of fluid phases must be used to fill all control volumes. The VOF model does not allow for voids where there is no fluid of any kind.

3- Can only work with cases with no more than one compressible ideal gas. However, compressible liquids can be defined with no limits using user-defined functions.

4- Potential limitations with streamwise periodic flow boundary conditions with either specific mass flow rate or pressure drop.

5- The second-order implicit time-stepping formulation is not compatible with and cannot be used with the VOF explicit scheme.

Note that all three models (mixture model, Eulerian model, and volume of fluids model) may possess minor limitations which are not included in the major limitations and may require the users' attention before their application to any specific problem.

Based on the strength and limitations of the above multiphase models, this study adopted the VOF model, since it offers the minimal computational load on the computer and sufficiently high accuracy required for this study. The following section offers the details of the VOF formulation process to study the current droplet breakup and generation problem.

4.3   Volume of Fluids Formulation

The generation of liquid droplets as explained earlier occurs through the liquid breakup process as the result of a dynamic flow interaction between liquid and gas which surrounds the liquid. To numerically investigate this multiphase flow problem, unsteady Navier-Stockes equations are required to describe the transient behavior of the flow consisting of the liquid (e.g., water) and gas (e.g., air) over time. It is necessary to make good and practically acceptable assumptions to obtain the sufficiently accurate practical solutions for the current problem in a timely manner. This assumption making process uses the inductive approach and thinking rather than the deductive scientific approach, according to (Saito, K., & Williams, F., 2015). It is one of most difficult processes in numerical and scale modeling; if the assumptions are correct, then the final numerical calculation results will be correct. Note: Chapter 6, section 6.1 ultrasonic pulsation atomizer provides specific assumptions employed for numerical modeling.

Here, the Mass, Momentum and Energy conservation equations in 2-D form are employed and all the equations are specified assuming that there is no mass source anywhere in the domain.

$$\frac{\partial \rho}{\partial t} + \nabla . (\rho \vec{V}) = 0 \tag{4-1}$$

$$\frac{\partial (\rho \vec{V})}{\partial t} + \nabla . (\rho \vec{V} \vec{V}) = -\nabla p + \nabla . \left[\mu (\nabla \vec{V} + \nabla \vec{V}^T) \right] + \rho \vec{g} + \vec{F}_\sigma \tag{4-2}$$

$$\frac{\partial}{\partial t} (\rho E) + \nabla . \left[\vec{V} (\rho E + P) \right] = \nabla . \left(k_{eff} \nabla T \right) \tag{4-3}$$

Where, $\vec{V} = (u, v)$ is the velocity vector, p is the pressure, $\vec{g}$ is the gravitational acceleration, μ is the viscosity of the working liquid, $\vec{F}$ is the surface tension force per volume, E is the energy, T is the temperature, and k_{eff} is the effective thermal conductivity.

The VOF model (Yang, Zhou, Zhang, & Wang, 2013) is the main method employed in this study to simulate two immiscible phases of air and liquid by solving a single set of momentum and energy equations and sharing the resulting velocity field and temperature among all the phases present in the domain. In addition, the volume fraction of particular phases in each cell throughout the model domain are tracked to monitor the changes of different fluid properties in the entire domain. Unfortunately, the shared-velocity-fields approximation has the lower accuracy in capturing the physical properties of cases where larger velocity differences exist in the phase interface regions.

The VOF model, an interface-capturing model, uses volume fraction to specify percentage of liquid and air in each control volume (cell) throughout the domain. This

volume fraction can take values between 0 and 1 in each cell, but the volume fractions of all the phases sum to unity. The volume fractions are given with the following equation:

For regions only including the representative phase
For interface region (regions including more than only one phase) $\quad \alpha = \begin{cases} 1 \\ 0 < \alpha < 1 \\ 0 \end{cases}$
For regions empty of the representative phase

Note that the interface region is a transition area, where the fluid is a mixture of two or more fluids at the same time during the simulation. With respect to the continuity equation and $D\alpha/Dt = 0$, the continuity equation on the interface areas become:

$$\frac{\partial \alpha}{\partial t} + \frac{\partial}{x_i}(V\alpha) = 0 \tag{4-4}$$

This equation needs to be solved for each of the phases and track the locations and interfaces. For a representative phase q, continuity equation gives us the following equation:

$$\sum_q \frac{1}{\rho_q}[\frac{\partial}{\partial t}(\alpha_q \rho_q) + \nabla.(\alpha_q \rho_q \vec{U}_q)] = \sum_q \frac{1}{\rho_q}\sum_{p=1}^{n}(\dot{m}_{pq} - \dot{m}_{qp}) \tag{4-5}$$

Where, $\dot{m}_{pq}$ is the mass transfer from phase p to phase q, and $\dot{m}_{qp}$ is the mass transfer from phase q to phase p at each interface.

This volume fraction equation is not solved for the primary phase, where a different constraint (to be explained later) is introduced. Equation (4-5) can be solved either using

explicit or implicit time discretization schemes. Using the explicit scheme, the final form of the equation is as follows:

$$\frac{\alpha_q^{n+1}\rho_q^{n+1} - \alpha_q^n\rho_q^n}{\Delta t}V + \sum_f (\alpha_{q,f}^n\rho_q\vec{U}_q^n) = V\left[\sum_{p=1}^n (\dot{m}_{pq} - \dot{m}_{qp})\right] \qquad (4\text{-}6)$$

Where, $n+1$ is the index for the current time step, n is the index for the previous time step, $\alpha_{q,f}$ is face value q^{th} volume fraction computed from compressive scheme (first- or second-order upwind, QUICK, modified HRIC, or CICSAM scheme), V is the volume of cell, and U_f is the volume flux through the face, based on normal velocity. Depending on the case and its governing physics, the implicit scheme can be used for time discretization as well by incorporating different interpolation schemes which would lead to a slightly different discretized forms for the volume fraction equation. The final form of the equation using the implicit scheme is provided in the following:

$$\frac{\alpha_q^{n+1}\rho_q^{n+1} - \alpha_q^n\rho_q^n}{\Delta t}V + \sum_f (\alpha_{q,f}^{n+1}\rho_q^{n+1}\vec{U}_q^{n+1}) = V\left[\sum_{p=1}^n (\dot{m}_{pq} - \dot{m}_{qp})\right] \qquad (4\text{-}7)$$

Since the implicit discretized equation requires the volume fraction values at the current time step (unlike the explicit scheme), a standard scalar transport equation needs to be solved iteratively for each of the secondary-phase volume fractions at each time step to obtain the final values.

For the primary phase in the domain (air), the volume fraction is obtained based on the following constraint:

$$\sum_{q=1}^{n} \alpha_q = 1 \qquad (4\text{-}8)$$

Where, α is the volume fraction, and q represents the phases in the system. The volume fraction of the secondary phase is obtained using one of the equations (4-6) or (4-7) and can be compared to the primarily phase's volume fraction calculated from equation (4-8).

The surface tension model available in ANSYS FLUENT is the continuum surface force (CSF) model presented by (Brackbill, Kothe, & Zemach, 1992). Using this model, the force source term in equation (4-2) can be further explained. In ANSYS FLUENT, the CSF model is used, and surface curvature is computed from the local gradients in the surface normal at each interface in the domain.

$$\vec{n} = \nabla \alpha_q \qquad (4\text{-}9)$$

$$\hat{n} = \frac{\vec{n}}{|\vec{n}|} \qquad (4\text{-}10)$$

The curvature k is defined in terms of the divergence of the unit normal, $\hat{n}$ (Brackbill et al., 1992) using the following equation:

$$k = \nabla.\nabla\hat{n} \qquad (4\text{-}11)$$

Writing the surface tension in terms of the pressure jump across the surface of the interface, the force at the surface then can be written using the divergence theorem. Equation (4-12) presents a simplified form of the surface tension force as a volume force when there are only two phases available at the interface.

$$\vec{F} = \sigma \frac{2\rho k \nabla \alpha_g}{\rho_l + \rho_g} \qquad (4\text{-}12)$$

Where, ρ is the volume-averaged density and k is the curvature of the gas–liquid interface and a property defined for the interface of each two fluid types.

The surface tension force, which may cause complications and difficulty in numerical calculations, can be estimated based on two non-dimensional numbers, the capillary number (Ca) and the weber number (We). The effects of the surface tension force can be ignored under the following conditions.

Surface tension effects can be neglected
Surface tension effects need to be considered

$$\begin{cases} Ca \gg 1 \ or \ We \gg 1 \\ Ca \ll 1 \ and \ We \ll 1 \end{cases}$$

A single momentum equation in VOF model is solved throughout the domain for all the cells in the domain, gathering the possible resulting velocity field and equating at the interface cells of two phases. Equation (4-6) is solved for each control volume in the domain to conclude the primarily phase's volume fraction, and the domain is shared by all phases. The properties are volume-averaged values based on the volume fractions in each cell. The final physical properties are, depending on the volume fraction in each of the cells, related to one of the phases (in case of having a volume fraction of 1) or a mix of some of the phases available in that cell (any other number than 1 for the volume fraction). To find the averaged value for the properties throughout the domain, for instance, one can

use the following equation, the weighted average of the same properties, for all different phases available in that cell.

$$\rho = \alpha_g \rho_g + (1 - \alpha_g)\rho_l \qquad (4\text{-}13)$$

Where, subscripts g and l represent gas and liquid phases, respectively. In general, the average of that property can be given for an n-phase system by the following equation:

$$\vartheta = \sum \alpha_q \vartheta_q \qquad (4\text{-}14)$$

Where, q shows the phase, for which we are attempting to compute the chosen property, and ϑ is the representative property. This equation can be used multiple times for all the different properties needed as the result of the simulation. Using all of the equations for all of the n phases, a total of (4n+1) equations are provided, while, 5n unknowns are needed to be calculated. Thus, additional (n-1) equations are needed for the system of equations. The same pressure field in the entire domain is given as a constraint:

$$p_q = p, \quad \forall q \in [1, n] \qquad (4\text{-}15)$$

Where, p is representing the pressure field, q is showing any chosen phase inside the domain and n is the maximum number of phases available in the domain.

There are other different constraints to couple pressure and velocity fields regarding the rest of the unknowns. The pressure implicit with splitting of the operators' scheme (PISO scheme) is employed along with skewness and neighbor corrections for coupling velocity and pressure fields. A geo-reconstruct scheme is also applied to make the

interfaces between different phases smoother, achieving a more realistic transfer of the properties from one phase to another. The equations can determine the values on different nodes, but not throughout the entire domain as a field. A pressure staggering and second-order upwind schemes are, therefore, utilized to interpolate the values in the regions between the nodes, where, no value is available. A variable time-stepping with a constraint of the global courant number equal to 0.2 is applied throughout this study to reduce the simulation time for all cases in this study.

4.4   Non-Newtonian Pseudo-Plastic Viscosity Models

The viscosity of common automotive water-borne (WB) paints displays non-Newtonian pseudo-plastic characteristics. For a non-Newtonian pseudo-plastic fluid, the viscosity tends to non-linearly reduce as the fluid is deformed. Figure 4.2 illustrates a typical behavior of viscosity with respect to shear rate. High viscosity values at low shear rates are required to guarantee high quality painted surface finish which promotes leveling and avoiding sagging, while low viscosity values at high shear rates are favor for enhancing atomization.
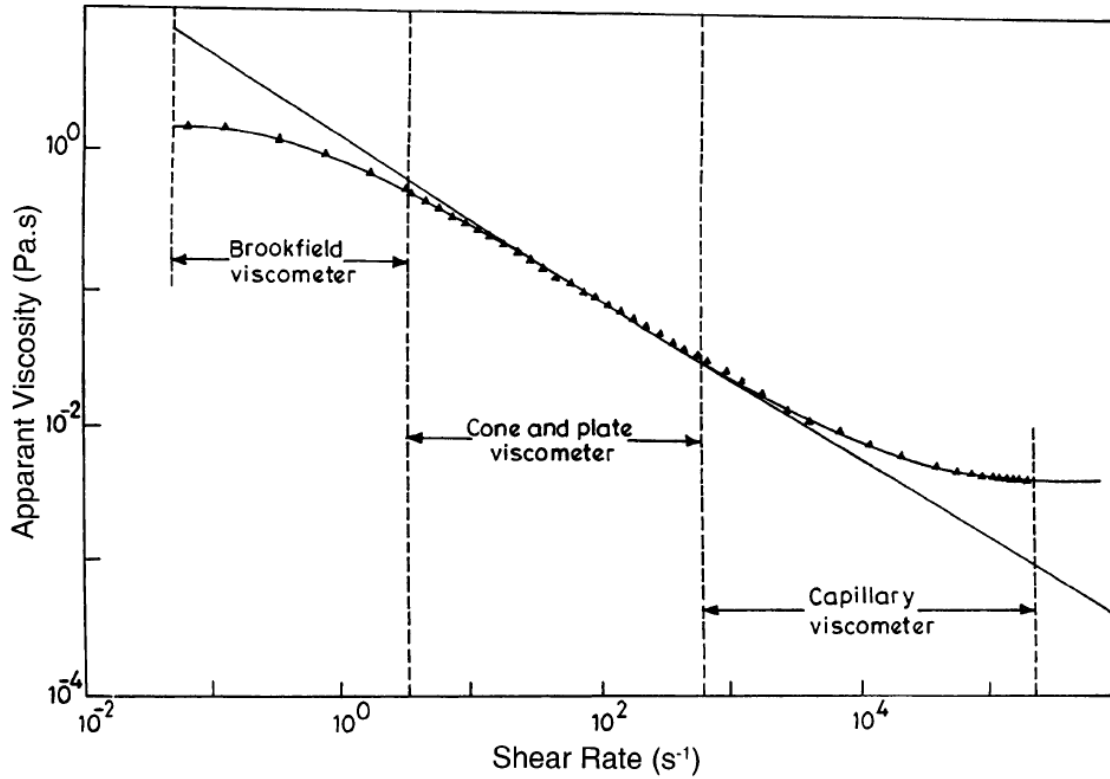
Figure 4.2 Typical rheological (pseudo-plastic) behavior of water-borne paints,
Reprinted/adapted by permission from Springer Nature: (Chhabra, 2010).

For incompressible Newtonian fluids, the shear stress is proportional to the rate of

deformation, $\ddot{D}$, thus:

$$\ddot{\tau} = \mu \ddot{D}$$ (4-16)

The rate of deformation can be defined using the following equation (4-17).

$$\ddot{D} = \left(\frac{\partial u_j}{\partial x_i} - \frac{\partial u_i}{\partial x_j} \right)$$ (4-17)

Where, μ is the viscosity, which is independent of the $\ddot{D}$ itself. Following the same formulation for some non-Newtonian fluids, the shear stress can similarly be written in terms of a non-Newtonian viscosity η, which is also called apparent viscosity.

$$\ddot{\tau} = \eta(\ddot{D})\ddot{D} \tag{4-18}$$

The non-Newtonian viscosity η is generally a function of all three invariants of the rate-of-deformation tensor $\ddot{D}$, while, η is assumed as only a function of the shear rate $\ddot{Y}$, the magnitude of the strain-rate tensor with the unit of s^{-1}. This shear rate is related to the second invariant of $\ddot{D}$ and is defined with the following equation.

$$\dot{\gamma} = \sqrt{0.5 \times \ddot{D} : \ddot{D}} \tag{4-19}$$

4.4.1   Temperature Dependent Viscosity

If the flow is non-isothermal, the temperature dependency on viscosity, as well as the shear rate dependency, are required to be considered. Therefore, a total viscosity is divided into two parts and calculated as:

$$\mu = \eta(\dot{\gamma})H(T) \tag{4-20}$$

Here, $H(T)$ is the temperature dependency of the fluid, known as the Arrhenius law.

$$H(T) = exp\left[\alpha\left(\frac{1}{T - T_0} - \frac{1}{T_\alpha - T_0}\right)\right] \tag{4-21}$$

Where, α is the activation energy, T_0 is customarily set to zero, while T_α is the reference temperature, at which $H(T) = 1$.

To model the non-Newtonian pseudo-plastic behavior of typical automotive waterborne paints, two different conditions: the power law model and Carreau model, could be adopted and are explained as follows.

4.4.2   Power Law Model for Non-Newtonian Viscosity

The power-law or Ostwald-deWaele model has been most widely used for the constitute equations to simulate transport processes of shear-rate-dependent viscosity fluids (R. B. J. A. R. o. F. M. Bird, 1976). Viscosity for the non-Newtonian power-law model is represented by the following equation (4-22).

$$\eta_{min} < \eta = k\dot{\gamma}^{n-1}exp\left(\frac{T_0}{T}\right) < \eta_{max} \tag{4-22}$$

Where, k (the consistency factor or index) is a measure of the average viscosity of the fluid and n (the behavior index or indicator) is a measure of the derivation from Newtonian fluid. The value n is used to determine the class of the fluid, as shown below.

$$\begin{cases} n < 1 \to Shear - thinning\ (pseudo - plastic)\ fluid \\ n = 1 \to Newtonian\ fluid \\ n > 1 \to Shear - thickening\ fluid \end{cases}$$

A modified power-law model caps the equation between the upper and lower limits. An upper limit η_{max} is necessary for shear-thinning fluids to eliminate the model's

singularity at zero shear rate. In a pipe flow, for example, the flow velocity is maximum at the axis where the strain rate is also zero. In the absence of this upper limit, the uncapped power law model would lead to unrealistically large apparent viscosity values. The upper and lower limit capping is necessary to follow the typical behavior of WB paints' viscosity. Note that the behavior of WB paints, however, resembles that of Newtonian fluid at very low shear rates. The same type of response, the second Newtonian viscosity range is observed at very high shear rates, where the apparent viscosity approaches that of the solvent.

The upper limit viscosity η_{max} and the lower limit viscosity η_{min} are specified based on experimental viscosity data and the Carreau non-Newtonian viscosity model is considered to make the current study relevant to automotive industry at large. Figure 4.3 presents water-borne paint viscosity vs. shear rate data. Two sets of data presented in the figure include: (1) data provided by TMC (Toyota Motor Corporation in Japan), and (2) data provided by TMMI (Toyota Motor Manufacturing Indiana) w/data measured at UK (A. J. S. Salazar, K. , 2008).
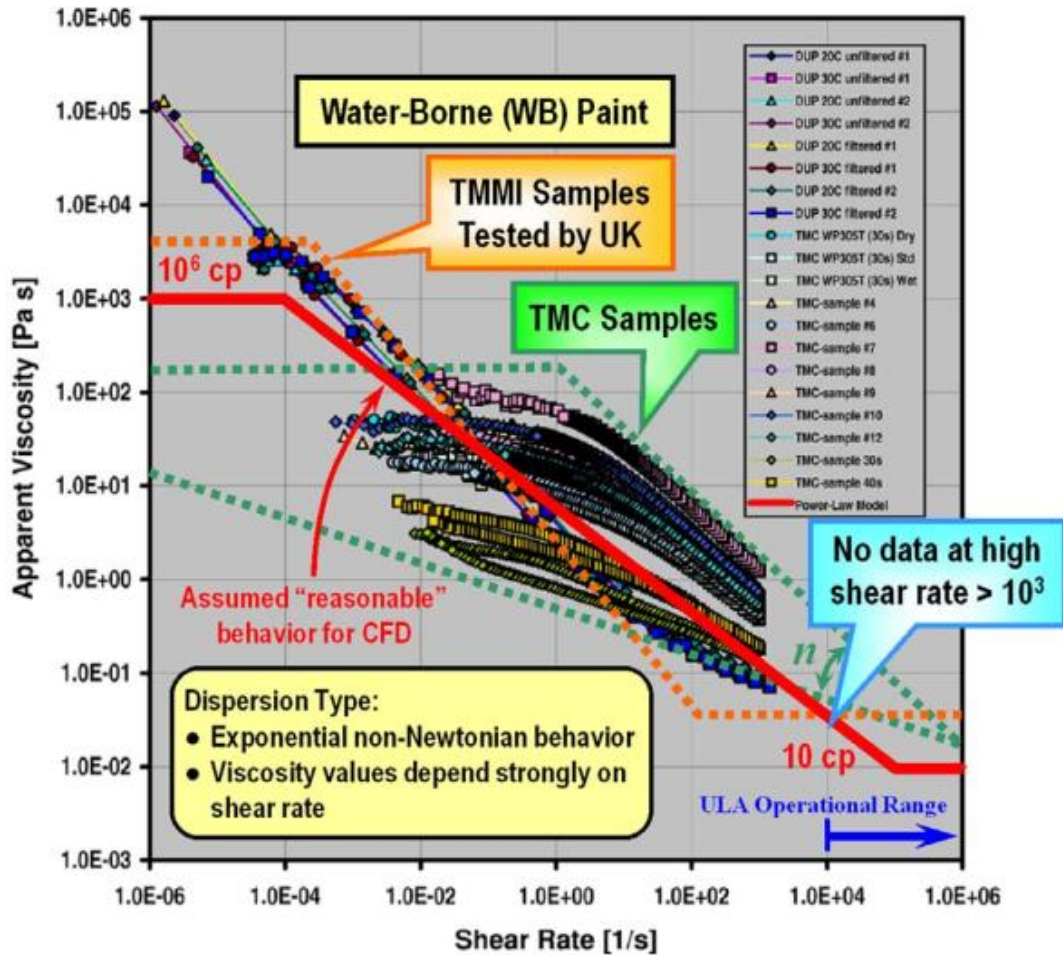
Figure 4.3 Water-borne paint viscosity vs. shear rate data. Two sets of data are presented: (1) data provided by TMC, and (2) Samples provided by TMMI w/data measured at UK (A.J. Salazar, K. Saito., 2008), reproduced with the permission of Dr. Kozo Saito.

These paint samples were tested at two different temperatures of 25 and 30 C twice to test the sensitivity of the paint viscosity to temperature variation, and no significant behavior was observed. Due to the significant difference in these two trends, a simple average between them was used to obtain the necessary data for numerical simulation. In addition, the input parameters k and n are also computed by curve fitting of the same data. Finally, T and T_0 are respectively the working and reference temperature. Often this

temperature-dependence of the viscosity is ignored by assuming $T_0 = 0$, which might have caused inaccurate computation results. If the viscosity from the power model is less than η_{min}, the value of η_{min} is used for computation, while if the computed viscosity is greater than η_{max}, the value of η_{max} is used.

4.4.3   Carreau Model for Pseudo-Plastic Fluids

The Carreau model (R. B. Bird, Armstrong, & Hassager, 1987; R. B. J. A. R. o. F. M. Bird, 1976) solves the inability of the power law model to describe the limiting low shear rate by introducing a low shear viscosity, η_0, and a time constant, λ, which sets the Newtonian limit in terms of the shear rate. This model attempts to describe a wide range of fluids by establishing a curve-fit to piece together functions for both Newtonian and shear-thinning (n < 1) non-Newtonian laws. In the Carreau model, the viscosity is expressed as in the following equation:

$$\eta = \eta_\infty + (\eta_0 - \eta_\infty) \times [1 + (H(T)\dot{\gamma}\lambda)^2]^{\frac{(n-1)}{2}} \qquad (4\text{-}23)$$

Which satisfies the following equation.

$$\begin{cases} \dot{\gamma} \to 0, \ \eta \to \eta_0 \\ \dot{\gamma} \to \infty, \ \eta \to \eta_\infty \end{cases} \qquad (4\text{-}24)$$

Where, η_0 and η_∞ are the upper and lower limits of the fluid viscosity, respectively and equation (4-23) still holds. The parameters n, λ, T_α, η_0, and η_∞ are dependent on the fluid itself. Parameter λ, is the time constant, and n is the power-law index.

There are, however, two other models available in ANSYS FLUENT to deal with modeling non-Newtonian flows that can be used depending on data available from the sample. These two additional models are the Cross Model and Herschel-Bulkley Model for Bingham plastics.

4.4.4 Cross Model

The Cross model for the viscosity is as follows:

$$\eta = H(T)\frac{\eta_0}{1 + (\dot{\gamma}\lambda)^{1-n}} \tag{4-25}$$

Where η_0 is zero-shear-rate viscosity, λ is the natural time (i.e., inverse of the shear rate at which the fluid changes from Newtonian to power-law behavior), and n is the power-law index.

Note that the Cross model is generally more suitable to describe the low-shear-rate behavior of the viscosity.

4.4.5 Herschel-Bulkley Model for Bingham Plastics

When both the shear stress and the strain rate are zero, the power law model becomes accurate. When the strain rate is zero, Bingham plastics exhibit a non-zero shear stress:

$$\ddot{\tau} = \ddot{\tau}_0 + \eta\ddot{D} \tag{4-26}$$

Where, τ_0 is the yield stress.

$$\begin{cases} \tau < \tau_0 \rightarrow The\ material\ remains\ rigid \\ \tau > \tau_0 \rightarrow The\ material\ flows\ as\ a\ power-law\ fluid \end{cases}$$

This model combines the effects of Bingham and power-law behavior in a fluid. For lower strain rates $\left(\dot{\gamma} < {}^{\tau_0}/_{\mu_0}\right)$, the material acts like high-viscos fluid with viscosity of μ_0. However, when the yield stress is passed, the fluid behavior can be described by a power law.

For $\dot{\gamma} > \dot{\gamma}_c$:

$$\eta = \frac{\tau_0}{\dot{\gamma}} + k\left(\frac{\dot{\gamma}}{\dot{\gamma}_c}\right)^{n-1} \tag{4-27}$$

And for $\dot{\gamma} < \dot{\gamma}_c$:

$$\eta = \tau_0 \frac{\left(2 - {}^{\dot{\gamma}}/_{\dot{\gamma}_c}\right)}{\dot{\gamma}_c} + k\left[(2-n) + (n-1)\frac{\dot{\gamma}}{\dot{\gamma}_c}\right] \tag{4-28}$$

Where, k is the consistency factor, and n is the power law index. Validation of the Numerical Simulation Model

Before conducting numerical simulation, it is necessary to validate the code developed in ANSYS FLUENT. To validate the in-house model, a separate model was created similar to that of (J. Castrejón-Pita et al., 2011) using the data provided earlier in this chapter. Figure 4.4 shows a simple illustration of how their system was set up to generate droplets.
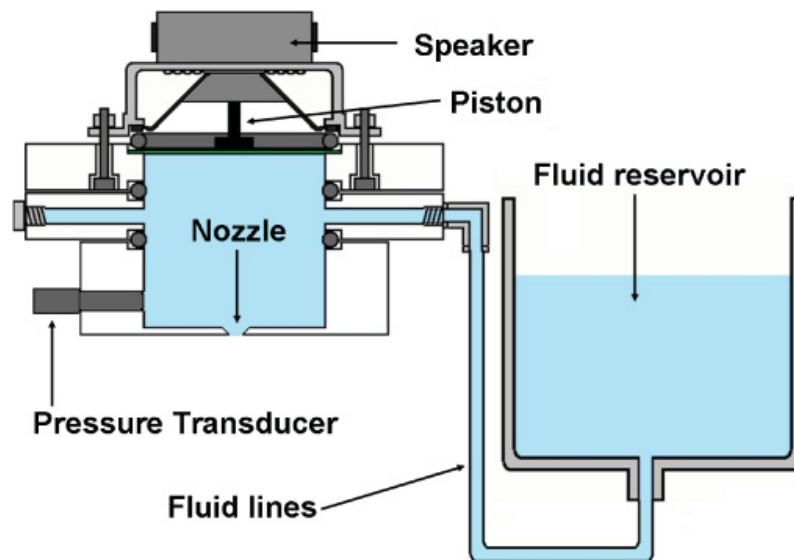
Figure 4.4 Simple illustration of the system employed in (J. Castrejón-Pita et al., 2011), reprinted with permission from the American Physical Society, Copyright 2011 by the American Physical Society, http://dx.doi.org/10.1103/PhysRevE.83.036306.

Figure 4.5 dimensions of the nozzle used in their study, which will be used for numerical provides calculations to validate the model.
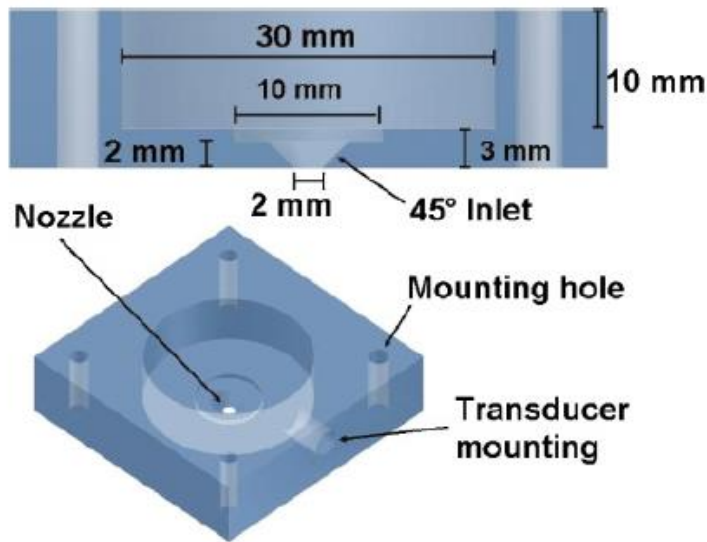
Figure 4.5 Schematics of the nozzle used in (J. Castrejón-Pita et al., 2011) , reprinted with permission from the American Physical Society, Copyright 2011 by the American Physical Society, http://dx.doi.org/10.1103/PhysRevE.83.036306.

To conduct the validation tests, the same system was studied using the numerical method selected for this study. The fluid used in their study was a mixture of 85% glycerol and 15% water with a final density of 1222 kg.m^{-3}, viscosity of 0.1 Pa.s, and surface tension of 0.064 N.m^{-1}. To validate the current CFD predictions, the droplet distance from the tip of the nozzle was plotted as a function of time and compared with the experimental and numerical results available in their paper (J. Castrejón-Pita et al., 2011).

Figure 4.6 compares the data obtained using the current numerical method and those obtained in (J. Castrejón-Pita et al., 2011). Very good agreement was observed between the results from the present model and the one used by the reference work, validating the current CFD model to be reasonably accurate in representing the governing physics of similar phenomena. The small difference between the numerical and experimental results shown in the figure may be due to two different numerical methods

and also the effect of gravity for the experiments, which was not included into the numerical calculations. This validation can justify the use of the current numerical model to investigate the detailed aspects of the droplet generation system and process.
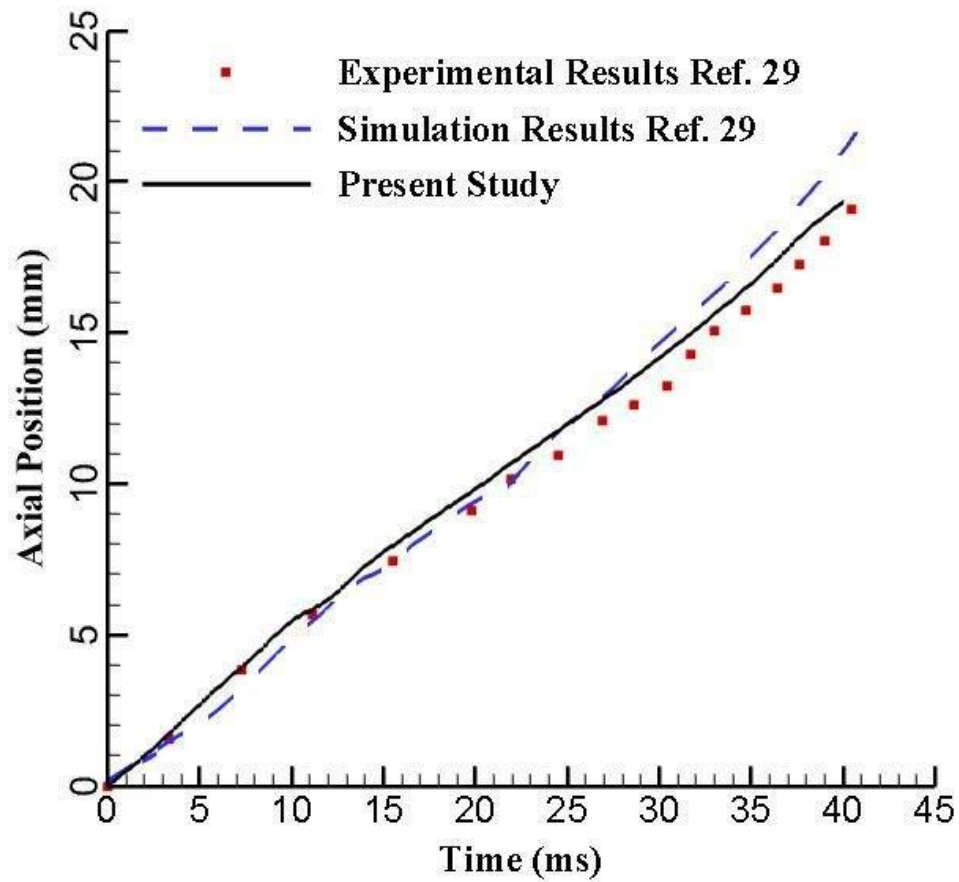
Figure 4.6 The droplet tip position over time, from (J. Castrejón-Pita et al., 2011) and using the current model for validation purposes.

4.5   Closure

Chapter 4 explained the concept of multiphase flow and introduced a total of five different multiphase flow models currently available in the latest version of ANSYS FLUENT commercial software. The volume of fluids (VOF) model was chosen for this study and its details were provided extensively. Assumptions employed to simplify the equations were listed and their reasons were explained. Different approaches to model the dependency of viscosity on the temperature and shear stress were specified and the different models available in ANSYS FLUENT were listed.

CHAPTER 5. SCALING ANALYSIS

5.1   Introduction

The scaling analysis is an effective tool to identify the effects of the influential parameters and the governing forces on the performance of the inkjet nozzles and the liquid breakup process. The law approach-based scaling analysis pioneered by R.I. Emori (Emori et al., 2000) is designed to enhance our understanding of physics that govern the liquid breakup phenomenon. Figure 5.1 shows the general diagram of the scale and numerical modeling, whose concept is applied to the following alternative numerical scaling approach. That is because the law approach-based scaling analysis can be extended to obtain the governing non-dimensional numbers by numerically studying the effects of all the significant parameters that influenced this numerical simulation.

A traditional scale modeling approach to this task will be a well-designed experiment that can satisfy the accuracy of the numerical simulation. This experiment requires high precision accuracy and is very difficult to design. As an alternative to this precision scale model experiment, a validated numerical model like the current one is thought to do this task systematically with acceptable accuracy. To that end, the following study was conducted by following the laws approach process (Emori et al., 2000). First, the major forces governing the process are assumed and parameters that constitute these forces were identified. Then a key parameter was selected, while keeping the rest of the parameters constant to numerically calculate the effects of the key parameter on the fluid dynamics of the droplets. Second, the key parameter was changed to a different parameter selected among the important parameters identified in the above and the same process was repeated.
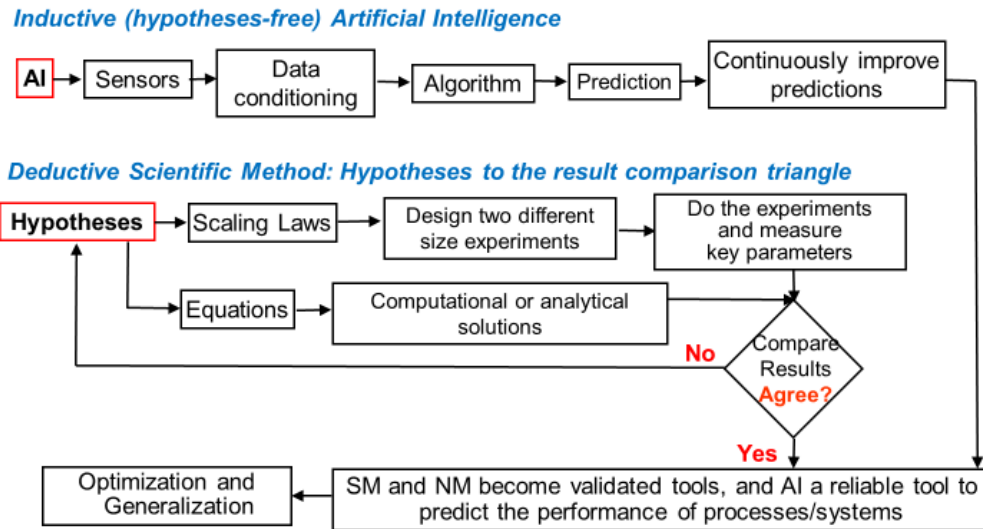
Figure 5.1 Diagram of artificial intelligence, and scale and numerical modeling. Scale and numerical modeling uses the deductive hypothesis-driven scientific method, while artificial intelligence uses the hypotheses-free inductive method, adopted from (K Saito, 2022), reproduced with the permission of Dr. Kozo Saito.

A liquid filament's jet breakup is caused by surface tension strangulation, which functions as a driving cause, while the inertia and viscous forces operate as retarding causes, suppressing filament breakup (Delhaye, Coutris, & Herran, 2013). As the result, two distinct pi-numbers that describe this competitive character have been identified; the Webber number, We, which is a ratio of the inertial force divided by the surface tension force, and the Reynolds number, Re, which is a ratio of the inertia force divided by the viscous force (Emori et al., 2000). Another dimensionless number is the Ohnesorge number, Oh, which can be calculated using the We and the Re numbers as $Oh = {We^{0.5}}/{Re}$. The following section explains the significance of this set of Pi numbers.

5.2 Major Pi Numbers Used in The Past Studies

Now that we know better about the mathematical formulations and since the scaling analysis will be an important part of presenting the results of our work, it would be beneficial to rewrite the equations based on modified terms to obtain their non-dimensional forms. The non-dimensional form of equations helps us identify the influential parameters and the governing forces affecting the liquid breakup process. The momentum equation provides the velocity field which is the main variable to observe the characteristics of the generated droplets. To obtain the non-dimensional form of the momentum equation, the following modified terms are defined:

$$\vec{X}*= \frac{\vec{X}}{R}, \vec{V}*= \frac{\vec{V}}{U} \tag{5-1}$$

$$t*= \frac{t}{R/U}, p*= \frac{p}{\rho U^2}$$

Where, U is the inlet velocity of the liquid flow (m/s) (characteristic velocity chosen in this work) and R is the nozzle radius (m) (characteristic length chosen in this work). Substituting these parameters into the momentum equation (4-2), the equation can be rewritten as follows:

$$\frac{U^2}{R}\left[\frac{\partial(\vec{V}*)}{\partial t*} + \nabla.(\vec{V}* \vec{V}*)\right] \tag{5-2}$$

$$= -\frac{U^2}{R}\nabla p* + \frac{U\mu}{\rho R^2}\nabla.\left[\nabla\vec{V}* + \nabla(\vec{V}*)^T\right]$$

$$+ \frac{\sigma}{\rho R^2}\nabla.[(I - \hat{n} \otimes \hat{n})|\vec{n}|]$$

Considering the Re and We numbers that have the following definitions;

$$Re = \frac{\rho U R}{\mu} \qquad (5\text{-}3)$$

$$We = \frac{\rho U^2 R}{\sigma}$$

The dimensionless momentum equation with these substitutions is as follows:

$$\frac{\partial(\vec{V}*)}{\partial t *} + \nabla . (\vec{V} * \vec{V} *) \qquad (5\text{-}4)$$

$$= -\nabla p * + \frac{1}{Re\left[\nabla \vec{V} * + \nabla(\vec{V} *)^T\right]\frac{1}{We}\left[(I - \hat{n} \otimes \hat{n})|\vec{n}|\right]}$$

This equation (5-4) indicates that the Re and We numbers can define the characteristics of the droplets ejected from the nozzle based on the operating conditions, while the characteristic velocity chosen for these two pi-numbers needs to be identified by adopting the assumptions for equation (4-2). Equation (5-4) also can be rewritten in terms of Oh number using the relationship among Re, We, and Oh numbers.

There have been recent studies attempting to provide some other dimensionless groups in terms of the droplets' properties to describe the ligament breakup process by (Castrejon-Pita et al., 2012; S. Hoath, Jung, & Hutchings, 2013), where the aspect ratio number l/R', with R being the radius of the cylindrical filament was introduced. However, as mentioned in the previous chapters, the process of droplet generation from the inkjet nozzles depends on the working liquid properties, the input conditions of the nozzle and the geometrical parameters of the nozzle. Thus, characterizing the atomization process based on non-dimensional groups depending on these factors can define the process more accurately.

5.3   Major governing Forces and Pi Numbers Used in This Study

The numerical experiment can be a viable alternative method in terms of efficiency and consistency, when scale model experiment faces difficulty, as explained earlier. Numerical experiment also has limitations associated with assumptions employed for calculations and governing equations, since they may not be able to precisely capture or represent the mechanism of the phenomena of concern. As to the role of experiments, it is noteworthy to mention that (Poozesh, 2021) recently addressed the emergence and surge of data-driven modeling as a new opportunity to leverage experimental data in model development, in comparison to the traditional first-principle-based scale modeling, which attempts to find pi-numbers made up of physical forces and energies that govern the phenomenon of concern and proper correlations among pi-numbers. The law approach (Emori et al., 2000) is available to accomplish the first aim, while scale model experiments achieve the second aim. His mention of data-driven modeling, such as artificial intelligence, can be added as a new tool to scale modeling (see Figure 5.1).

A total of six different forces are assumed to be significant for numerical model calculations in conjunction with the performance of the inkjet nozzle and the process of breaking up the liquid ligaments. They are: (1) inertial force of air (F_1), (2) inertial force of liquid (F_2), (3) viscous force of air acting on droplet surface (F_3), (4) viscous force of liquid (F_4), (5) surface tension force of liquid (F_5), and (6) the dynamic pressure force (flow oscillation force) (F_6) which causes oscillation of liquid flow. Applying the law approach scale modeling theory (Emori et al., 2000), the following five independent non-dimensional numbers (pi-numbers) can be formed from these six different forces. They are, for example, according to the law approach theory:

$$\pi_1 = \frac{F_1}{F_2} \tag{5-5}$$

$$\pi_2 = F_2/F_3$$

$$\pi_3 = F_3/F_4$$

$$\pi_4 = F_4/F_5$$

$$\pi_5 = F_6/F_5$$

Theoretically, the above five independent principal pi-numbers are sufficient to study the performance of the inkjet nozzle. However, the Capillary number (Ca), defined as the ratio of viscous drag force to surface tension force and the Strouhal number (St), defined as the ratio of flow oscillation force to inertial force of liquid, can be added as auxiliary pi-numbers, since the viscous drag force in the Ca number and the flow oscillation force in the St number are functions of the Re number. These two pi-numbers will interest inkjet nozzle design engineers and researchers in this field. The Ca number and the St number can be respectively described with the principal pi-numbers as follows: $Ca = \pi_3\pi_4$, $St = \pi_5/(\pi_2\pi_3\pi_4)$.

$$\pi_1 = \frac{Inertial\ force\ of\ air}{Inertial\ force\ of\ liquid} = \frac{(\rho U R)_a}{(\rho U R)_l} \tag{5-6}$$

$$\pi_2 = \frac{Inertial\ force\ of\ liquid}{Viscous\ force\ of\ air} = \frac{(\rho U R)_l}{(\mu)_a}$$

$$\pi_3 = Re_l = \frac{Inertial\ force\ of\ liquid}{Viscous\ force\ of\ liquid} = \frac{(\rho U R)_l}{\mu_l}$$

$$\pi_4 = We_l = \frac{Inertial\ force\ of\ liquid}{Surface\ Tension\ force} = \frac{(\rho U^2 R)_l}{\sigma_l}$$

$$\pi_5 = \Omega^2 = \frac{Flow\ oscillation\ force}{surface\ tension\ force} = \frac{(f^2\rho R^3)_l}{\sigma_l}$$

$$Ca_l = \frac{Viscous\ drag\ force}{Surface\ Tension\ force} = \frac{(\mu U)_l}{\sigma_l} = \pi_3\pi_4$$

$$St_l = \frac{Flow\ oscillation\ force}{Inertial\ force\ of\ liquid} = \frac{FR}{U_l} = \pi_5/(\pi_2\pi_3\pi_4)$$

Where, ρ is the density of the liquid/air flows (Kg/m^3), f is the frequency of pulsation (kHz), U is the inlet velocity of the liquid/air flows (m/s) (characteristic velocity chosen in this work is the liquid inlet velocity), R is the nozzle radius (m) (characteristic length chosen in this work), and σ is the surface tension of the liquid flow (N/m).

The shaping air also plays an important role in determining the outcome of the atomization, while the liquid velocity was found to be more influential in the process, and hence, was chosen as the characteristic velocity for simplicity for the rest of this study. Efforts were made to find a characteristic velocity that can improve the performance of the data correlation, but no successful and clear correlation appeared in the process, indicating that the selection of characteristic parameters may be more complicated than just the difference between the shaping air velocity and the liquid velocity. Finding the most appropriate correlations between the two velocities merits further studies on scaling analysis approach for similar cases.

5.4   Closure

This chapter summarized the scaling analysis, as an effective tool to study the effects of various parameters on the ligament breakup process. Applying the law-approach scaling analysis, the major forces that affect the process of droplet generation were identified, the non-dimensional form of the momentum equation was derived, and principal Pi numbers were obtained. These principal Pi numbers are expected to influence the quality of droplets generated from the in-house inkjet nozzle. Chapter 6 will use these principal pi-numbers to predict the performance of the nozzle based on the introduced conditions and create the performance behavior diagrams for the nozzle based on the operating conditions.

CHAPTER 6. RESULTS AND DISCUSSION

This chapter presents the results of the current study and discussion to promote our understanding and interpretation of these results. The results are presented in various graphs to evaluate the jetting conditions and the characteristics of the generated droplets for each set of working conditions. The results of this study were presented in three main sections, each of which specifically discussed one of the droplet-generator designs whose details were provided in chapters 3 and 4. The unique features including the advantages and disadvantages for each of the designs are summarized here to specify the merits of each towards the mentioned goal of this study.

6.1 Ultrasonic Pulsation Atomizer

This section presents numerical calculation results on the ultrasonic paint atomizer (UPA) inkjet printhead for discussion and interpretation. Using sinusoidal pulsation waves, this model showed significant improvements in generating a stream of mono-dispersed droplets that can help achieve the main goal of this study. The following assumptions were made to simplify the CFD modeling and reduce the computation load of the study, without altering the major governing physics that control the problem.

1. The internal liquid and air flows are laminar.

2. All the phenomena are axisymmetric.

3. Airflow is treated incompressible due to a low Mach number phenomenon.

4. The liquid transport properties are constant.

5. Atomization occurs at atmospheric conditions.

6. Evaporation of the liquid ligament and droplets is neglected, since the flow time scale is much faster than the liquid heat transfer time (for the estimate, see the note below); thus, the energy equation was not employed for numerical simulation. Note that the flow time, $t_f = R/u$, and the liquid heat transfer time, $t_h = R^2/\alpha_l$, where R = nozzle radius and α_l = thermal diffusivity of water. Using R = 0.5 mm, u = 100 mm/s, and α_l = 0.15 mm^2/s, $t_f = 5 \times 10^{-3}$ s and t_h = 1.7 s. Thus, $t_f \ll t_h$.

7. The fluid in the CFD modelling is water (or water-based liquid under a special condition).

8. The 2-D computational model was created and calculated first, then it was expanded to the 3-D model using the post-processing tools available in ANSYS FLUENT, due to the characteristics of the problem.

The first step was to generate a 2D domain that can represent the inkjet printhead accurately, given the assumptions listed above. A high-quality computational grid needs to be created on this 2D domain afterward to be used in ANSYS FLUENT software. Figure 6.1 illustrates this computational domain and the associated computational grid. The grid encompasses the relevant region inside UPA up to 3.5 mm and 1.25 mm outside the nozzle respectively in the axial and radial directions, and 0.3 mm and 0.25 mm respectively in the axial and radial directions inside the nozzle. More cells are generated in regions with higher intensity gradients to accurately reflects the governing physics. The smallest grid edge size employed is 25 microns in size. Various grid setups were generated to accurately capture the physical forces that govern the phenomenon. The grid independence was achieved with a total of 21,067 cells.
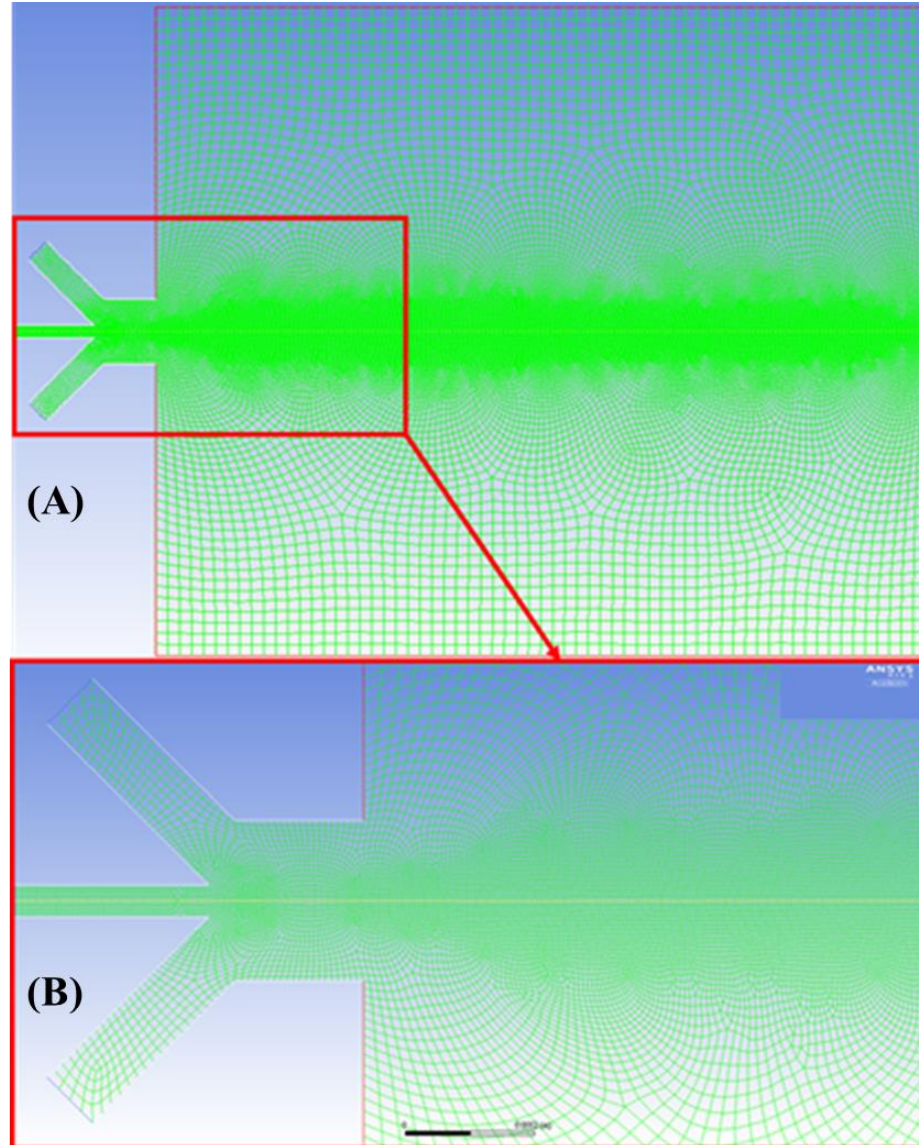
Figure 6.1 A) Overall view of the grid generated for the numerical model. B) Illustration of the smaller and finer cells generated along the trajectory of the droplets.

No-slip boundary condition was employed for all the solid boundaries. A wet contact angle (an acute angle) was imposed inside the nozzle, where the liquid is flowing, and a non-wet contact angle (an obtuse angle) was used for all other solid boundaries. A

constant velocity was imposed on the air inlets and a modified sinusoidal wave was imposed on the liquid inlet.

To impose the sinusoidal wave as liquid inlet velocity, a user-defined function (UDF) was developed to enforce this boundary condition to the liquid inlet every timestep. Finally, a pressure outlet boundary was imposed to model the environment outside the computational domain. The following equation (6-1) was used to introduce the pulsation to the liquid inlet.

$$U(t) = |U_{max}Sin(2\Pi ft)| \qquad\qquad (6\text{-}1)$$

After creating the numerical models and computational grid, the effects of various factors on the quality of the generated droplets can be investigated. The droplet parameters, which can determine the optimal conditions to produce quality droplets, included droplet diameter, distance between each pair of droplets (frequency of generation), ligament breakup length and the chance of satellite droplet generation. The range of inlet velocities needs to be determined based on the assumption that the nozzle has an acceptable performance (able to generate a stream of mono-dispersed droplets). It further requires studying the effects of liquid properties and to assess the performance of the nozzle with water-based paint.

.

6.1.1   Droplet Characteristics

This section focuses on the effects of different factors on the performance of the nozzle. The factors studied include the liquid and air inlet velocities, liquid viscosity and pulsation frequency.

This section is to study the effects of liquid and air inlet velocities on the production of quality droplets and determine the acceptable range of these two factors for studying the rest of effective parameters. Figure 6.2 presents the effects of liquid inlet velocity on droplets' quality in volume fraction contour for three different liquid inlet velocities with air inlet velocity of 10 m/s. Figure 6.3 presents the effects of air inlet velocity on droplets' quality in volume fraction counter for five different air inlet velocities with liquid inlet velocity of 3 m/s.
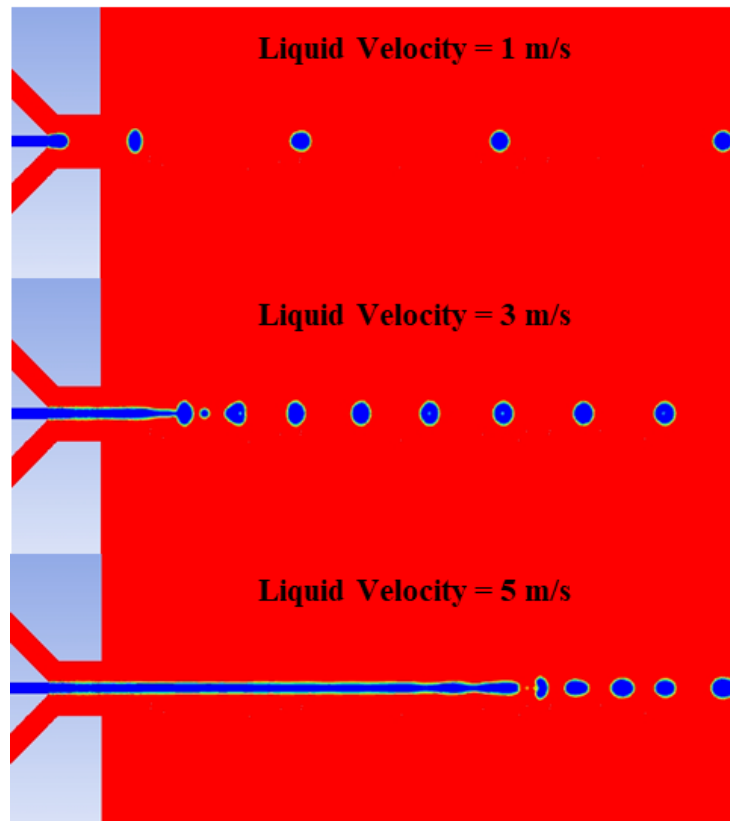
Figure 6.2 Effects of liquid inlet velocity on droplets' quality for three different liquid inlet velocities with air inlet velocity of 10 m/s (Volume Fraction Contour).

Figure 6.2 demonstrates that an increase in the liquid inlet velocity decreased the spacing of the drops, implying a higher droplet formation frequency from the nozzle. An increase in the liquid inlet velocity can also significantly increase the liquid ligament breakup length, indicating that an increase in the liquid inlet velocities and thus liquid inertial force will require a higher airflow shear-force to assist to break up the droplets. This also indicates that the location of the nozzle must be sufficiently away from the target surface for coating with quality drops and there will be a certain maximum liquid inlet velocity limit beyond which a continuous liquid spray jet will be produced. By reducing the droplet distancing, the nozzle can be placed closer to the target, preventing a change in the droplet trajectory which may be caused by undesirable forces such as the surface tension and gravity and increasing the overall transfer efficiency.

Diameter of droplets is another important parameter for production of quality droplets and coating as explained in the previous chapters. The droplet diameter ranging between 70 μm and 76 μm presented in Figure 6.2 is deemed acceptable for such purposes. Table 6.1 presents the magnitude of four dimensionless numbers, the Re, We, Oh and Ca, all based on the liquid flow and properties, as a function of liquid inlet velocity, 1, 3 and 5 m/s. Further extensive discussion on the scaling aspects of Figure 6.2 and Figure 6.3 will appear later in this chapter. For the rest of the study in this work, the liquid inlet velocity of 3 m/s was selected to achieve a suitable balance among all the parameters. Note that Figure 6.2 and Figure 6.3 results and Table 6.1 represent typical cases among other additional calculations made.

Table 6.1. Dimensionless numbers associated with cases provided in Figure 6.2.

Liquid inlet Velocity (m/s)	Re_l	We_l	Oh_l	Ca_l
1	24.88	0.35	0.02	0.01
3	74.64	3.12	0.02	0.04
5	124.40	8.67	0.02	0.07

6.1.1.2   Effects of Air Inlet Velocity

This section discusses the effects of air velocities on the liquid atomization process and the optimum air velocity on production of the quality droplets. To that end, the effect of a total of ten different air inlet velocities on the atomization process were calculated. Figure 6.3 presents the effects of typical five different air inlet velocities, 2.5, 5.0, 10, 15 and 20 m/s, with the fixed liquid velocity of 3 m/s in volume fraction counter on production of quality droplets. These five different air inlet velocities were selected since they can effectively represent the effects of the air inlet velocity on the atomization process and the characteristics of the generated droplets from the nozzle.

Although the introduction of air is thought necessary to break up droplets, the quality of the drops with the air velocity is frequently overlooked in the literature. Behavior graphs have been introduced in the literature in terms of non-dimensional numbers such as Reynolds number, whereas the air velocity is assumed to remain constant during many of the investigations. Even though the air inlet is generally necessary to help with the breakup phenomenon, the quality of the droplets is usually affected negatively by air inlets. Thus, reducing the air inlet velocity has merits in most cases for similar applications.
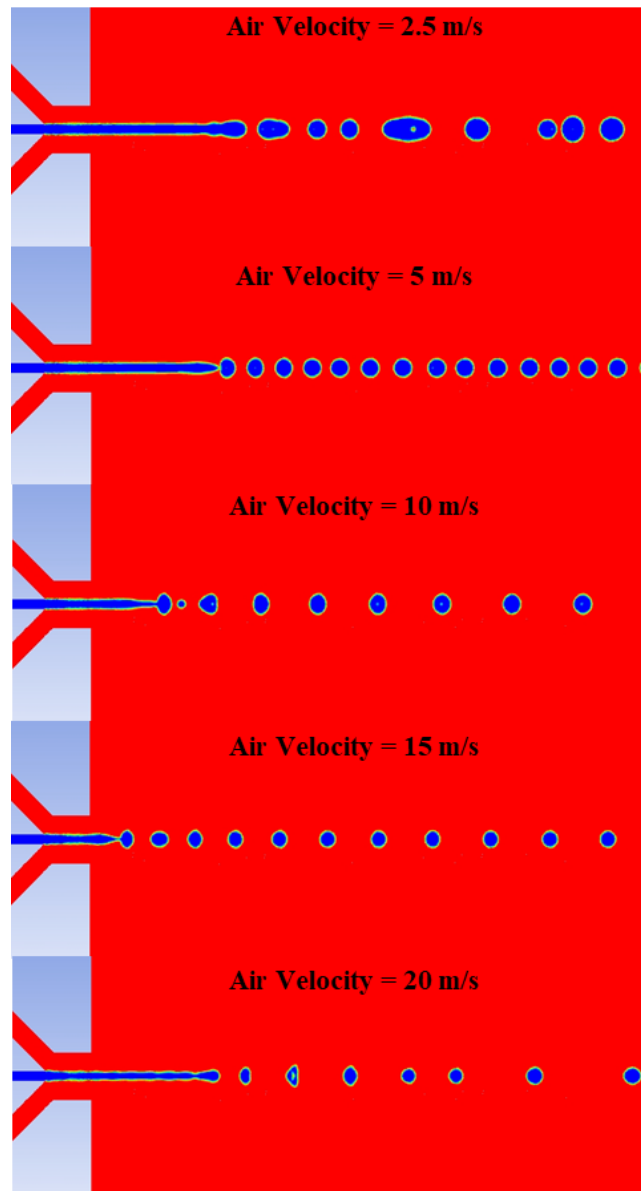
Figure 6.3 Effects of air inlet velocity on droplets' quality for five different air inlet velocities with liquid inlet velocity of 3 m/s (Volume Fraction Contour).

Figure 6.3 shows that an increase in the air inlet velocity decreased the ligament breakup length in lower air inlet velocities, possibly because the surface tension force of the liquid becomes stronger than the viscous force of the liquid in breaking up the droplets.

A reversed trend, however, was observed for air inlet velocities higher than 15 m/s as the liquid ligament breakup length increased with an increase in the air inlet velocity any further. The quality of the droplet stream was negatively affected for very high air inlet velocities and increased droplet shedding phenomena was observed, indicating the significance of identifying the optimum air inlet velocity which can be adjusted based on the nozzle shape, size and inlet liquid velocity. In this study, however, the nozzle's minimal air velocity that can help produce the monodispersed droplet stream was selected for the rest of the study.

Figure 6.3 also shows that droplet diameters decreased with increasing the air inlet velocity. Note that the droplet diameter increased from 65μm to 76μm whose changing range is acceptable as quality droplets, indicating that the ultrasonic pulsation atomizer can produced monodisperse droplets even without pulsation waves under the right working conditions. To keep the monodispersed and uniform droplet spacing, the optimum air velocity must be calculated to maintain the balance between the beneficial droplet diameter and the acceptable maximum droplet shedding and the air inlet velocity of 10 m/s was selected for the rest of this study. This 10 m/s air inlet velocity was effective in the droplet production phenomenon, but not 5 m/s or less, because the coalescence propensity of liquid drops is increased in higher viscous fluids requiring higher air velocities to overcome this tendency. Table 6.2 presents the four dimensionless numbers associated with data in Figure 6.3, the Re, We, Oh, and Ca, all based on the characteristic parameters of the inlet air whose definition was given in the chapter 5. Further detailed discussion on the significance of these non-dimensional numbers on the inkjet design will appear later in this chapter.

Table 6.2. Dimensionless numbers associated with cases provided in Figure 6.3.

Air inlet Velocity (m/s)	Re_a	We_a	Oh_l	Ca_a
2.5	62.2	2.17	0.02	0.03
5	124.4	8.67	0.02	0.07
10	248.8	34.69	0.02	0.14
15	373.2	78.05	0.02	0.21
20	497.61	138.75	0.02	0.28

6.1.1.3   Effects of Pulsation Frequency

Now that we know the nozzle under the current study can produce a mono-dispersed stream of droplets, the next step is to study the effects of liquid inlet pulsation on the performance of the liquid breakup and the characteristics of the generated droplets. For this purpose, a range of pulsation frequencies from 0 to 120 kHz were introduced to the nozzle and the quality of the droplets emanated from the nozzle were compared. Figure 6.4 demonstrates the results for a selective range of frequencies in terms of volume fraction contours, when the waveform was employed with a peak inlet liquid velocity of 3 m/s, inlet air velocity of 10 m/s and with a range of pulsation frequencies between 10 to 80 KHz. Figure 6.4 shows that the spacing between the droplets and diameter of droplets are significantly affected by the imposed pulsation frequencies, indicating the pulsation frequency as one of the significant parameters to control the size and spacing of the droplets.
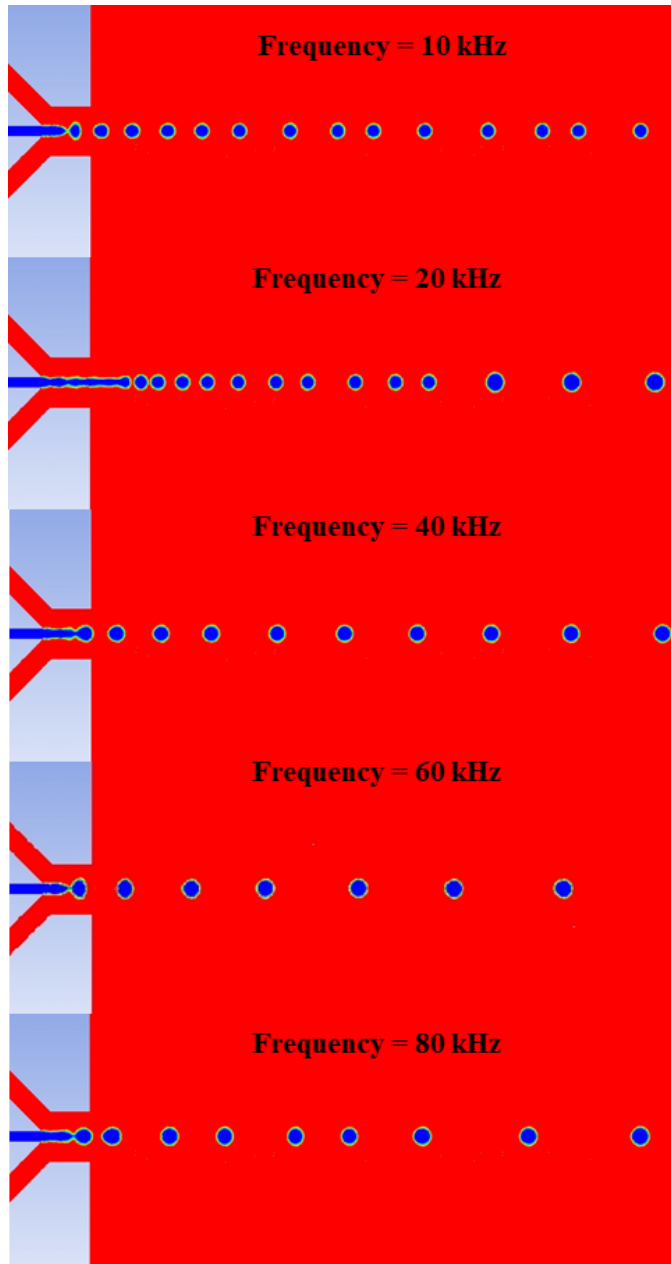
Figure 6.4 Effects of the pulsating frequency on the performance of the UPA nozzle and droplets' properties for air and peak liquid inlet velocities of 10 and 3 m/s (Volume Fraction Contour).

Figure 6.4 shows that by employing low frequency waves as the inlet velocity, the droplets became smaller in size and the frequency of generation is decreased. Comparison among three figures, Figure 6.2, Figure 6.3 and Figure 6.4, indicates that the ligament

breakup length decreased by employing low to medium frequency waves. The droplet sizes can be further decreased with an increase in frequency of pulsation for lower frequencies. There was, however, an optimum condition observed, at which the droplets' diameter was minimum and a further increase caused an increase in the droplet sizing. This behavior may well be due to coalescence of the liquid droplets at higher frequencies. The slight velocity difference between droplets and the short distance between each two consecutive drops, caused the coalescence to happen more and the droplets are merged, creating a larger mean diameter. This can also be seen by looking at the droplet distancing as it decreases up to the same point and then increases as the frequency increases further, resulted from the coalescence of the two consecutive droplets, which had a really short distance between them.

The observed trend is different from the liquid ligament breakup, which was continuously decreased until a certain frequency, depending on the inertial force of the liquid. The liquid ligament breakup stayed approximately the same after that frequency. A shorter breakup length was resulted from the fact that lower forces are required from the air stream as the pulsation was introduced. It caused the breakup point to move closer to the nozzle itself, which is a benefit since the pulsing wave allows the nozzle to be placed closer to the targeted surface increasing the transfer efficiency.

The droplet diameter ranged from 48 μm to 76 μm, presented in Figure 6.4, is a significant reduction in diameter in comparison to the results from Figure 6.2 and Figure 6.3, indicating that application of the pulsation to the nozzle rather than a constant liquid inlet velocity can significantly reduce the diameter of the droplets. Excessively high-frequency pulsations, however, can cause a negative undesirable shedding in the droplets

and may not reflect a consistent pattern in droplet distance or sizing. Interestingly, the author of this dissertation study experienced that the maximum pulsation frequency to obtain the uniform quality droplets was approximately 80 kHz for this current ultrasonic pulsation atomizer design.

Table 6.3 presents five dimensionless numbers associated with the data in Figure 6.4, the Re, We, Oh, Ca and Omega, all based on the characteristic parameters related to the liquid. It indicates the physical behavior of the flow independent of the nozzle specifications in comparison to Table 6.1 and Table 6.2 .

Table 6.3. Dimensionless numbers associated with cases provided in Figure 6.4.

Liquid Inlet Frequency (kHz)	Re_l	We_l	Oh_l	Ca_l	Omega
10	74.64	3.12	0.02	0.04	0.15
20	74.64	3.12	0.02	0.04	0.29
40	74.64	3.12	0.02	0.04	0.59
60	74.64	3.12	0.02	0.04	0.88
80	74.64	3.12	0.02	0.04	1.18

The current study shows that the inkjet nozzle can produce fine-quality and mono-disperse droplets without employing pulsation waves in a limited fashion. Introducing pulsation waves as additional parameters to the paint chamber, however, can enhance our capability to control the quality and attributes of the droplets. The performance can even be enhanced based on the properties required by choosing the right wave specifications to the nozzle.

The next step to assess the possibility of using this UPA for applications such as automotive coating and painting is to evaluate the performance of the nozzle with higher viscosity working fluids e.g. those similar to the viscosity of the actual paint used in this industry. As mentioned before, the exact data for the industrial paints is not easily available since they are kept under strict confidentiality. Even those that are available are generally outdated, but they still can provide a good benchmark to work with. Since the exact data is not available and this is a preliminary study to assess this possibility, a constant typical viscosity was selected to represent the high range viscosity for the rest of the simulations, which is about 10 times as viscos as normal working water.

6.1.1.4   Effects of Liquid Viscosity

In this section, the performance of the inkjet nozzle is studied when the viscosity of the working liquid was increased. A range of viscosities from the normal water viscosity up to 10 times the water viscosities were considered, and the results were compared. Figure 6.5 presents the results for this comparison in terms of volume fraction contours, when the constant liquid and air velocities of 3 m/s and 10 m/s are employed, and the liquid viscosity is changed from $1\mu_w$ to $10\mu_w$.
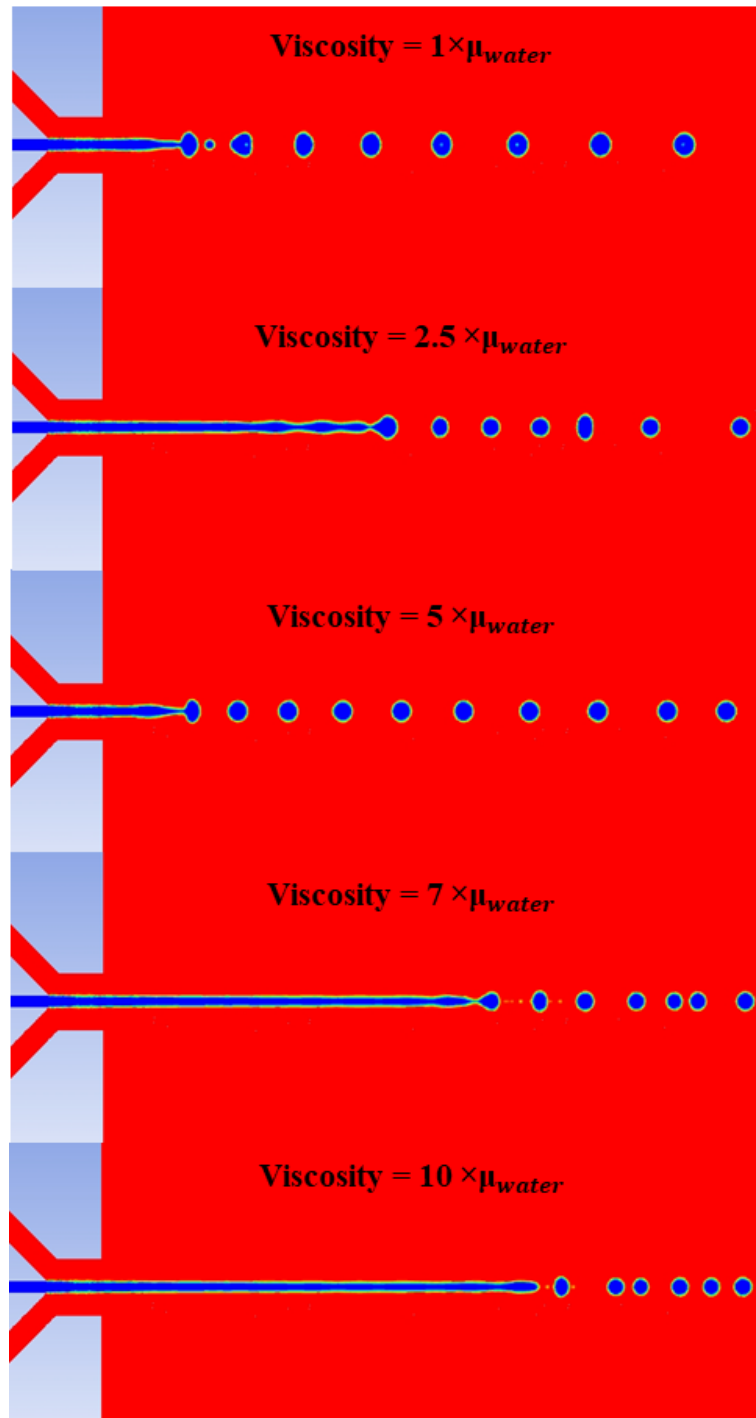
Figure 6.5 Effects of working liquid viscosity on the performance of the UPA nozzle without pulsation for liquids with up to 10 times more viscous than water for constant air and liquid inlet velocities of 10 and 3 m/s (Volume Fraction Contour). Figure 6.5 shows that when no pulsation was applied, increasing liquid viscosity

While using higher viscosity liquids to represent the working paint in automotive sectors, smaller droplet sizes can be a considerable advantage. This observation is slightly different for higher viscosity fluids as the droplets are accompanied with satellite droplets that can negatively affect the process. In addition, with an increase in working liquid viscosity, the spacing between consecutive droplets has decreased. This behavior is more likely due to high viscosity fluids' greater tendency to resist the surface tension force components between air and liquid, as well as breakup phenomenon. With working liquid viscosity, however, the ligament breakup length does not exhibit such straightforward patterns. The ligament breakup length increased with a rise in liquid viscosity for lower working liquid viscosities, closer to the viscosity of water. After that, the trend was shown to reverse to a liquid of five times of water viscosity. Then the same increasing behavior was observed again as the result of an increase in the fluid viscosity. This behavior shows that, depending on the application, this UPA can be operated at an optimal working state, such as requiring a higher or lower generation frequency or placing the nozzle closer or farther away from the targeted substrate. Note that the exact optimum conditions may be influenced by the air or inlet velocities as well. To ensure that the droplet sizes produced at this stage of the study are in the acceptable range, the droplet diameters for the cases showed in Figure 6.5 are measured and resulted in a diameter range of 58 μm and 86 μm.

Now that the design can work with higher viscosity fluids (at least up to $5\mu_w$) without the need for pulsation, the effects of pulsation frequency on the process can be numerically assessed. For this purpose, the performance of the nozzle was compared for two liquid viscosities of $5\mu_w$ and $10\mu_w$, each with and without pulsation and the results are presented below.
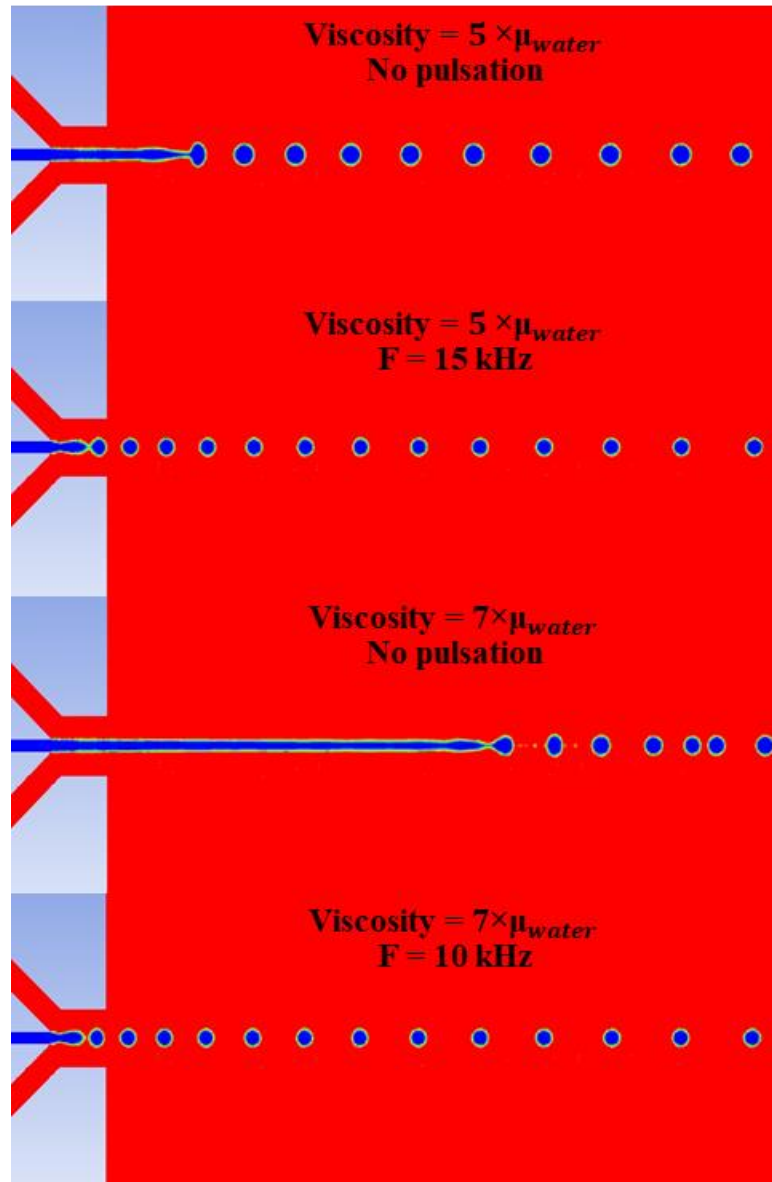
Figure 6.6 Effects of low frequency pulsation on the quality of droplets using high viscosity working liquid for air and liquid inlet velocities of 10 and 3 m/s (Volume Fraction Contour).

Figure 6.6 presents the volume fraction contours for the two cases mentioned above, where the constant liquid and air inlet velocities of 3 m/s and 10 m/s are employed to the nozzle. For the case with working liquid of $5\mu_w$, the frequency of 15 kHz was

selected, while for the case with working liquid of $7\mu_w$, the pulsation frequency of 10 kHz was selected. Note that multiple pulsation frequencies were tested for each case, however, only the results representing the lowest droplet diameter and the highest generation frequency were presented. Figure 6.6 shows that the quality of droplets emanated from the nozzle under low frequency pulsation was significantly improved. In addition, the introduction of pulsation helped to decrease the diameter of the droplets. Moreover, introducing the low frequency pulsation helped to atomize the working liquid of $7\mu w$ to produce a stream of monodisperse droplets.

Ligament breakup length is another parameter of interest to be studied for more viscous fluids, since it enables us to move the nozzle closer to the targeted substrate, which helps to increase the transfer efficiency. This positive trend was observed for all the cases studied in this work, while Figure 41 represents two cases. Higher frequencies of pulsation, however, did not show favorable results and qualities of droplets for higher viscosity fluids. With the pulsation of 10 kHz, the droplet diameter decreased to 55 μm for $5\mu_w$, while with the pulsation of 15 kHz, it decreased to 57 μm for and $7\mu_w$.

Table 6.4 presents the dimensionless numbers associated with the data in Figure 6.5 and Figure 6.6 to better relate them to the physical behavior of the flow independent of the nozzle specifications.

Table 6.4. Dimensionless numbers associated with cases provided in Figure 6.5 and Figure 6.6.

Liquid Viscosity ($\times\mu_w$)	Liquid Inlet Frequency (kHz)	Re_l	We_l	Oh_l	Ca_l	Omega
1	0	74.64	3.12	0.02	0.04	0
2.5	0	29.86	3.12	0.06	0.1	0
5	0	14.93	3.12	0.12	0.21	0
5	15	14.93	3.12	0.12	0.21	0.22
7	0	10.66	3.12	0.17	0.29	0
7	10	10.66	3.12	0.17	0.29	0.15
10	0	7.46	3.12	0.24	0.42	0

Overall, based on the findings shown, this model can produce a small mono-disperse stream of WB paint droplets if the right conditions are met. Furthermore, even without using waveform pulsations, the UPA design can produce quality droplets at higher viscosities, closer to the range of viscosities of working paints in the automotive coating industries for some cases.

Even though the qualitative results from this section can show promising evidence towards achieving the goal of this study, there is a need to assess the performance of such nozzles with different conditions using more quantitative methods. One of the best tools for conducting such studies is the scaling analysis technique. In this section, an extensive scaling analysis study was conducted to study the performance of a similar nozzle under

various working conditions. This would help predict the results from the atomization using a specific set of input conditions before conducting the actual experiments.

6.1.2 Behavior Diagram based on Scaling Analysis

After creating the numerical model and successfully simulating fluid dynamics of the droplet formation and transport behavior, it is interesting to numerically study the effects of all significant parameters that influenced this phenomenon (Masoud Arabghahestani et al., 2021). A traditional scale modeling approach to this task will be a well-designed experiment that can satisfy the accuracy of the numerical simulation and the seven assumptions employed in this section for the numerical model calculations.

This experiment is difficult as explained earlier, so a validated numerical model like the current one can do this task systematically, as it is explained in the following. First, we select a key parameter while keeping the rest of the parameters constant to numerically assess the effects of the key parameter on the fluid dynamics of the generated droplets. Then the key parameter will be changed to another parameter and repeat the numerical calculations by following the same procedure for another factor. There was a total of six key parameters (major forces) to be assessed in conjunction with the performance of the inkjet nozzle and the process of breaking up the liquid ligament as explained in the previous chapter.

These six different forces include: (1) the inertial force of air (F1), (2) the inertial force of liquid (F2), (3) viscous force of air acting on droplet surface (F3), (4) viscous force of liquid (F4), (5) surface tension force of liquid (F5), and (6) the dynamic pressure force (flow oscillation force) (F6) which causes oscillation of liquid flow. Applying the law

approach scale modeling theory (Emori et al., 2000), five independent non-dimensional numbers can be formed that are presented in equation (5-5) in the previous chapter. Using these five numbers plus Ca and St. numbers, the performance of the nozzle can be studied under various working conditions. To better present the results, we selected the following two cases; the first case, case 1, dealt with droplet generation with no pulsation, while the second case, case 2, dealt with the liquid flow with pulsation to generate the flow oscillations.

Case 1: The liquid flow without pulsation.

With this assumption, the Strouhal and Ω numbers will not affect the numerical calculations, and Case-1 is controlled by five pi-numbers: π_1 through π_4 as principal pi-numbers and the Ca number as auxiliary pi-number. Three different graphs, Re (π_3) vs. Ca, We (π_4) vs. Ca, and π_1 vs. π_2, were created to analyze the effects of the governing forces; the inertial force of air and liquid, the viscous force of air and liquid, and the surface tension force of the liquid.

Figure 6.7 and Figure 6.8 show that three principal pi-numbers govern the jetting process without oscillation and air inertial forces. As shown from the data in Figure 6.7, there is a maximum Re number for each Ca number with which condition the nozzle can generate a stream of monodispersed droplets. For example, suppose the viscous force is kept constant while increasing the Re number by increasing the inertial force of the liquid. In that case, the surface tension force of the working fluid needs to be changed not to produce satellite droplets. An increase in the Ca number decreases the maximum Re number, a maximum inertial force at which the breakup occurs. This figure also shows that

that the Ca number has less influence on the atomization process in higher Re number regions. Note that the range for which the nozzle can generate monodispersed droplet streams in higher Ca numbers is very narrow since the nozzle's performance decreases significantly for working liquids with higher viscosity. Figure 6.8 presents this information with a different scale. The Re-Ca graph can also be shown in a We-Ca graph since the surface tension was assumed to be constant.
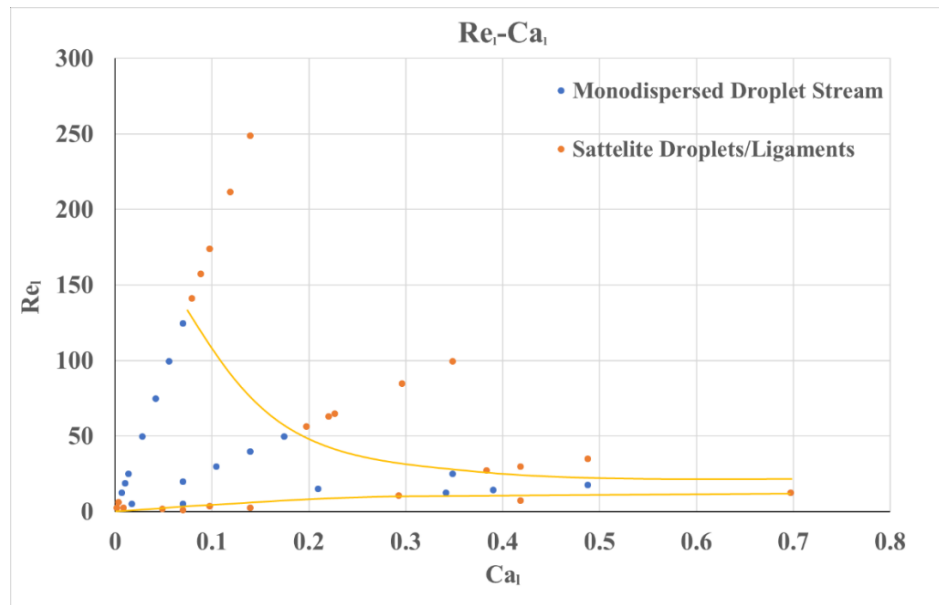
Figure 6.7 Jetting behavior diagram separating the regions with monodispersed droplet stream and satellite droplets droplet generation/ligament in terms of Re and Ca numbers.
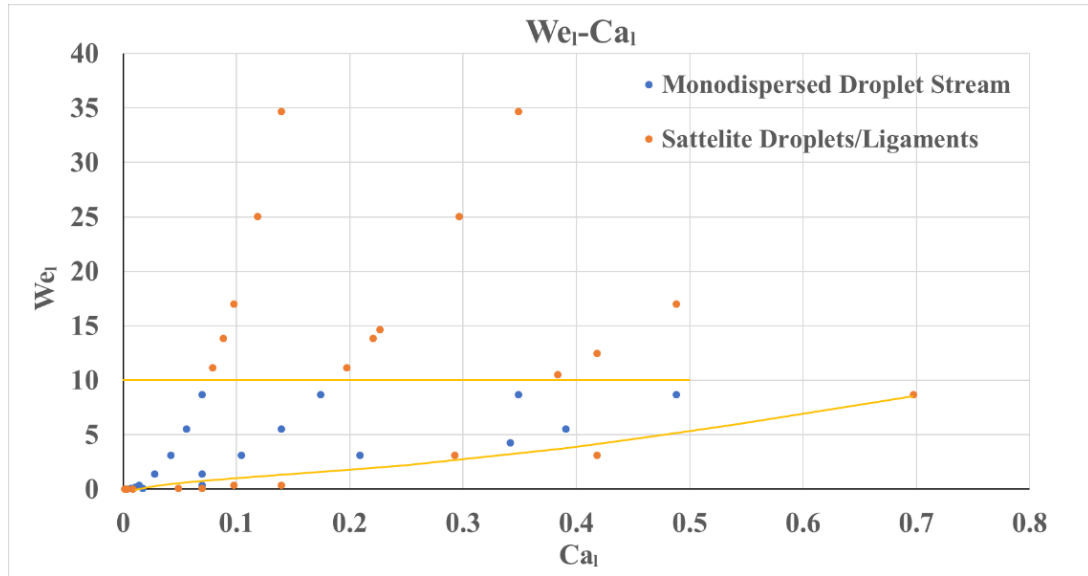
Figure 6.8 Jetting behavior diagram separating the regions with monodispersed droplet stream and satellite droplets droplet generation/ligament in terms of We and Ca numbers.

As mentioned before, shaping air can have significant influence on the quality of the droplets generated from the nozzle. Therefore, we focused on observing its effects for determining the ideal air velocity that allows for producing mono-dispersed droplet stream. The following section assesses the impact of shaping air velocity on the atomization process with two principal pi-numbers, π_1 and π_2, which count on the effects of the inertial force of the liquid, the inertial force of the air, and the viscous force of the air.

Figure 6.9 presents the jetting behavior diagram of the nozzle in terms of the two pi-numbers, π_1 and π_2. The liquid inlet velocity was changed from 0.5 m/s to 5.67 m/s, and the air velocity was changed from 0 to 20 m/s to study their effects on the atomization process, while the air and liquid viscosities, surface tension, and air and liquid densities were kept constant. Note that, it can be seen from the data in this figure that the nozzle is not capable of producing acceptable droplets without introducing shaping air to the nozzle, meaning $\pi_1 = 0$.

112

Figure 6.9, unlike Re-Ca and We-Ca graphs, shows a transition area boundary between the two regions as a solid line was not possible due to uncertainties in the atomization process and the numerical assumptions or simply due to the hardship of separating the quality of the droplets qualitatively. The data shows that for each specific π_2 number, there was a minimum and a maximum shaping air velocity to control the atomization process and ensure the generation of monodispersed drops. The minimum air velocity increases with an increase in the inertial force of the liquid. In contrast, the change in the maximum air velocity is much more significant. For higher liquid inertial forces, the production of quality droplets becomes less influenced by the shaping air, and the average shaping air velocity required to produce quality droplets is lower. There may be a minimum liquid inertial force to generate a droplet stream due to the nozzle surface's wettability effects.
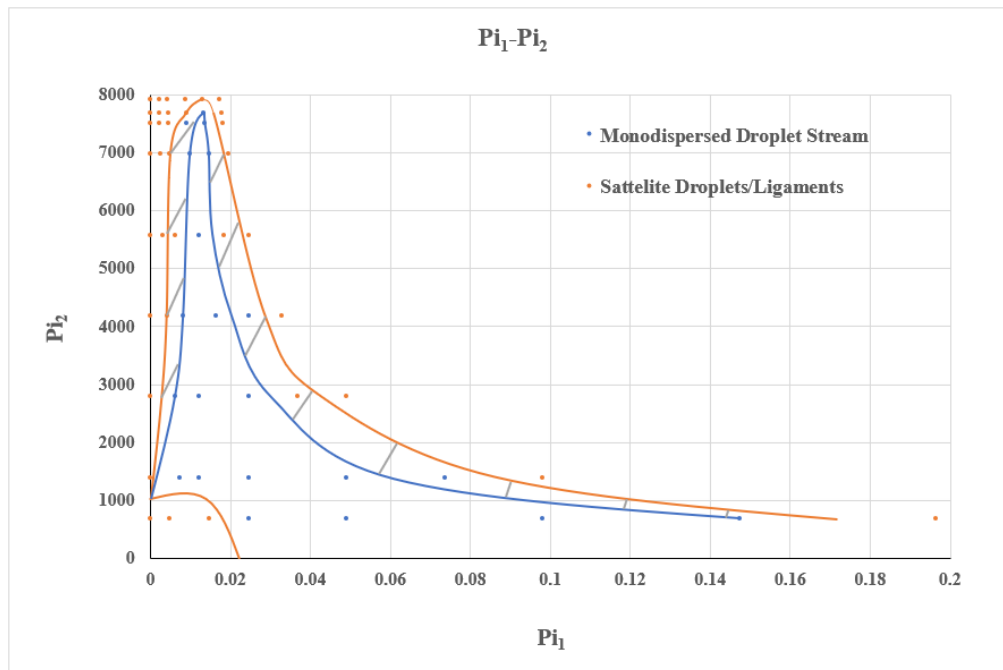
Figure 6.9 Jetting behavior diagram separating the regions with monodispersed droplet stream and satellite droplets droplet generation/ligament in terms of π_1 and π_2 numbers.

Case 1: The liquid flow with pulsation.

This case includes the form of sinusoidal waves in liquid inlet velocity and studies the effects of the pulsation frequency on the droplet generation process. Figure 6.10 shows Re (π_3) vs. St. The interactions among the inertial force of liquid, viscous force of liquid, and flow oscillation force were calculated by keeping all other forces constant. Figure 6.11 shows Re vs. Ω^2 (π_5), where the interactions of the inertial force of liquid, the viscous force of liquid, surface tension force, and flow oscillation force were calculated by keeping all other forces constant. These two figures present the jetting behavior diagram of the nozzle under the conditions that the air velocity, surface tension, liquid and air densities, and the geometric properties of the nozzle are constant, while the liquid inlet velocity was changed from 1 m/s to 5 m/s and the liquid viscosity from μ_w up to $10\mu_w$.

Figure 6.10 shows that there is a maximum St. number for each Re number for which the generation of uniform droplet stream is possible. The maximum frequency is relatively low for high Re numbers, while it increases with a decrease in the Re number. This data is useful to generate smaller droplets with relatively low liquid droplet speeds (i.e., low inertial forces of liquid). For very low Reynolds numbers (e.g., high viscosity working liquids such as industry paints), the range of frequencies that can be used is minimal as it can be seen for lower Re numbers in Figure 6.10 and Figure 6.11. This confirmed that generating droplets using higher viscosity working liquid was more challenging and required specific frequencies. Note that generation of monodispersed droplet stream was possible without frequency in most cases except when the viscosity was

very high ($7\mu_w$), for which there was a minimum frequency (10 kHz) required. Figure 6.11

shows this information in terms of Re and Ω^2. The data in the two graphs can easily be

converted to each other since the surface tension was assumed to be constant in all cases.
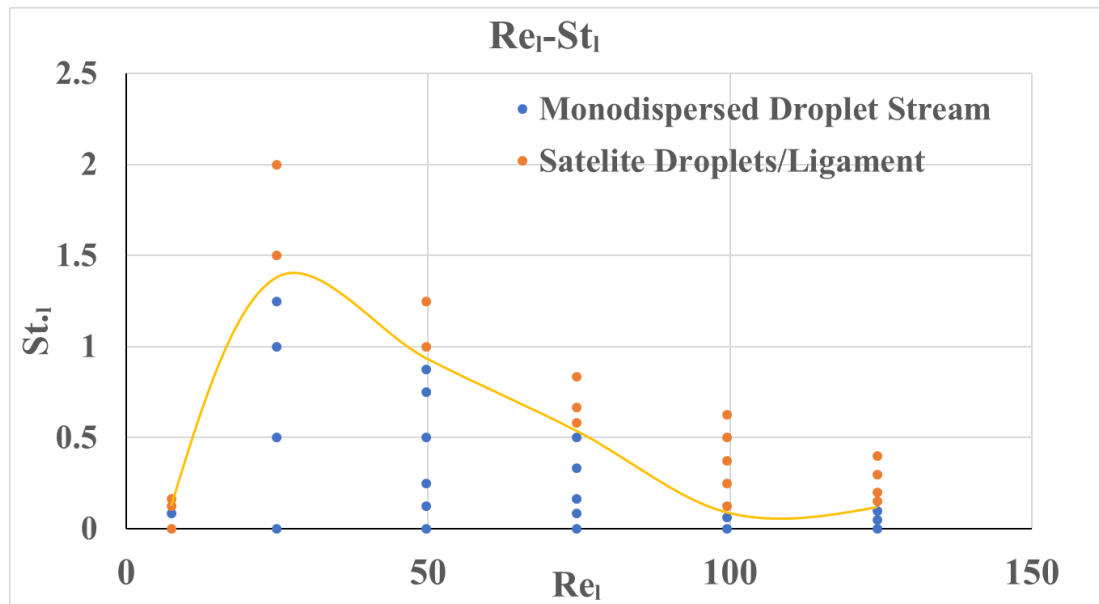
Figure 6.10 Jetting behavior diagram separating the regions with monodispersed droplet stream and satellite droplets droplet generation/ligament in terms of Re and St. numbers.
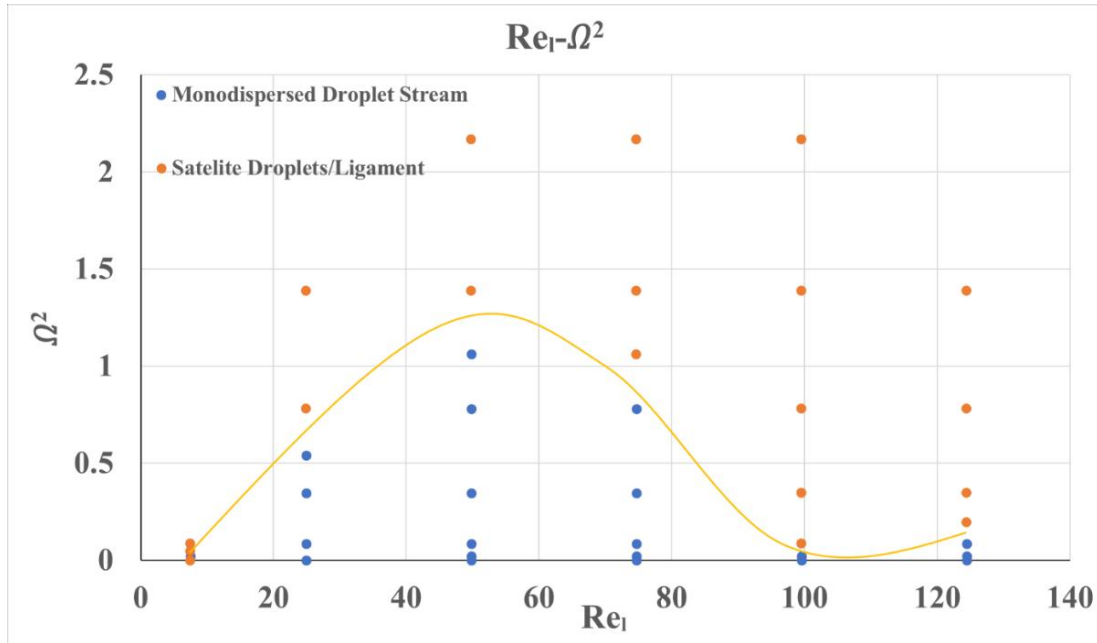
Figure 6.11 Jetting behavior diagram separating the regions with monodispersed droplet stream and satellite droplets droplet generation/ligament in terms of Re and Ω^2 numbers.

6.1.3   Summary of The Results

The effects of various influential parameters on the performance of the nozzle were analyzed in this section. These parameters include air velocity, liquid velocity, pulsation frequency, and the working liquid viscosity. The design was shown to be able to generate monodispersed droplets from normal water under various working conditions. In addition, addition of the pulsation to the nozzle offers a higher control over the droplets' characteristics and can reduce their size without decreasing the nozzle orifice diameter to deal with complications arising from the very small size nozzles. The frequency can also help with reducing the air velocity required to provide the additional force needed for liquid ligament breakup. The results from this section also showed that the design can work with liquids with much higher viscosities, especially those close to the viscosities of industrial paints, given the optimum conditions introduced to the nozzle.

6.2 Single-Piezo-Driven DOD (SPD) Inkjet Printhead

In this section, the main results related to the SPD inkjet printhead are presented and discussed. Using sinusoidal pulses to the piezo sensor, this model showed significant improvements in generating a stream of mono-dispersed droplets that can help achieve the main goal of this study. First, it is required to briefly summarize the assumptions, to neglect the least influential mechanisms, made for simplicity of the CFD modeling and reducing the computation load of the studies. The main numerical assumptions are similar to those used for the UPA model and they are listed in the following as well:

1. The internal liquid and air flows are laminar.

2. All the phenomena are axisymmetric.

3. Airflow is treated incompressible due to low Mach number.

4. The liquid transport properties are constant.

5. Atomization occurs at atmospheric conditions.

6. Evaporation of the liquid ligament and droplets is neglected throughout the simulations; thus, the energy equation was left out of the simulations. This assumption is due to the fact that the flow time scale is much faster than the liquid heat transfer time (for the estimate, see the assumptions for UPA nozzle).

7. The fluid in the CFD modelling is water (or water-based liquid under a special condition).

8. The computational model was assumed to be 2-D for the first steps of this work. The results can later be presented in 3D levels using the post-processing tools available in ANSYS FLUENT, due to the characteristics of the problem.

Similar to the previous model, the first step is to generate a 2D domain that can represent the inkjet printhead accurately, given the assumptions listed above. A high-quality computational grid needs to be created on this 2D domain afterward to be used in ANSYS FLUENT software. Figure 6.12 illustrates this computational domain and the computational grid that are generated and used for the rest of the work in this section. The grid encompasses the relevant region inside the inkjet nozzle system (from the actuator to the nozzle orifice), and 0.5 mm and 0.25 mm in the axial and radial directions outside the nozzle, respectively. More cells are generated in regions with higher intensity gradients in order to reach higher accuracy and capture the real physics with a higher precision. These regions include the area around the trajectory of the droplets (axis of the computational domain), regions close to the nozzle orifice, anywhere that there is a sharper change in the geometry of the nozzle and the area near the piezo sensor. The smallest grid edge size employed is 27.2 microns in size. Various grid setups were generated to accurately capture the physics that control the phenomenon. To ensure the grid independency of the model, we found that a total of 45,787 cells were necessary to provide the results presented in this work with acceptable accuracy.
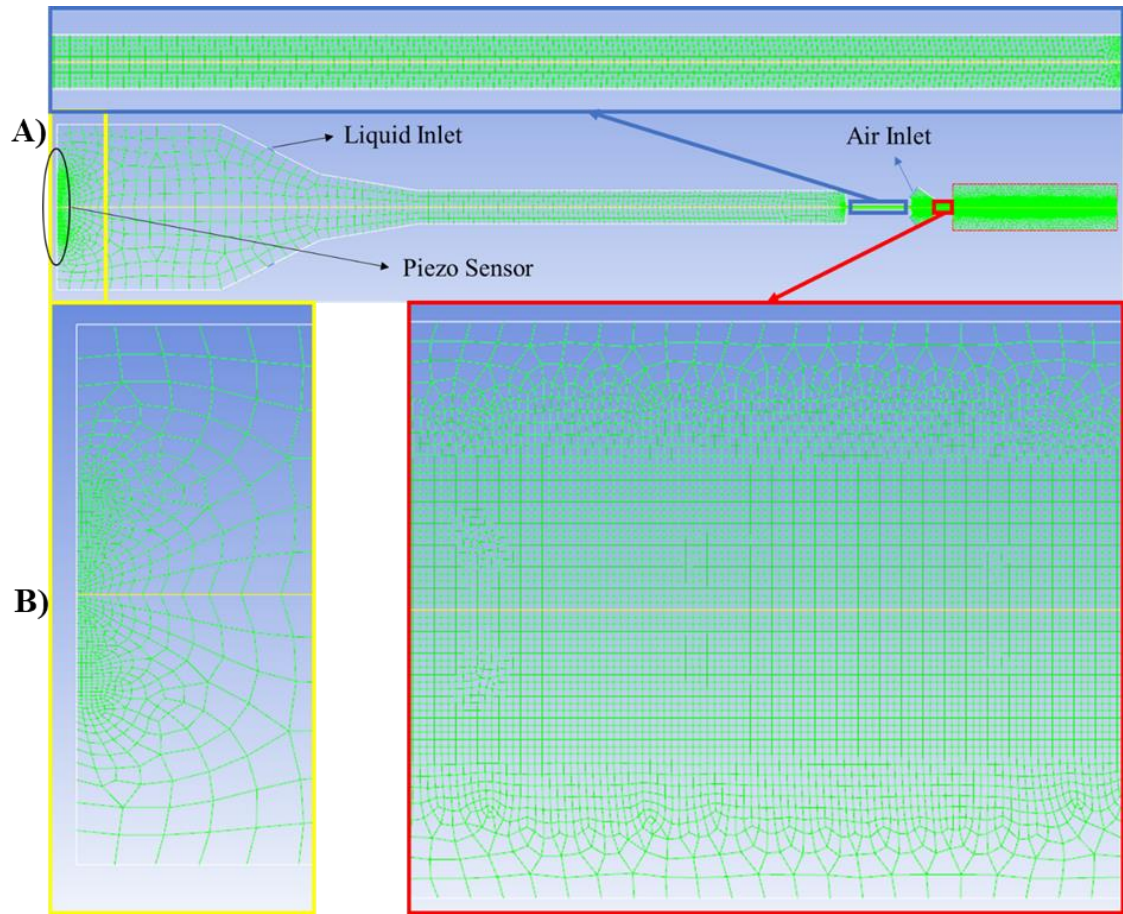
Figure 6.12 A) Overall view of the grid generated for the SPD numerical model. B) Illustration of the smaller and finer cells generated for regions with higher gradients.

No-slip boundary condition was employed for all the solid boundaries. A wet contact angle (an acute angle) was imposed inside the nozzle, where the liquid is flowing, and a non-wet contact angle (an obtuse angle) was used for all other solid boundaries. A constant velocity was imposed on the air inlets and the liquid velocity was adjusted in a way that the pressure inside the paint chamber stays constant throughout the simulation. The movement of the piezo sensor was introduced to the software using a UDF script that defines the velocity of the transducer in terms of time to test the effects the piezo on the

generated droplet. The following equation presents the equation of motion for the piezo transducer over time.

$$U_A(t) = U_{A_{max}} Sin(2\Pi f t) \tag{6-2}$$

Where, $U_{A_{max}}$ is the maximum velocity of the piezo sensor and f_A is the frequency of the movement. It is worthy to mention that the movement of the piezo sensor is modeled using a rigid body movement script. Since the movement of the piezo sensor changes the structure of the model in its vicinity, the generated mesh needs to be modified after each time step. However, since the movement of the piezo sensor was only horizontal, the dynamic mesh option can be employed to adjust the mesh in that region throughout the simulation with enough accuracy. Thus, a dynamic mesh option using only layering feature was employed to follow the movement of the piezo sensor after each time step. Note that a few tests were conducted to monitor the fineness of the grid using various grid modification models and it was found that using more simplistic models suffice to capture the phenomena in that vicinity with acceptable accuracy.

Finally, a pressure outlet boundary was imposed to model the environment outside the computational domain and the paint chamber needs to be filled with paint entirely at the beginning of the simulation. For this purpose, the zone inside the paint chamber was patched with the liquid at t = 0 which is the only initial condition that needed to be defined.

After creating the numerical models and computational grid, effects of various factors on the quality of the generated droplets can be investigated. The droplet characteristics that are the targets of this study are droplet diameter, distance between each pair of droplets (frequency of generation), ligament breakup length and the possibility of

satellite droplet generation. If these parameters can be kept at optimal conditions, the nozzle will be capable of producing more controllable droplets and thus, achieving a higher transfer efficiency in the process. Note that the range of air inlet velocities for this design needs to be determined, assuming that the nozzle has an acceptable performance (able to generate a stream of mono-dispersed droplets) to be able to further study the effects of liquid properties and assess the performance of the nozzle with water-based paints. In the following section, the effects of different working factors on the characteristics of the droplets are investigated.

6.2.1   Effects of Air Inlet Velocity

This section studies the effects of air velocity on the performance of the nozzle with the pulsation frequency of 40 kHz for the piezo sensor. The air velocity was changed from 0 m/s to 20 m/s to obtain an acceptable range of the air velocity to be used for the rest of this study. Figure 6.13 shows effects of the air inlet velocity on droplets' quality for five different air velocities in volume fraction contour for the piezo displacement of 0.034 μm and frequency of 40 kHz. The lower air velocities are usually preferred to control droplet properties in a certain way although there is a minimum air velocity to maintain the droplets' kinetic energy that is required to carry them towards the targeted substrate. Therefore, the preferred air velocity needs to be found considering the balance between these two factors.
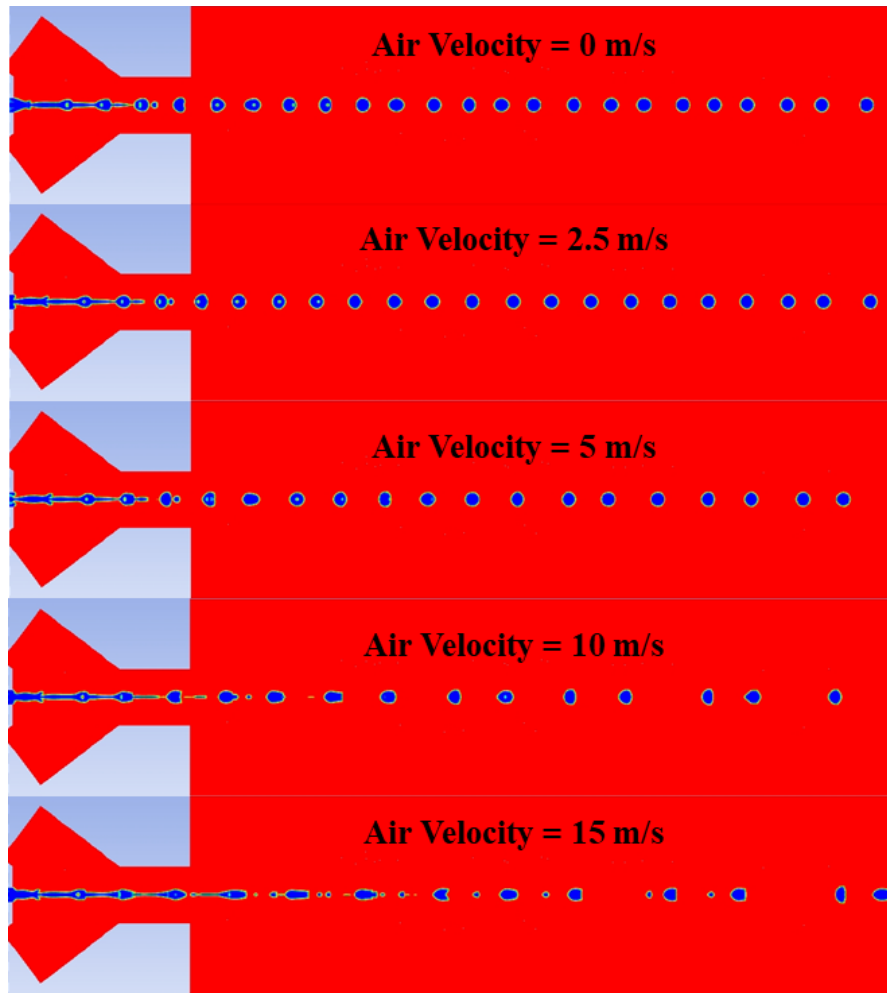
Figure 6.13 Effects of the air inlet velocity on droplets' quality for five different air velocities with piezo displacement and frequency of 0.034 μm and 40 kHz (Volume Fraction Contour).

Figure 6.13 shows that the air velocity does not significantly influence the droplets' characteristics unlike for the UPA model. That is because for low to medium air velocities, the droplets' kinetic energy mainly comes from the piezo sensor; and to affect the droplets, higher air velocities are required. The SPD-DOD model, unlike UPA model, can produce a stream of monodispersed droplets even without introducing the air velocity, and can increase the kinetic energy of the droplets. Note that the gravity effect is neglected in these

simulations and this gravity can have more significant effects in the absence of the shaping air.

Figure 6.13 also shows that higher air velocities increase the probability of satellite droplets and oddly shaped droplets. Very high air velocities increase the droplet size slightly and produces the more oval-shaped droplets and non-uniform sizes drops. Overall, the air velocity does not present significant effects on the droplets unless for very high velocities. Since the droplets were the most uniform and with kinetic energy deemed to be more favorable for the case with air velocity of 5 m/s, this velocity was considered for the rest of the studies in this section unless otherwise is stated.

6.2.2   Effects of Piezo Sensor Displacement

The piezo sensor displacement is usually very limited, depending on the commercial piezo transducer at-hand. It is worthy to understand the effects from this displacement on the performance of this model to select the right piezo sensors, which are available in the market. Figure 6.14 shows the effects of piezo displacement in volume fraction contour on the performance of the nozzle with piezo frequency of 50 kHz and air velocity of 5 m/s.
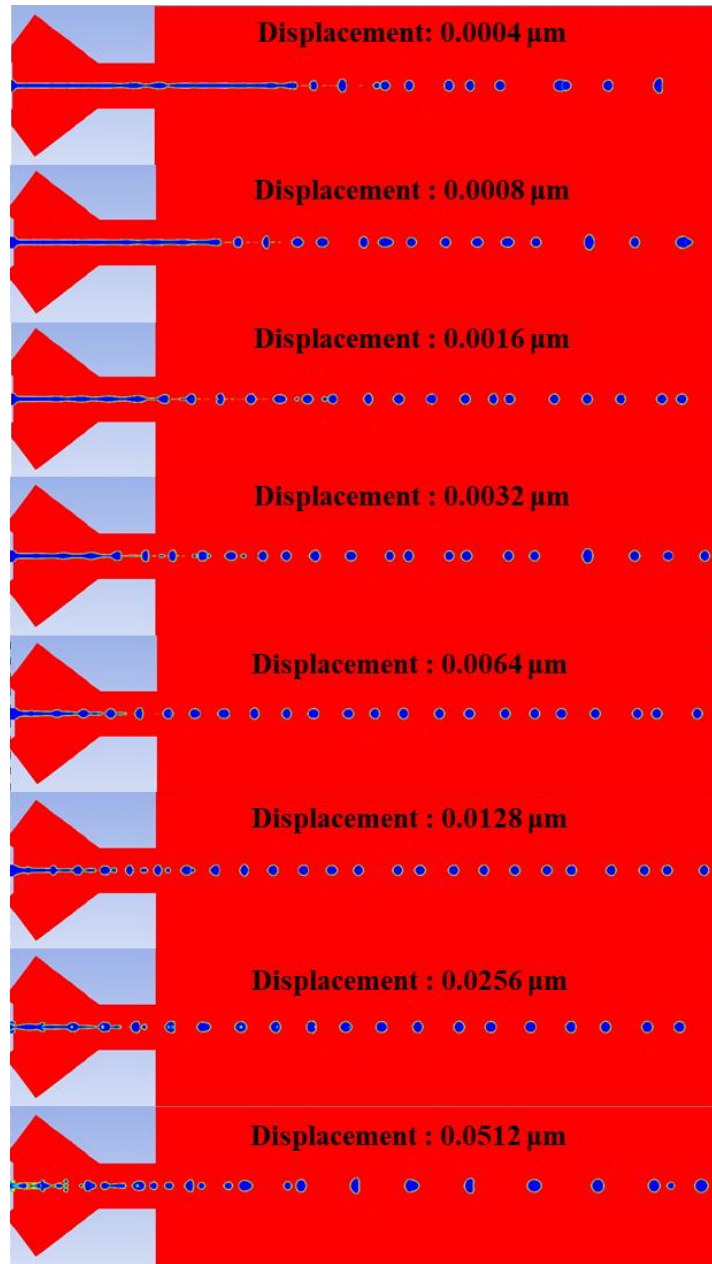
Figure 6.14 Effects of piezo displacement on the performance of the nozzle with piezo frequency of 50 kHz and air velocity of 5 m/s (Volume Fraction Contour).

Figure 6.14 shows that for lower piezo displacements, the droplet coalescence was occurring, and because of this reason, long tailed liquid ligaments are created before their breakup. With an increase in the displacement, this long-tailed ligaments disappeared.

124

There is a range that the nozzle was capable of generating a stream of mono-dispersed droplets with no negative effects such as satellite droplets or droplet coalescence.

Performance of the nozzle depends on other factors such as the frequency, but the effects of the piezo displacement are expected to stay relatively similar for different working conditions. To obtain the range for the piezo displacement for the nozzle that can lead to acceptable droplets for the targeted application, preliminary numerical calculations were made to get a better idea about these effects, however, these results are not presented here due to its preliminary nature. A noteworthy point: effects of the piezo displacement and piezo frequency are not independent, and this graph could be slightly different for another range of piezo frequencies.

6.2.3   Effects of Piezo Frequency

This section is devoted to studying the effects of one of the most important factors on performance of the nozzle, the piezo sensor frequency. The air velocity was assumed to be constant at 5 m/s and both the piezo displacement and frequency were changed to study the droplets' characteristics. The reason for changing the piezo displacement at the same time with the piezo frequency was to keep the maximum velocity of the piezo motion constant, since it controls the volume flow rate of the paint that is pushed towards the nozzle orifice due to the movement of the piezo transducer. Figure 6.15 shows effects of piezo frequency in volume fraction contour on the performance of the nozzle with air velocity of 5 m/s for five different values of piezo displacement and frequency.

125
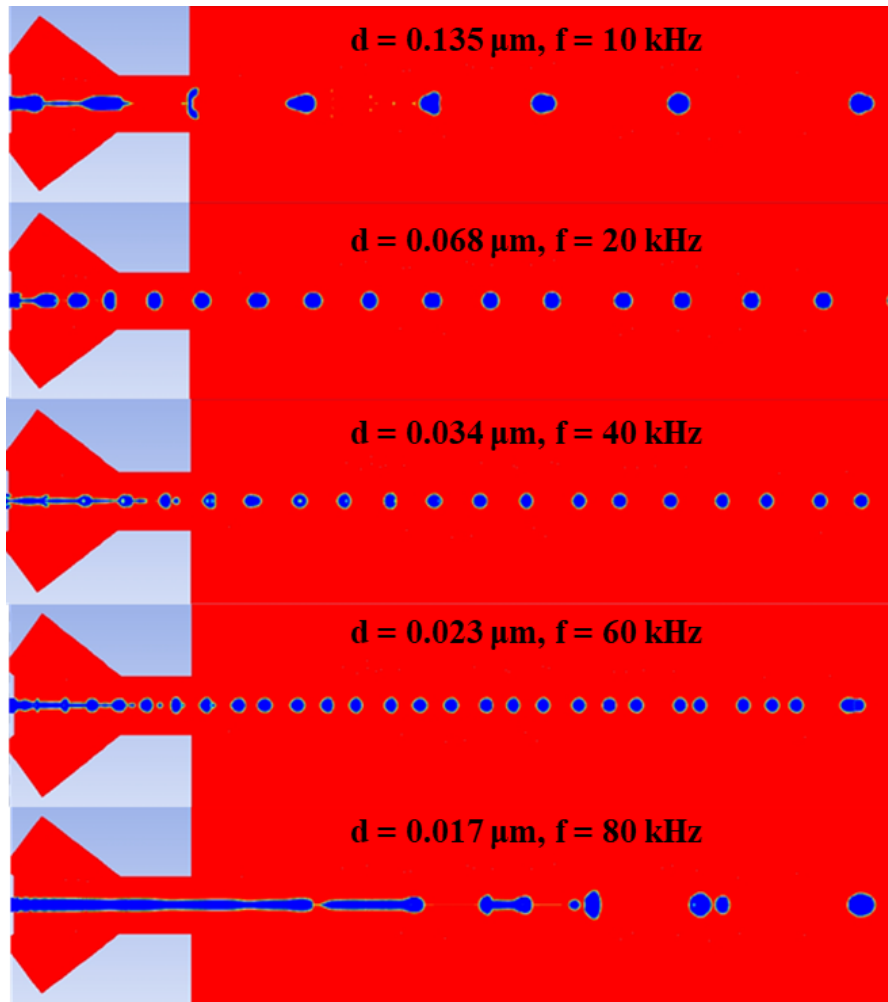
Figure 6.15 Effects of piezo frequency on the performance of the nozzle with air velocity of 5 m/s (Volume Fraction Contour).

As can be seen in Figure 6.15, increasing the frequency, until 60 kHz, improved the quality of the droplets generated from the nozzle. This includes reducing the ligament breakup length, decreasing the droplet diameters, spacing, and even improving the shape of the drops e.g. ensuring close to uniform sphere-shaped droplets as the result. These results were expected since with an increase in the frequency, the kinetic energy of the droplets also increased, providing the energy required to overcome the surface tension force to break the ligament faster. As the result, the smaller diameter droplets were

produced. For very high frequencies such as 80 kHz, however, the droplets were mostly erratic and there was a higher chance for droplet coalescence, due to the overpowering kinetic energy from the piezo transducer. This will increase the chance of non-uniform or satellite droplets, thereby decreasing the quality of the droplets. The above results may be different for nozzles whose working conditions are different, however, the trend is likely the same when the selected working parameters are within the range of producing monodispersed droplets.

6.2.4   Effects of Liquid Viscosity

Figure 6.16 shows the effects of the liquid viscosity on the performance of the nozzle and the quality of the drops. For this study, the goal is to find out how well the nozzle can work with higher viscosity fluids, especially those closer to the industrial paint's viscosity. For this purpose, the air velocity and piezo frequencies were selected to be those that we observed the best nozzle performance for the nozzle; frequency of 40 kHz and air velocity of 5 m/s. Performance of the nozzle depends on other factors, as it was mentioned before, and thus the droplets may be different for different frequencies or piezo displacements for the same viscosity. However, this graph is meant to provide an example of the performance and show that the nozzle is capable of working with higher viscosity fluids as well.
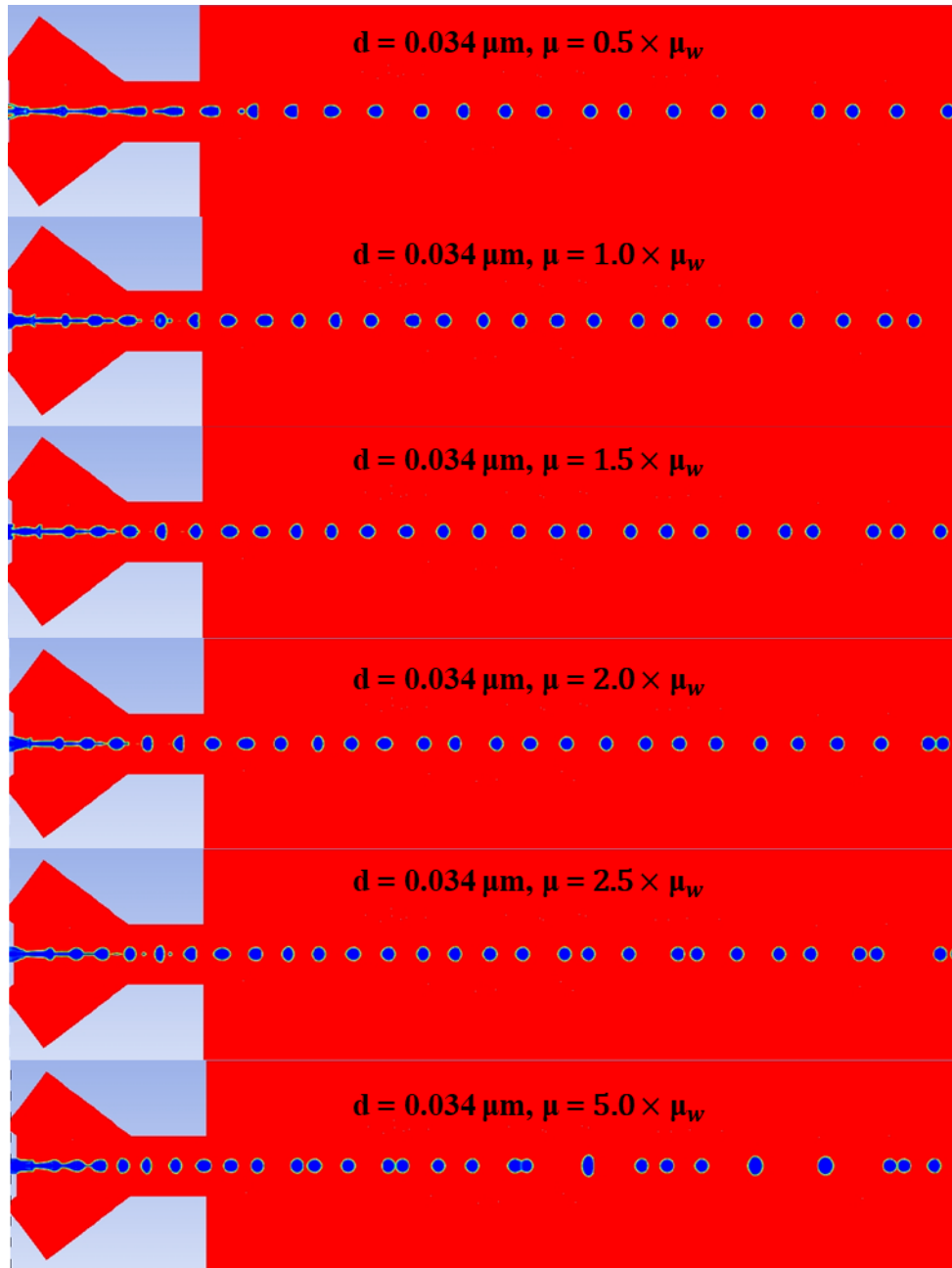
Figure 6.16 Effects of liquid viscosity on the performance of the nozzle with air velocity of 5 m/s and piezo frequency of 40 kHz (Volume Fraction Contour).

As it can be seen from this data, the nozzle was capable of performing the atomization with generating a stream of monodispersed droplets as the result for working liquids of up to $2.5 \times \mu_w$. This maximum viscosity was lower than what we observed for

UPA, however this design can provide higher degrees of control over the droplets'
properties. For example, this design offers a better control to decrease the droplet diameters
even further and with the help of the pulsation frequency, it can generate the desired
droplets with lower air velocities, which is an important feature of this design. In addition,
with further modification to the model, it may be capable of working with even higher
viscosity fluids, which will be presented in the following section. Note that the optimum
working conditions for the nozzle are expected to provide a higher margin for the
maximum viscosity that the nozzle can work with. However, to better analyze this goal,
extensive numerical and experimental tests are required in the future.

6.2.5   Summary of the results

The effects of various influential parameters on the performance of the nozzle were
analyzed in this section. These parameters include air velocity, piezo maximum
displacement and frequency and the working liquid viscosity. The design was shown to be
able to generate mono-dispersed droplet stream from normal water with lower air velocities
even without piezo pulsation. This is especially important knowing that higher air
velocities are known to affect the quality of the droplets and/or their trajectory in a negative
way in automotive painting and coating section. Thus, reducing the minimum air velocity
that the nozzle can work with has exceptional merits for these applications. In addition,
this design was observed to provide a higher degree of control over the characteristics of
the droplets which can be a perfect tool for the applications of target for this dissertation.
Lastly, the nozzle was shown to be capable of producing high quality droplets from higher
viscosity working fluids to some degree that is the first step to ensure that the nozzle can

129

be used for atomizing the industrial degree paints used in automotive painting and coating sections.

6.3 Double-Piezo-Driven DOD (DPD) Inkjet Printhead

This section presents results and discussion on the DPD inkjet printhead. The working concept of DPD-DOD is similar to the SPD-DOD nozzle concept. The only difference is that DPD-DOD has an additional piezo sensor to assist breaking up high viscous liquids. For the DPD-DOD, the piezo sensor used for SPD-DOD is kept in the same location and a new piezo sensor which operates perpendicular to the first piezo sensor is added inside the nozzle (not inside the paint chamber). These two piezo sensors will be operated by different sinusoidal pulses and the equations for these pulse waves will appear later in this section. The assumptions employed for DPD-DOD model calculations are essentially the same as the ones used for the UPA and SPD models, but they are restated below for the convenience of readers.

1. The internal liquid and air flows are laminar.

2. All the phenomena are axisymmetric.

3. Airflow is treated incompressible due to low Mach number.

4. The liquid transport properties are constant.

5. Atomization occurs at atmospheric conditions.

6. Evaporation of the liquid ligament and droplets is neglected throughout the simulations; thus, the energy equation was left out of the simulations. This assumption is due to the fact that the flow time scale is much faster than the liquid heat transfer time (for the estimate, see the assumptions for UPA nozzle).

7. The fluid in the CFD modelling is water (or water-based liquid under a special condition).

8. The computational model was assumed to be 2-D for the first steps of this work. The results can later be presented in 3D levels using the post-processing tools available in ANSYS FLUENT, due to the characteristics of the problem.

The first step, which is similar to the previous SPD-DOD model, is to generate a 2D domain that can represent the inkjet printhead accurately, under the assumptions listed above and the general working concept of the nozzle. A high-quality computational grid needs to be created on this 2D domain for the use of ANSYS FLUENT software.

Figure 6.17 illustrates this computational domain and the computational grid that are generated and used through the rest of this section. The grid encompasses the relevant region inside the inkjet nozzle system (from the actuator to the nozzle orifice), that is, 0.5 mm in the axial direction outside the nozzle, and 0.25 mm in the radial direction outside the nozzle. The rest of procedures share exactly the same steps explained in the section 6.2 SPD-DOD inkjet printhead on pages 128 and 129 and not repeated here.
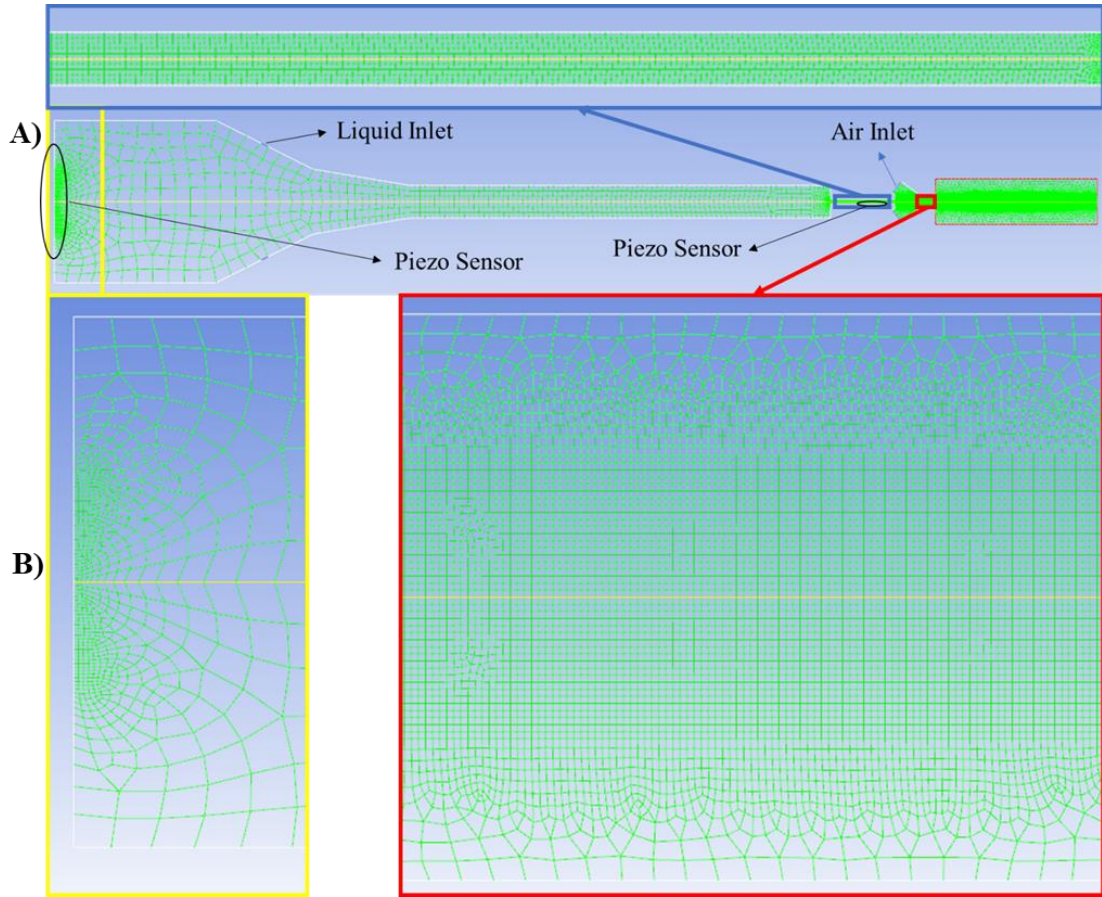
Figure 6.17 A) Overall view of the grid generated for the DPD numerical model. B) Illustration of the smaller and finer cells generated for regions with higher gradients.

The movement of the piezo sensors was introduced to the software using a single UDF script that would define the velocity of the transducers in terms of time to test the effects the two piezo sensors on the generated droplets. For the ease of understanding, the first piezo sensor is called actuator and the second piezo is called piezo sensor for the rest of this section. The following equation presents the equations of motion for the piezo transducers over time.

$$U_A(t) = U_{A max} Sin(2\Pi f_A t) \tag{6-3}$$

$$V_p(t) = V_{P_{max}} Sin(2\Pi f_P t)$$

Where, $V_{p_{max}}$ and $U_{A_{max}}$ are respectively the maximum velocity of the piezo sensor and the actuator, and f_P and f_A are respectively the frequency of the movement for piezo sensor and the actuator. The only difference between the movements of the piezo sensor and the actuator, is the direction of the movements; the piezo sensor moves along the y axis, while the actuator moves along the x axis. The movements of the two transducers are modeled using a rigid body movement script.

The generated mesh needs to be modified after each time step, since the movement of the sensors changes the structure of the model in their vicinities. The dynamic mesh option can be employed to adjust the mesh in that region throughout the simulation, since their movements were simple and along only one axis. Tests conducted to monitor the fineness of the grid using various grid modification models found that rather simplistic models suffice to capture the phenomena in that vicinity with acceptable accuracy. In addition, a pressure outlet boundary was imposed to model the environment outside the computational domain. Lastly, the paint chamber needs to be entirely filled with paint at the beginning of the simulation, so that the zone inside the paint chamber was patched with the liquid at t = 0, the only initial condition that needed to be defined.

After creating the numerical models and computational grid, effects of various factors on the quality of the generated droplets can be investigated. The droplet characteristics that are the targets of this study include droplet diameter, distance between each pair of droplets (frequency of generation), ligament breakup length and the possibility of satellite droplet generation. If these parameters can be kept at optimal conditions, the

nozzle will be capable of producing more controllable droplets, and thus, achieving a higher transfer efficiency in the process. The range of air inlet velocity for this design needs to be determined, assuming that the nozzle is able to generate a stream of mono-dispersed droplets. It is required to further study the effects of liquid properties and assess the performance of the nozzle with water-based paint. The air velocity had the same exact effects on the droplets as the DPD design is very similar to SPD nozzle, thus, the air velocity was assumed to be 5 m/s for the rest of the study in this section (the same as for the SPD nozzle). The following section investigates the effects of different working factors on the characteristics of the droplets.

6.3.1 Effects of The Printhead's Working Conditions on the Droplets

Both SPD-DOD and DPD-DOD designs are constructed based on many different parameters. The effects of each parameter on the performance of each design require an independent numerical parametric study including a constrained case when only the limited piezo sensors are available. To that end, the performance of each nozzle with normal water as the working liquid in the nozzle needs to be analyzed. Considering the tests from the previous section and the similarities in the design for these two inkjet nozzles, the air velocity, 5 m/s, was applied for numerical tests, the liquid velocity was adjusted to keep the inside chamber pressure stay constant, and the maximum velocities of the piezo sensors were assumed to be the same for all the tests conducted in this section.

Figure 6.18 shows the effects of the two piezo sensors' characteristics on the performance of the nozzle and the optimum working conditions, where, d_A and d_P. are respectively the maximum displacements for the actuator and the piezo sensor.
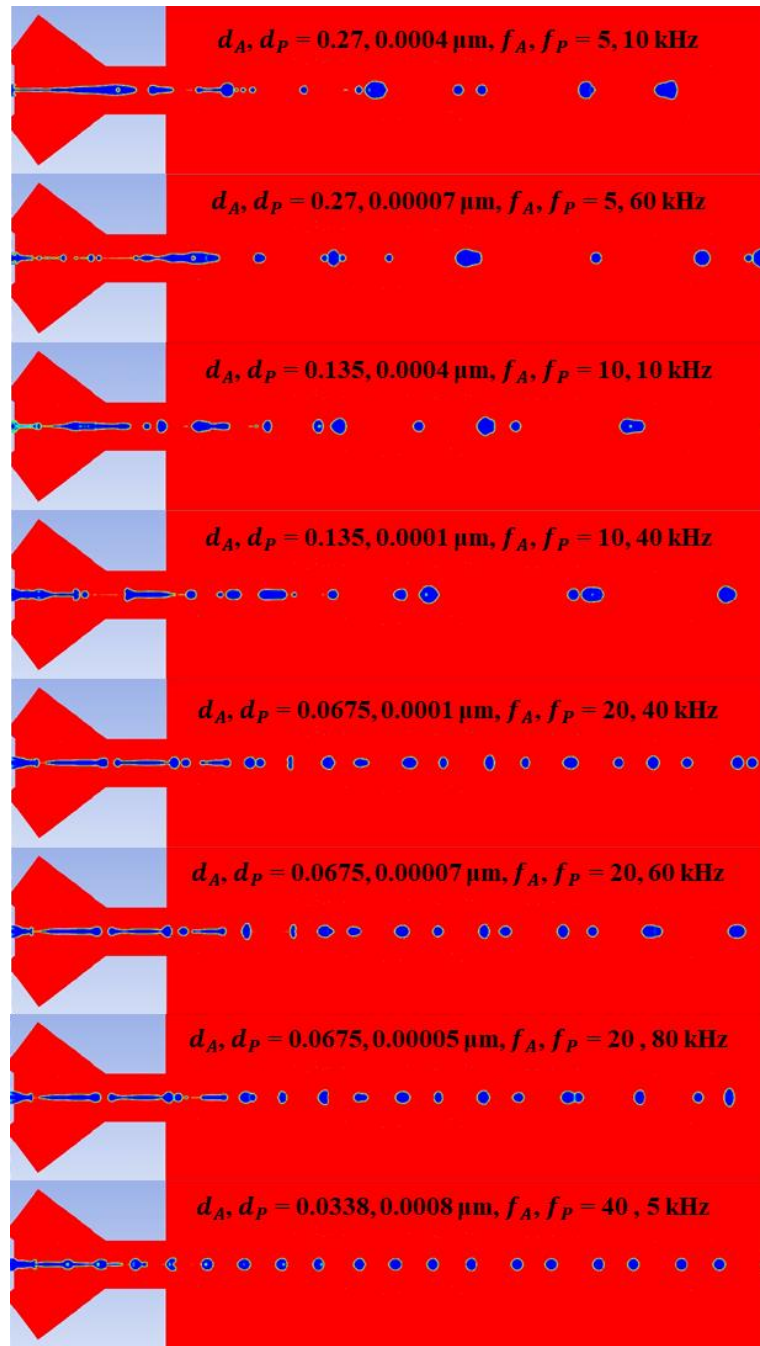
Figure 6.18 Effects of the eight different piezo characteristics in volume fraction contour on the performance of the nozzle (Volume Fraction Contour).

Figure 6.18 clearly indicates the actuator frequency to be the main factor to control the generation of uniform droplets from the nozzle, while the piezo sensor's frequency is a minor factor. Note that this piezo sensor can still provide more control for some cases to

135

change the outcome of the atomization process. Figure 6.18 shows that the nozzle can produce acceptable-range-diameter droplets for higher actuator frequencies (e.g., $f_A = 40$ kHz which was shown to be the best performance for the previous model), even with relatively low piezo frequencies.

It would be beneficial to investigate the effects of the piezo sensor and why it may add more favorable controls over the droplet's characteristics for the targeted industrial applications. Figure 6.19 presents the effects of the piezo sensor frequency on the performance of the nozzle for $f_A = 40$ kHz, and Figure 6.20 presents the same effects for $f_A = 60$ kHz. Figure 6.19 and Figure 6.20 show that with an increase in the piezo sensor's frequency for a specific actuator's frequency, only a mild effect compared to the effect of actuator, appeared on the droplets' size, but assisted the liquid ligament breaking up process. Figure 6.20 shows the liquid ligament breakup decreased slightly with an increase in the piezo sensor's frequency. An increase in the piezo sensor's frequency to very high values will have negative effects, as can be seen in the last test in Figure 6.19, such as generation of satellite droplets and droplet's coalescence, which shares the same trend as the actuator.
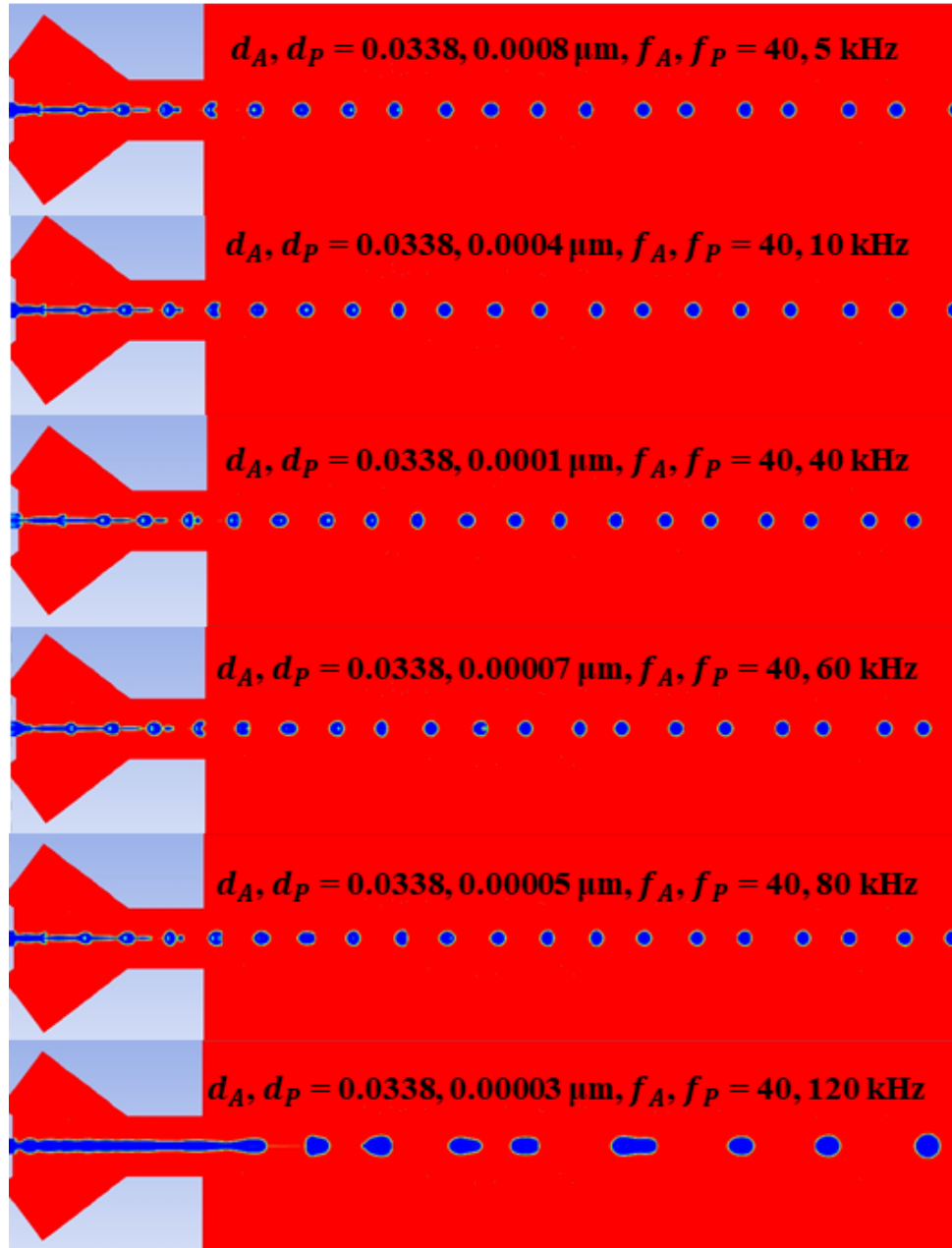
Figure 6.19 Effects of the piezo sensor frequency in volume fraction contour on the generated droplets from the nozzle with actuator's frequency of 40 kHz (Volume Fraction Contour).
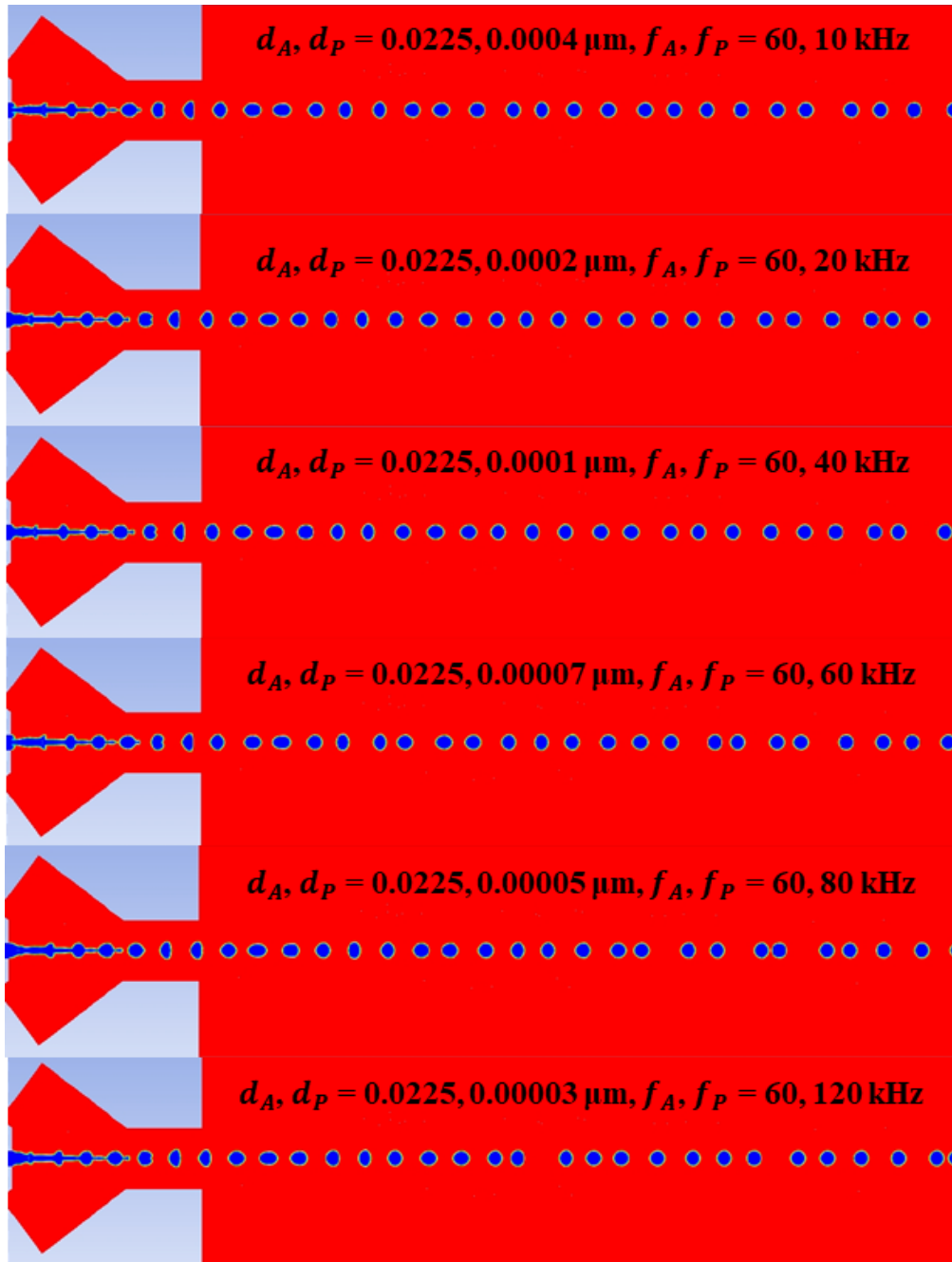
Figure 6.20 Effects of the piezo sensor frequency in volume fraction contour on the generated droplets from the nozzle with actuator's frequency of 60 kHz (Volume Fraction Contour).

The maximum frequency for the piezo sensor for the nozzle to operate in an acceptable range may depend on the actuator's specifications and its frequency, since the actuator introduces more energy to the liquid than the piezo sensor. A very high piezo frequency of 120 kHz in Figure 6.20 did not affect the droplet generation characteristics than the same actuator frequency in Figure 6.19. Additional numerical tests can help further quantify the effects of the actuator and piezo sensors on the droplets' size. A more quantitative analysis of the data in Figure 6.19 shows that an increase in the piezo sensor's frequency decreased the average droplet diameter from 64 μm to 55 μm which is a 14% deduction, while this analysis on the data from Figure 6.20 shows that the decrease was from 50 μm to 44 μm, which is a 12% reduction. It may be possible to further reduce the diameter of droplet beyond 44 μm, by finding the optimum nozzle's geometry and the exact properties of the piezo transducers. This is a worthy study to continue. Finally, the performance of the nozzle with higher viscosity fluids is ready to be numerically tested as shown in the next section.

6.3.2   Effects of Liquid Viscosity of The Performance of The Nozzle

This section is to assess the potentials of this nozzle design to work with higher viscosity fluids, the first step toward the application of the nozzle in automotive coating and painting industries. Parameters including air velocity, the frequency and amplitude for both the piezo sensor and the actuator were selected and the effect of each of these parameters on the performance of the nozzle for high viscous fluids were numerically studied. Figure 6.21 presents effects of the liquid viscosity in volume fraction contour on the performance of the inkjet nozzle with the piezo and actuator frequency fixed at 40 kHz,

139

$d_A = 0.0338$ µm and $d_P = 0.0001$ µm. The air velocity was also fixed at 5 m/s. As it can be seen, the nozzle can handle higher viscosity fluid; for example, an increase in the viscosity up to $3 \times \mu_{water}$ had very minimal effects on the nozzle's performance, and reduced the liquid ligament breakup length, which is an additional positive effect.

With a further increase in the liquid viscosity after $7 \times \mu_{water}$, the liquid ligament breakup length was increased, which is considered as a mild negative effect. For the liquid viscosity $9 \times \mu_{water}$ and higher, the performance of the inkjet nozzle became unacceptable as the liquid with $10 \times \mu_{water}$ represents the case in Figure 6.21. Comparison between the results in Figure 6.21 and in Figure 6.16 shows the additional second piezo sensor can significantly help to improve the performance of the nozzle under higher viscosity fluids. Based on the limited data regarding the viscosity values of typical industrial paint (presented in Figure 4.3), this DPD design is promising to be able to handle high viscous working liquids. For the maximum $9 \times \mu_{water}$ viscosity fluids where the current nozzle failed to perform adequately, the nozzle with higher frequencies or different maximum displacements may be able to overcome the current limitation. Therefore, further numerical tests and corresponding precision experiments will clarify these promising performances.
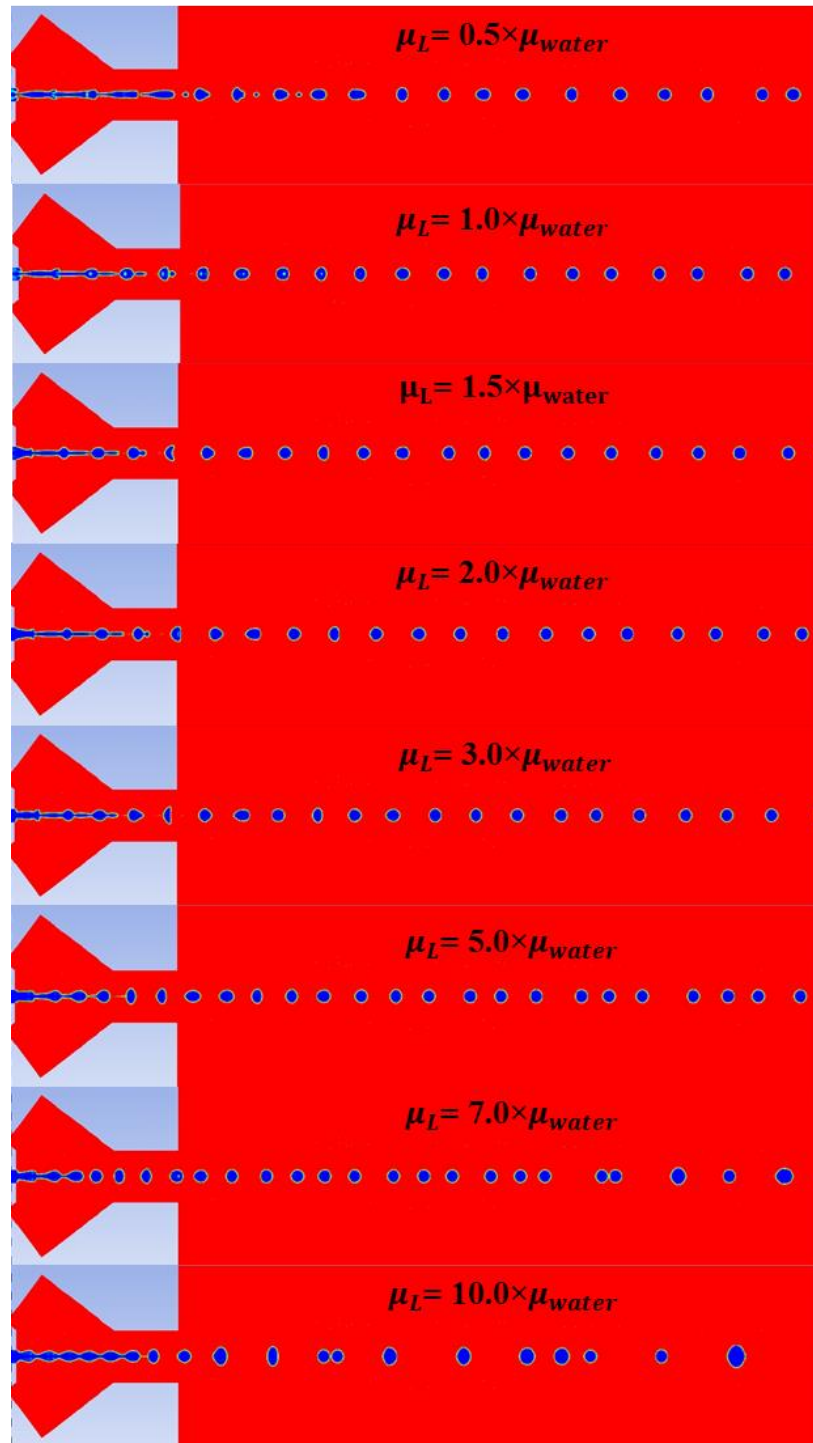
Figure 6.21 Effects of the liquid viscosity in volume fraction contour on the performance of the inkjet nozzle with piezo and actuator frequency of 40 kHz, d_A = 0.0338 μm and d_P = 0.0001 μm (Volume Fraction Contour).

6.3.3   Summary of The Results

This section numerically examined the effects of various influential parameters on the performance of the DPD nozzle. These parameters include the piezo sensor frequency, the actuator frequency, their maximum displacements, and the effects of the liquid viscosity on the performance of the nozzle. The design was shown to be able to generate mono-dispersed droplets from normal water with a wide range of piezo sensor's frequencies. Addition of the second piezo sensor was less effective in the nozzle's performance than the actuator's frequency, as it was expected. However, the second piezo sensor helped better control the droplet diameter and droplet generation frequency, given that the nozzle is working in the optimum range already without introducing the frequency to this second piezo sensor. This chapter showed a high performance of the nozzle with high viscose fluids whose viscosity is nine times water viscosity, and the results are significant for typical high viscous industrial paints.

CHAPTER 7. CONCLUSIONS, CONTRIBUTIONS AND FUTURE STUDY

7.1   Conclusions

This dissertation numerically studied the fluid mechanical process of ligament breakup and droplet generation from inkjet nozzles. Based on the results, new types of inkjet printheads were proposed for automotive coating and painting industries. This numerical study was meant to improve the performance of three modified inkjet printhead designs. The CFD simulations were conducted using each of these models separately with water-bone paint and with changing viscosities. For each design, the effect of various influential parameters on the performance of each inkjet nozzle was numerically studied, and the performance of the SPD nozzle with high viscosity fluids was assessed.

The ultrasonic pulsation atomizer (UPA) model, the simplest design among all studied cases in this dissertation, showed promising results using modified sinusoidal waves as the pulsation to reduce the droplets' size without reducing the nozzle orifice size. This was particularly helpful to avoid the nozzle clogging and similar problems due to the reduced nozzle orifice diameter. The results showed that the nozzle can generate droplets up to 40% smaller than the orifice size if the right conditions are introduced to the nozzle. The effects of other influential parameters on the nozzle's performance were also studied to help improve the droplet quality and transfer efficiency.

For the UPA model, a numerical scaling analysis was conducted to analyze the correlations between single monodispersed droplet stream and satellite droplet jetting conditions and provide jetting behavior diagrams to predict the performance of the inkjet nozzles under different conditions. Six different mechanical forces were identified for controlling the quality of the droplets and the performance of the nozzle. They are the

inertial force of air, the inertial force of liquid, viscous force of air acting on droplet surface, the viscous force of liquid, surface tension force of liquid, and dynamic pressure force (flow oscillation force). Furthermore, the jetting behavior diagrams of the UPA nozzle was created for different conditions by identifying five independent pi-numbers (principal pi-numbers) with significant effects on the nozzle's performance.

Advanced nozzle designs, SPD-DOD and DPD-DOD, in comparison to the simple UPA, were introduced to provide more control over the characteristics of the droplets generated. The effects of various working parameters were studied on the performance of the nozzle using normal water as the working liquid and the optimum conditions were identified. Waves with different pulsation frequencies and maximum displacements were introduced to the piezo sensor to understand the behavior of the nozzle with these conditions with the potential aim of reducing the droplet size without reducing the nozzle orifice size. The new types of nozzle showed promising results to work with very low air velocities which is the basis of increasing the TE as the result in automotive coating and painting industries. The SPD-DOD was found to be capable of working with higher viscosity paints for industrial applications.

The DPD-DOD was introduced taking advantage of two piezo sensors with the aim of providing more controls over the droplets' characteristics and it showed excellent capabilities to reduce the droplet size further. The DPD-DOD design was able to generate a monodispersed droplet stream from very high viscosity working fluids up to nine times more viscos than normal water. This viscosity is well within the range of the viscosities of the normal paints used in this industry.

144

7.2   Contributions of This Dissertation

This dissertation conducted CFD modeling to produce mono-dispersed well-controlled-size droplets of water bone paints using inkjet atomizing nozzles for coating and painting industries. The grand aim of this dissertation research is to create a new coating method to provide full and precise control over the droplet size and increase transfer efficiency of the coating process in automotive industries. Specific outcomes from this research include a new inkjet design which can fully control the droplet characteristics, work with fluids whose viscosity is nine times higher than the viscosity of water, and reduce the droplet size up to 55% without reducing the orifice size. As a result, the over-sprayed paints can be significantly reduced since the dependency of the droplet generation on the air velocity was drastically reduced and the droplets can be generated on an on-demand basis. This is a positive contribution to clean environment. Finally, a numerical scaling study produced jetting behavior diagrams to correlate single monodispersed droplet stream with satellite droplet jetting conditions. The diagrams are expected to predict the performance of the inkjet nozzles under different conditions, thus help researchers for an effective design of new inkjets for specific applications.

7.3   Future Study Recommendations

Five possible future studies are as follows:

(1) Finding the optimized working conditions for each atomizer design using experimental methods.

(2) Investigating the nozzle performance using different wave inputs to the piezo sensors and comparing the results to understand the advantages and

disadvantages of each wave form. To that end, the optimum working conditions need to be identified for each design separately.

(3) Scaling analysis on the correlations between the single monodispersed droplet stream and satellite droplet jetting conditions for the SPD and DPD designs as it probably requires some experimental testing to facilitate the investigations.

(4) Developing an advanced model, which can handle the variation of surface tension force with temperature, to accurately estimate actual non-Newtonian behaviors of industrial paints.

(5) Applying the current study to investigate effective inkjet designs with the metallic-flakes-added paints, which are common in coating car shells in automotive industries.

Acknowledgments

Nomenclature

Ca	Capillary number
Ca_a	Air Capillary number
Ca_l	Liquid Capillary number
d_A	Maximum displacement for the actuator
d_P	Maximum displacement for the piezo sensor
F	Surface tension force per volume
f	Pulsation frequency
f_i	Inertial force
f_σ	Surface tension force
f_μ	Viscous force
f_A	Frequency of movement for the actuator
f_P	Frequency of movement for the piezo sensor
$\vec{g}$	Gravity
$H(T)$	Temperature dependency of the fluid
k	Curvature of the gas–liquid interface
k_{eff}	Effective thermal conductivity
$\hat{n}$	Unit vector normal to the interface
Oh_l	Liquid Ohnesorge number
p	Pressure
R	Nozzle radius
Re	Reynolds number
Re_a	Air Reynolds number
Re_l	Liquid Reynolds number
St	Strouhal number
TE	Transfer efficiency

T	Temperature
U	Velocity magnitude
U_f	Volume flux through the face
$U(t)$	Inlet velocity in terms of time
$U_A(t)$	Actuator inlet velocity in terms of time
U_{max}	Amplitude of sinusoidal inlet velocity
$U_{A_{max}}$	Amplitude of sinusoidal inlet velocity for the actuator
$\vec{V}$	Velocity vector
V	Volume of the cell
$V_p(t)$	Piezo sensor inlet velocity in terms of time
$V_{P_{max}}$	Amplitude of sinusoidal inlet velocity for the piezo sensor
VOF	Volume of fluids
We	Weber number
We_a	Air Weber number
We_l	Liquid Weber number
π	Pi number
Ω	Omega number
σ	Surface Tension
μ	Viscosity
μ_w	Viscosity of water
ρ	Density
α	Volume fraction
ρ	Volume-averaged density
$\ddot{D}$	Rate of deformation
$\ddot{\tau}$	Shear stress
$\dot{\gamma}$	Shear rate
$\dot{m}_{pq}$	Mass transfer from phase p to phase q,
$\dot{m}_{qp}$	Mass transfer from phase q to phase p.

REFERENCES

Akafuah, N. K., Salazar, A. J., Saito, K., & Srinivasan, V. (2009). *Ultrasonically Driven Cavitating Atomizer: Prototype Fabrication and Characterization.* Paper presented at the ASME 2009 Fluids Engineering Division Summer Meeting.

Andersson, B. (2013). *Modeling and simulation of rotary bell spray atomizers in automotive paint shops*: Chalmers Tekniska Hogskola (Sweden).

Antonopoulou, E., Harlen, O., Rump, M., Segers, T., & Walkley, M. (2021). Effect of surfactants on jet break-up in drop-on-demand inkjet printing. *Physics of fluids, 33*(7), 072112.

Antonopoulou, E., Harlen, O., Walkley, M., & Kapur, N. (2020). Jetting behavior in drop-on-demand printing: Laboratory experiments and numerical simulations. *Physical Review Fluids, 5*(4), 043603.

Arabghahestani, M., Akafuah, N., Li, T., & Saito, K. (2022). A CFD-based scaling analysis on liquid and paint droplets moving through a weak concurrent airflow stream. *Progress in Scale Modeling, an International Journal, 3*(1), 3.

Arabghahestani, M., Akafuah, N. K., & Saito, K. (2021). Computational fluid dynamics and scaling study on ultrasonic pulsation atomizer for waterborne paint. *Atomization and Sprays, 31*(3).

Arabghahestani, M., & Karimian, S. (2017). Molecular dynamics simulation of rotating carbon nanotube in uniform liquid argon flow. *Journal of Molecular Liquids, 225*, 357-364.

Arabghahestani, M., Poozesh, S., & Akafuah, N. K. (2019). Advances in Computational Fluid Mechanics in Cellular Flow Manipulation: A Review. *Applied Sciences, 9*(19), 4041.

Avvaru, B., Patil, M. N., Gogate, P. R., & Pandit, A. B. (2006). Ultrasonic atomization: effect of liquid phase properties. *Ultrasonics, 44*(2), 146-158.

Bang, K. H., Kim, J. M., & Kim, D. H. (2003). Experimental study of melt jet breakup in water. *Journal of nuclear science and technology, 40*(10), 807-813.

Basaran, O. A. (2002). Small-scale free surface flows with breakup: Drop formation and emerging applications. *American Institute of Chemical Engineers. AIChE Journal, 48*(9), 1842-1848.

Bergwerk, W. (1959). Flow pattern in diesel nozzle spray holes. *Proceedings of the Institution of Mechanical Engineers, 173*(1), 655-660.

Bernardini, G. L., Rampy, B. A., Howell, G. A., Hayes, D. J., & Frederickson, C. J. J. J. o. n. m. (1991). Applications of piezoelectric fluid jetting devices to neuroscience research. *38*(1), 81-88.

Bird, R. B., Armstrong, R. C., & Hassager, O. (1987). Dynamics of polymeric liquids. Vol. 1: Fluid mechanics.

Bird, R. B. J. A. R. o. F. M. (1976). Useful non-Newtonian models. *8*(1), 13-34.

Brackbill, J. U., Kothe, D. B., & Zemach, C. (1992). A continuum method for modeling surface tension. *Journal of Computational physics, 100*(2), 335-354.

Brennan, T. M. (1999). Method and apparatus for conducting an array of chemical reactions on a support surface. In: Google Patents.

Brown, C. T., & McDonell, V. G. (2006). *Near field behavior of a liquid jet in a crossflow.* Paper presented at the Proceedings of the ILASS Americas, 19th Annual Conference on Liquid Atomization and Spray Systems.

Burr, R. F., Tence, D. A., Le, H. P., Adams, R. L., & Mutton, J. C. (1996). Method and apparatus for producing dot size modulated ink jet printing. In: U.S. Patent No. 5,495,270.

Caglar, U. (2010). Studies of inkjet printing technology with focus on electronic materials.

Carrino, L., Moroni, G., & Polini, W. J. J. o. M. P. T. (2002). Cold plasma treatment of polypropylene surface: a study on wettability and adhesion. *121*(2-3), 373-382.

Castrejón-Pita, A., Castrejón-Pita, J., & Martin, G. (2012). A novel method to produce small droplets from large nozzles. *Review of scientific instruments, 83*(11), 115105.

Castrejon-Pita, A. A., Castrejon-Pita, J. R., & Hutchings, I. M. (2012). Breakup of liquid filaments. *Physical review letters, 108*(7), 074506.

Castrejón-Pita, J., Morrison, N., Harlen, O., Martin, G., & Hutchings, I. (2011). Experiments and Lagrangian simulations on the formation of droplets in drop-on-demand mode. *Physical Review E, 83*(3), 036306.

Chen, A. U., & Basaran, O. A. (2002). A new method for significantly reducing drop radius without reducing nozzle radius in drop-on-demand drop production. *Physics of fluids, 14*(1), L1-L4.

Chhabra, R. P. (2010). Non-Newtonian fluids: an introduction. In *Rheology of complex fluids* (pp. 3-34): Springer.

Chuang, M. Y. (2011). Medicine injection into skin with heater chip. In: Google Patents.

Conner, D. C., Atkar, P. N., Rizzi, A. A., & Choset, H. (2002). *Development of deposition models for paint application on surfaces embedded in/spl Ropf//sup 3/for use in automated path planning.* Paper presented at the Intelligent Robots and Systems, 2002. IEEE/RSJ International Conference on.

Conner, D. C., Greenfield, A., Atkar, P. N., Rizzi, A. A., Choset, H. J. I. T. o. A. S., & Engineering. (2005). Paint deposition modeling for trajectory planning on automotive surfaces. *2*(4), 381-392.

Conto, F. P. (2019). *Breakup of liquid jets: the capillary retraction.* Queen Mary University of London,

Darroch, J. (1997). The HVLP revolution: The basics of buying HVLP spray equipment. *Furniture Design & Manufacturing, 69*, 100-106.

Darwish Ahmad, A., Abubaker, A. M., Salaimeh, A. A., & Akafuah, N. K. (2018). Schlieren visualization of shaping air during operation of an electrostatic rotary bell sprayer: Impact of shaping air on droplet atomization and transport. *Coatings, 8*(8), 279.

Darwish Ahmad, A., Singh, B. B., Doerre, M., Abubaker, A. M., Arabghahestani, M., Salaimeh, A. A., & Akafuah, N. K. (2019). Spatial Positioning and Operating Parameters of a Rotary Bell Sprayer: 3D Mapping of Droplet Size Distributions. *Fluids, 4*(3), 165.

Delhaye, J.-M., Coutris, N., & Herran, L. (2013). *Drop-on-Demand: A Scale Analysis.* Paper presented at the ASME International Mechanical Engineering Congress and Exposition.

Dombrowski, N., & Lloyd, T. (1972). The spread of liquid on a rotating vane. *Chemical Engineering Science, 27*(5), 1003-1012.

Domnick, J., Scheibe, A., & Ye, Q. (2005). The Simulation of the Electrostatic Spray Painting Process with High-Speed Rotary Bell Atomizers. Part I: Direct Charging. *Particle & Particle Systems Characterization, 22*(2), 141-150.

Domnick, J., Scheibe, A., & Ye, Q. (2006). The Simulation of Electrostatic Spray Painting Process with High-Speed Rotary Bell Atomizers. Part II: External Charging. *Particle & Particle Systems Characterization, 23*(5), 408-416.

Dong, H., Carr, W. W., & Morris, J. (2006). An experimental study of drop-on-demand drop formation. *Physics of fluids, 18*(7), 072102.

Edgerton, H. E., Hauser, E. A., & Tucker, W. (1937). Studies in drop formation as revealed by the high-speed motion camera. *Journal of Physical Chemistry, 41*(7), 1017-1028.

Eggers, J., & Dupont, T. F. (1994). Drop formation in a one-dimensional approximation of the Navier–Stokes equation. *Journal of fluid mechanics, 262*, 205-221.

Emori, R., Saito, K., & Sekimoto, K. (2000). Scale models in engineering (Mokei Jikken no Riron to Ohyou). *Gihodo Publishing Co., Tokyo, Japan, 20*(0), 0.

Eshkalak, S. K., Chinnappan, A., Jayathilaka, W., Khatibzadeh, M., Kowsari, E., & Ramakrishna, S. (2017). A review on inkjet printing of CNT composites for smart applications. *Applied Materials Today, 9*, 372-386.

Fakhfouri, V., Cantale, N., Mermoud, G., Kim, J., Boiko, D., Charbon, E., . . . Brugger, J. (2008). *Inkjet printing of SU-8 for polymer-based MEMS a case study for microlenses.* Paper presented at the 2008 IEEE 21st International Conference on Micro Electro Mechanical Systems.

Fettis, G. (2008). *Automotive paints and coatings*: John Wiley & Sons.

Fischer, A. C., Mäntysalo, M., & Niklaus, F. (2020). Inkjet printing, laser-based micromachining, and micro–3D printing technologies for MEMS. In *Handbook of silicon based MEMS materials and technologies* (pp. 531-545): Elsevier.

Fromm, J. (1982). A numerical study of drop-on-demand ink jets.

Frost, A. (1981). Rotary atomization in the ligament formation mode. *Journal of Agricultural Engineering Research, 26*(1), 63-78.

Gan, H., Shan, X., Eriksson, T., Lok, B., & Lam, Y. (2009). Reduction of droplet volume by controlling actuating waveforms in inkjet printing for micro-pattern formation. *Journal of micromechanics microengineering, 19*(5), 055010.

Gao, J., Hossain, A., Matsuoka, T., & Nakamura, Y. (2017). A numerical study on heat-recirculation assisted combustion for small scale jet diffusion flames at near-extinction condition. *Combustion and flame, 178*, 182-194.

Ghosh, T., Rezaee, M., Honaker, R. Q., & Saito, K. (2015). Scale and numerical modeling of an air-based density separator. In *Progress in Scale Modeling, Volume II* (pp. 225-238): Springer.

Grant, R. P., & Middleman, S. (1966). Newtonian jet stability. *AIChE Journal, 12*(4), 669-678.

Guettler, N., Knee, P., Ye, Q., & Tiedje, O. (2020). Initial droplet conditions in numerical spray painting by electrostatic rotary bell sprayers. *Journal of Coatings Technology and Research, 17*(5), 1091-1104.

Gueyffier, D., Li, J., Nadim, A., Scardovelli, R., & Zaleski, S. (1999). Volume-of-fluid interface tracking with smoothed surface stress methods for three-dimensional flows. *Journal of Computational physics, 152*(2), 423-456.

151

Hauser, E., Edgerton, H. E., Holt, B., & Cox Jr, J. (2002). The Application of the High-speed Motion Picture Camera to Research on the Surface Tension of Liquids. *The Journal of Physical Chemistry, 40*(8), 973-988.

Heitbrink, W. A., Verb, R. H., Fischbach, T. J., & Wallace, M. E. (1996). A comparison of conventional and high volume-low pressure spray-painting guns. *American Industrial Hygiene Association Journal, 57*(3), 304-310.

Henderson, D. M., Pritchard, W. G., & Smolka, L. B. (1997). On the pinch-off of a pendant drop of viscous fluid. *Physics of fluids, 9*(11), 3188-3200.

Hines, R. (1966). Electrostatic atomization and spray painting. *Journal of Applied Physics, 37*(7), 2730-2736.

Hoath, S., Jung, S., & Hutchings, I. (2013). A simple criterion for filament break-up in drop-on-demand inkjet printing. *Physics of fluids, 25*(2), 021701.

Hoath, S. D. (2016). *Fundamentals of inkjet printing: the science of inkjet and droplets*: John Wiley & Sons.

Hollister, S. J., Lin, C., Saito, E., Lin, C., Schek, R., Taboas, J., . . . Diggs, A. (2005). Engineering craniofacial scaffolds. *Orthodontics & craniofacial research, 8*(3), 162-173.

Hon, S., Kwok, K., Li, H., & Ng, H. J. R. o. s. i. (2010). Self-focused acoustic ejectors for viscous liquids. *81*(6), 065102.

Huang, H., Lai, M.-C., & Meredith, W. (2000). *Simulation of spray transport from rotary cup atomizer using KIVA-3V.* Paper presented at the ICLASS 2000.

Im, K.-S., Lai, M.-C., Yu, S.-T. J., & Matheson Jr, R. R. (2004). Simulation of spray transfer processes in electrostatic rotary bell sprayer. *J. Fluids Eng., 126*(3), 449-456.

Janna, W. S. (1976). Drop-size distributions of sprays produced by fan-jet pressure nozzles.

Kim, E., & Baek, J. (2012). Numerical study on the effects of non-dimensional parameters on drop-on-demand droplet formation dynamics and printability range in the up-scaled model. *Physics of fluids, 24*(8), 082103.

Kimura, J., Kawana, Y., & Kuriyama, T. (1989). An immobilized enzyme membrane fabrication method using an ink jet nozzle. *Biosensors, 4*(1), 41-52.

Kimura, J., Kawana, Y., & Kuriyama, T. J. B. (1989). An immobilized enzyme membrane fabrication method using an ink jet nozzle. *4*(1), 41-52.

Kolakovic, R., Viitala, T., Ihalainen, P., Genina, N., Peltonen, J., & Sandler, N. (2013). Printing technologies in fabrication of drug delivery systems. *Expert opinion on drug delivery, 10*(12), 1711-1723.

Kumar, A. R., Arya, S., Levy, A., Schafrik, S., Wedding, W. C., & Saito, K. (2020). Scale and numerical modeling to determine operating points of a non-clogging Vortecone filter in mining operation. *Progress in Scale Modeling, an International Journal, 1*(1), 7.

Kuwana, K., Hassan, M., Singh, P., Saito, K., & Nakagawa, J. (2008). Scale-model experiment and numerical simulation of a steel teeming process. *Materials and Manufacturing Processes, 23*(4), 407-412.

Kuwana, K., Sekimoto, K., Saito, K., & Williams, F. A. (2008). Scaling fire whirls. *Fire Safety Journal, 43*(4), 252-257.

Laurell, T., Wallman, L., Nilsson, J. J. J. o. M., & Microengineering. (1999). Design and development of a silicon microfabricated flow-through dispenser for on-line picolitre sample handling. *9*(4), 369.

Lee, H.-H., Chou, K.-S., & Huang, K.-C. (2005). Inkjet printing of nanosized silver colloids. *Nanotechnology, 16*(10), 2436.

Lee, I., Kim, D., Koo, J. J. A., & Sprays. (2012). Liquid jet breakup structure and transfer efficiency of a two-stage air-blast injector. *22*(7).

Lefebvre, A. H. J. C., New York. (1989). Atomization and Sprays, Hemisphere Pub. *1989*.

Lessing, J., Glavan, A. C., Walker, S. B., Keplinger, C., Lewis, J. A., & Whitesides, G. M. (2014). Inkjet Printing of conductive inks with high lateral resolution on omniphobic "Rf paper" for paper-based electronics and MEMS. *Advanced Materials, 26*(27), 4677-4682.

Li, H., Pokhrel, S., Schowalter, M., Rosenauer, A., Kiefer, J., & Mädler, L. (2020). The gas-phase formation of tin dioxide nanoparticles in single droplet combustion and flame spray pyrolysis. *Combustion and flame, 215*, 389-400.

Lin, S. P., & Reitz, R. D. (1998). Drop and spray formation from a liquid jet. *Annual Review of Fluid Mechanics, 30*(1), 85-105.

Liou, J.-C., & Wu, C.-C. (2017). Design and fabrication of microfluidic inkjet chip with high voltage ESD protection system for DNA droplets arrangement and detection. *Microsystem Technologies, 23*(1), 199-213.

Liu, H. (2002). *Science and Engineering of Droplets:: Fundamentals and Applications*. Appl. Mech. Rev: William Andrew.

Liu, J., Yu, Q., & Guo, Q. (2012). Experimental investigation of liquid disintegration by rotary cups. *Chemical Engineering Science, 73*, 44-50.

Lohse, D. (2022). Fundamental fluid dynamics challenges in inkjet printing. *Annual Review of Fluid Mechanics, 54*, 349-382.

López, F. V., Diez, A., & Odriozola, A. (2007). Inkjet printing of conductive and resistive coatings. *International polymer processing, 22*(1), 27-33.

Mahmood, M. A. (2021). 3D printing in drug delivery and biomedical applications: A state-of-the-art review. *Compounds, 1*(3), 94-115.

Maisch, P., Tam, K. C., Fecher, F. W., Egelhaaf, H.-J., Brabec, C. J., Scheiber, H., & Maier, E. (2016). *Inkjet printing of highly conductive nanoparticle dispersions for organic electronics.* Paper presented at the 2016 12th International Congress Molded Interconnect Devices (MID).

Mark, A., Andersson, B., Tafuri, S., Engstrom, K., Sorod, H., Edelvik, F., & Carlson, J. S. (2013). Simulation of electrostatic rotary bell spray painting in automotive paint shops. *Atomization and Sprays, 23*(1).

Marshall, W. R. (1954). *Atomization and spray drying*. [New York: American Institute of Chemical Engineers.

Masters, K. (1979). Spray drying handbook. Retrieved from http://books.google.com/books?id=xblTAAAAMAAJ.

Mei, J., Lovell, M. R., & Mickle, M. H. (2005). Formulation and processing of novel conductive solution inks in continuous inkjet printing of 3-D electric circuits. *IEEE transactions on electronics packaging manufacturing, 28*(3), 265-273.

Nakamura, Y., Yamashita, H., & Saito, K. (2006). A numerical study on extinction behaviour of laminar micro-diffusion flames. *Combustion theory and modelling, 10*(6), 927-938.

Nasr, G. G., Yule, A. J., & Bendig, L. (2013). *Industrial sprays and atomization: design, analysis and applications*: Springer Science & Business Media.

Nukiyama, S., & Tanasawa, Y. (1938). An Experiment on the Atomization of Liquid. : 4th Report, The Effect of the Properties of Liquid on the Size of Drops. *Transactions of the Japan Society of Mechanical Engineers. A, 5*, 136-143.

Osman, H., Adamiak, K., Castle, G. P., Fan, H.-T., & Simmer, J. (2015). *Comparison between the numerical and experimental deposition patterns for an electrostatic rotary bell sprayer.* Paper presented at the ASME International Mechanical Engineering Congress and Exposition.

Pendar, M.-R., & Páscoa, J. C. (2019). Numerical modeling of electrostatic spray painting transfer processes in rotary bell cup for automotive painting. *International Journal of Heat and Fluid Flow, 80*, 108499.

Peng, H., Wang, N., Wang, D., & Ling, X. (2016). Experimental study on the critical characteristics of liquid atomization by a spinning disk. *Industrial & Engineering Chemistry Research, 55*(21), 6175-6185.

Perçin, G., Atalar, A., Levent Degertekin, F., & Khuri-Yakub, B. T. J. A. p. l. (1998). Micromachined two-dimensional array piezoelectrically actuated transducers. *72*(11), 1397-1399.

Poozesh, S. (2015). Inkjet Printing: Facing Challenges and Its New Applications in Coating Industry.

Poozesh, S. (2021). Data-driven tools guided by first-principles for scale modeling. *Progress in Scale Modeling, an International Journal, 2*(1), 1.

Poozesh, S., Akafuah, N., & Saito, K. (2015). *Numerical simulation of a coating sprayer capable of producing controllable paint droplets* (0148-7191). Retrieved from

Poozesh, S., Akafuah, N. K., Campbell, H. R., Bashiri, F., & Saito, K. (2020). Experimental and mathematical tools to predict droplet size and velocity distribution for a two-fluid nozzle. *Fluids, 5*(4), 231.

Poozesh, S., Saito, K., Akafuah, N. K., & Graña-Otero, J. (2016). Comprehensive examination of a new mechanism to produce small droplets in drop-on-demand inkjet technology. *Applied Physics A, 122*(2), 110.

Rayleigh, L. (1892). XIX. On the instability of cylindrical fluid surfaces. *The London, Edinburgh, Dublin Philosophical Magazine Journal of Science, 34*(207), 177-180.

Reitz, R., & Bracco, F. (1982). Mechanism of atomization of a liquid jet. *The physics of Fluids, 25*(10), 1730-1742.

Reitz, R. D. (1978). *Atomization and other breakup regimes of a liquid jet.* (PhD), Harvard University,

Saito, K. (2008). *Progress in Scale Modeling: Summary of the First International Symposium on Scale Modeling (ISSM I in 1988) and Selected Papers from Subsequent Symposia (ISSM II in 1997 Through ISSM V in 2006)*: Springer Science & Business Media.

Saito, K. (2022). The Lecture Note on ME 565: Scale Modeling in Engineering. *Department of Mechanical Engineering, University of Kentucky, Lexington, KY, 40506.*

Saito, K., & Williams, F. (2015). Scale modeling in the age of high-speed computation. In *Progress in Scale Modeling, Volume II* (pp. 1-18): Springer, Cham.

Sakai, S. (2000). *Dynamics of piezoelectric inkjet printing systems.* Paper presented at the NIP & Digital Fabrication Conference.

Salazar, A. J. (2013). Computational modeling of relevant automotive rotary spray painting process. In *Automotive Painting Technology* (pp. 47-95): Springer.

Salazar, A. J. S., K. . (2008). Novel automative spray painting systems: Computational fluid dynamics study of ultrasonic ligament atomizer. *IAES Final Report, project sponsored by Toyaota Motor Corporation.*

Schick, R. (2006). Spray technology reference guide: Understanding drop size, Spray analysis and research services. *Spray Drying Systems Co.*

Schonhorn, H. (1967). Surface Tension-Viscosity Relationship for Liquids. *Journal of Chemical and Engineering Data, 12*(4), 524-525.

Shi, X., Brenner, M. P., & Nagel, S. R. (1994). A cascade of structure in a drop falling from a faucet. *Science, 265*(5169), 219-222.

Shirinzadeh, B., Cassidy, G., Oetomo, D., Alici, G., Ang Jr, M. H. J. R., & Manufacturing, C.-I. (2007). Trajectory generation for open-contoured structures in robotic fibre placement. *23*(4), 380-394.

Srinivasan, V. (2006). A numerical study of a new spray applicator.

Swerin, A. (2018). Dimensional Scaling of Aqueous Ink Imbibition and Inkjet Printability on Porous Pigment Coated Paper–A Revisit. *Industrial & Engineering Chemistry Research, 57*(49), 16684-16691.

Sziele, D., Brüggemann, O., Döring, M., Freitag, R., & Schügerl, K. J. J. o. C. A. (1994). Adaptation of a microdrop injector to sampling in capillary electrophoresis. *669*(1-2), 254-258.

Tan, Y.-M., & Flynn, M. R. (2000). Experimental Evaluation of a Mathematical Model for Predicting Transfer Efficiency of a High Volume? Low Pressure Air Spray Gun. *Applied Occupational and Environmental Hygiene, 15*(10), 785-793.

Toda, K., Salazar, A., & Saito, K. (2012). *Automotive painting technology: A Monozukuri-Hitozukuri perspective*: Springer.

Wang, Y., Bokor, J., & Lee, A. (2004). *Maskless lithography using drop-on-demand inkjet printing method* (Vol. 5374): SPIE.

Wang, Z., & Nagao, Y. (2014). Effects of Nafion impregnation using inkjet printing for membrane electrode assemblies in polymer electrolyte membrane fuel cells. *Electrochimica Acta, 129*, 343-347.

Wijshoff, H. (2010). The dynamics of the piezo inkjet printhead operation. *Physics reports, 491*(4-5), 77-177.

Wijshoff, H. (2018). Drop dynamics in the inkjet printing process. *Current opinion in colloid & interface science, 36*, 20-27.

Wilson, E. B. (1990). *An introduction to scientific research*: Courier Corporation.

Yang, F. L., Zhou, S. J., Zhang, C. X., & Wang, G. C. J. K. J. o. C. E. (2013). Mixing of initially stratified miscible fluids in an eccentric stirred tank: Detached eddy simulation and volume of fluid study. *30*(10), 1843-1854.

Ye, Q., & Domnick, J. (2017). Analysis of droplet impingement of different atomizers used in spray coating processes. *Journal of Coatings Technology and Research, 14*(2), 467-476.

Zhang, D., & Stone, H. A. (1997). Drop formation in viscous flows at a vertical capillary tube. *Physics of fluids, 9*(8), 2234-2242.

Zhang, W., Liu, H., Liu, C., Jia, M., & Xi, X. (2019). Numerical investigation into primary breakup of diesel spray with residual bubbles in the nozzle. *Fuel, 250*, 265-276.

Zhang, X. (1999). Dynamics of growth and breakup of viscous pendant drops into air. *Journal of colloid and interface science, 212*(1), 107-122.

Zhang, X., & Basaran, O. A. (1995). An experimental study of dynamics of drop formation. *Physics of fluids, 7*(6), 1184-1203.

Masoud Arabghahestani

Education

Doctorate Degree in Mechanical Engineering – Anticipated: December 2022
University of Kentucky, Lexington, KY

Master of Science in Aerospace Engineering - October 2015
Amirkabir University of Technology, Tehran, Iran

Bachelor of Science in Aerospace Engineering - September 2013
Amirkabir University of Technology, Tehran, Iran

Publications

Journal Papers

Arabghahestani, M., Akafuah, N., Li, T., & Saito, K. (2022). A CFD-based scaling analysis on liquid and paint droplets moving through a weak concurrent airflow stream. Progress in Scale Modeling, an International Journal, 3(1), 3.

Babaei, A., & Arabghahestani, M. (2021). Free vibration analysis of rotating beams based on the modified couple stress theory and coupled displacement field. Applied Mechanics, 2(2), 226-238.

Arabghahestani, M., Akafuah, N. K., & Saito, K. (2021). Computational fluid dynamics and scaling study on ultrasonic pulsation atomizer for waterborne paint. Atomization and Sprays, 31(3).

Arabghahestani, M., Poozesh, S., & Akafuah, N. K. (2019). Advances in computational fluid mechanics in cellular flow manipulation: A review. Applied Sciences, 9(19), 4041.

Darwish Ahmad, A., Singh, B. B., Doerre, M., Abubaker, A. M., Arabghahestani, M., Salaimeh, A. A., & Akafuah, N. K. (2019). Spatial positioning and operating parameters of a rotary bell sprayer: 3D mapping of droplet size distributions. Fluids, 4(3), 165.

Presentations/Proceedings:

Arabghahestani, M., Akafuah, N. K., Li, T. X., & Saito, K. A CFD-Based Scaling Analysis on Liquid Droplets Moving Through A Weak Concurrent Airflow Stream. In International Symposium on Scale Modeling 02-04 March 2022, Napoli (Italy) (p. 102).